

**Wechselwirkung von dünnen Schichten aus HVZ
Polyestern im wässrigen Medium mit Modellproteinen**

*Investigation of adsorption of model proteins on hyperbranched
aromatic polyester thin films in aqueous media*

DISSERTATION

zur Erlangung des akademischen Grades

Doktor rerum naturalium

(Dr. rer. nat.)

vorgelegt

der Fakultät Mathematik und Naturwissenschaften
der Technischen Universität Dresden

von

Yulia Mikhaylova

(Master's degree in Chemistry)

geboren am 20. September 1976 in Tver, Russland

Gutachter: Prof. Dr. rer. nat. habil. Brigitte Voit
Dr. rer. nat. habil. Reinhard Miller
Prof. Dr. rer. nat. habil. Thomas Wolff

Eingereicht am: 06.03.2006

Tag der Verteidigung: 11.05.2006

Acknowledgments

I have spent more than three years conducting my project work at the Analytical Department of the Institute of Macromolecular Chemistry at the Leibniz Institute of Polymer Research (IPF) in Dresden. It has been a time of great experience and a lot of interesting work. Many people have contributed in making my stay here very pleasant. Thanks. There are some persons, that I especially would like to thank. Those are:

Prof. Dr. Brigitte Voit, my supervisor, for giving me the opportunity to do this project work. With her guidance and interest I was able to complete my work successfully.

Dr. Klaus-Jochen Eichhorn, my second supervisor, the project leader and head of the Analytical Department, for always taking time to answer my questions, his suggestions, hints and overall backing helped me to a large extent to reach the final goal, and for being so enthusiastic and friendly.

Dr. Karina Grundke, the second project leader (Sonderforschungsbereiches 287 - B6), for her interest to my work and the helpful discussions.

Dr. Victoria Dutschk for the help in discussions of contact angle measurement results. Many thanks for Mrs. Nicole Petong for her help in performing many of ADSA experiments. Dr. Cornelia Bellmann for the electrokinetic measurements and for helpful discussions. Dr. Dirk Schmaljohann and Dr. Doris Pospiech for the synthesis of hyperbranched aromatic polyesters. Dr. Martin Müller for the help in performing protein adsorption experiments by ATR-FTIR spectroscopy and for all the pleasant discussions we had.

I would like also to express my sincere thanks to all co-workers of the Analytical Department, especially to: Dr. Hartmut Komber for the great help in the interpretation of the NMR spectra and for the clever tips regarding purification. Mr. Dieter Voigt, Dr. Alben Lederer, and the assistances Mrs. Petra Treppe and Mrs. Christina Harnisch deserve my gratitude for the Liquid Chromatography measurements. Mrs. Liane Häussler and Mrs. Kerstin Arnhold for the DSC and TGA measurements. I thank also to Liane, my office neighbour, for her kind and friendly attitude to me

during all time. I thank Mrs. Gudrun Adam for the IR measurements and for help in the interpretation of the “hundreds” of FTIR spectra. My gratitude goes to Mr. Roland Schulze for the greatest help in the ellipsometric measurements and for the coming every time when I was crying “please, Roland, help”. Mrs. Beate Weiße, our secretary, for the help me solving practical matters of any kind.

I would like to thank my colleagues for the nice time I spent here and their helpful advices: Martin Gernert, Martin Messerschmidt, Renata Keska, Dr. Dirk Schmaljohann, Dr. Detlev Beyerlein, Stefan Gramm, Dr. Valentina Pitto, Dr. Felix Braun, Arnulf Scheel, Sven Fleischmann, Alla Synytska, Leonid Ionov, Dr. Denis Usov, Dr. Ihor Tokarev, Mikhail Motornov, Phylip Volodin, Dr. Nikolay Houbenov, Dr. Alexander Sydorenko, Senta Reichelt, Andreas Korwitz, Dr. Marta Millaruelo-Boira, Barbara Sieczkowska, Ute Stephan, Falko Schallausky, and all the rest of my colleagues and friends who helped me with various things. No one is forgotten, although not mentioned.

I am particularly indebted to Dr. Marina Dudkina and Prof. Andrei Tenkovsev for very kind attitude to me during all time and especially during the first weeks in Germany. I thank Dr. Alexander Pavlov for his great advises and help during my study at the Tver State University, and especially for his friendship. Prof. Pavel Pakhomov for his supervision during my Master’s Diploma at the Tver State University; without his support I would not be in IPF.

I am very grateful to my family: my husband Martin, my mother and father, my sister Valentina and her daughter Yulia, who gave the incredible love and support during all time.

Contents

Motivation	5
Goals	6
Outline	7

Chapter 1

Theoretical background for the experimental techniques

1.1. Ellipsometry	8
1.2. Contact Angle method	12
1.3. Electrokinetic method	15
1.4. Infrared Spectroscopy	17
1.5. Atomic Force Microscopy	19

Chapter 2

Characterisation of hyperbranched aromatic polyesters

2.1. Hyperbranched polymers (HBP): a promising class of materials	20
2.2. Characterisation of hyperbranched aromatic polyesters with different functional groups: Materials and Methods	23
2.3. Molecular structure analysis of HBPs in the liquid and solid state	25
2.4. Comparison of molar masses of HBPs determined by different type of chromatographic systems	29
2.5. Thermal properties of HBPs	35

Chapter 3

Characterisation of the film properties of hyperbranched aromatic polyesters

Chapter 3.1: Temperature-dependent FTIR spectroscopic and thermoanalytic studies of hydrogen bonding of hydroxyl terminated hyperbranched aromatic polyester, HBP-OH

3.1.1. Role of supramolecular interactions in HBPs	39
3.1.2. Application of “heating-annealing-cooling” cycles to study the hydrogen network formation in HBP-OH	40
3.1.3. Hydrogen bonds formation and reorganisation during “heating-annealing-cooling” cycles	42
3.1.4. Effect of the “heating-annealing-cooling” cycles on the glass transition temperature of HBP-OH	51
3.1.5. Hydrogen bonding in HBP-OH: summary	52

Chapter 3.2: Characterisation of the properties and swelling behaviour of HBP thin films

3.2.1. Swelling of polymer films: why to study?	53
3.2.2. Wafer cleaning technology	55
3.2.3. Thin film preparation	56
3.2.4. Methods applied to characterise HBP thin films in dry state and aqueous media	57
3.2.5. Role of end groups functionality on the surface properties of HBP films: -OH, -COOH, -OH/OCOCH ₃ and -OCOCH ₃	60
3.2.6. Stability, equilibrium swelling, kinetics and swelling degree of HBP thin films in aqueous media	63
3.2.7. Conclusions	72

Chapter 3.3: Preparation and characterisation of grafted films of carboxyl terminated hyperbranched aromatic polyester, HBP-COOH

3.3.1. Hyperbranched polymers on solid surfaces	73
3.3.2. Hyperbranched molecules with carboxyl terminal groups: Grafting to a solid surface (silicon wafer)	74
3.3.3. Analytical methods	75
3.3.4. Fabrication of surface attached HBP-COOH by “grafting to” technique	76
3.3.5. Summary	81

Chapter 4**Adsorption of model proteins**

4.1. Theory of protein adsorption	83
4.1.1. Structure of protein molecule	83
4.1.2. Factors affecting protein folding and stability in aqueous medium	84
4.1.3. Protein Adsorption: Fundamental Principles	86
4.1.4. Factors influencing the protein adsorption at solid/liquid interface	87
4.2. Monitoring the protein adsorption on solid surfaces	90
4.2.1. Materials used in the adsorption experiments: polymers (HBP-OH, HBP-OH/OCOCH ₃ , HBP-OCOCH ₃), proteins (LSZ, HSA), buffer	91
4.2.2. <i>In situ</i> ellipsometry studies of protein layers adsorbed at solid/liquid interfaces: Comparison between experimental data for adsorption kinetics of LSZ and HSA on HBP-OH films	93
4.2.3. <i>In situ</i> Attenuated Total Reflection Fourier Transform Infrared (ATR-FTIR) Spectroscopy: a complementary analytical tool for protein adsorption studies	97
4.2.4. Axisymmetric Drop Shape Analysis by Profile applied <i>in situ</i> to study kinetics of protein adsorption at HBPs and PS surfaces	98

4.2.5. Adsorption kinetics of LSZ and HSA at solid/liquid interface of HBP-OH, HBP-OH/OCOCH ₃ , HBP-OCOCH ₃ and PS films	100
4.2.6. Adsorption isotherms and adsorbed layer structure	109
4.2.7. Summary, remarks to protein adsorption.	110
5. Summary and outlook of dissertation	112
List of symbols and abbreviations	116
References	118

Motivation

Both dendrimers and hyperbranched polymers (HBP) are three-dimensional highly branched macromolecules with numerous functional groups. Because of their unique physical and chemical properties such as low viscosity, high solubility determined by the branching and the high functionality of these macromolecules, dendrimers and HBPs are a promising class of materials for different chemical, physical and biomaterial applications [Fre02]. In contrast to dendrimers, HBPs do not have a perfect three-dimensional globular molecular structure and can be obtained by an easy one step polycondensation or polyaddition of an AB_n -type monomer [Voi00, Jik01, Mor03, Gao04, Voi05] that makes it an even more attractive and perspective material.

For the most of potential applications and bio-chemical / bio-physical processes of both fundamental and technological aspects, the bulk properties of a material such as structure and composition, the thermal behaviour, the molar mass and polydispersity are of critical importance if subsequent coatings will be prepared. Thus, surfaces of polymer films with predictable changing properties as well as the control of these properties are more suitable for different kinds of coatings. The development of new polymers that have all of the desired characteristics is costly and unprofitable. In this field, HBP have become more important due to their low cost and easy synthetic procedure. Many HBP such as hyperbranched poly(amide)s [Cos00], hyperbranched poly(amine ester)s [Lim01] and oligosaccharides with branched architecture [Kad98], have been tested in bio-aspects as potential bio-carriers and bio-sensors. In this connection, HBP films containing high density of functional groups can bind biomolecules with greater sensitivity than SAMs (self-assembled monolayers) or linear polymers. At the same time, HBP molecules can be designed to have a rather open structure, allowing the biomolecules penetrate the film more easily than in conventional polymer films [Gao04]. All these factors make HBPs attractive for different bio-applications.

Goals

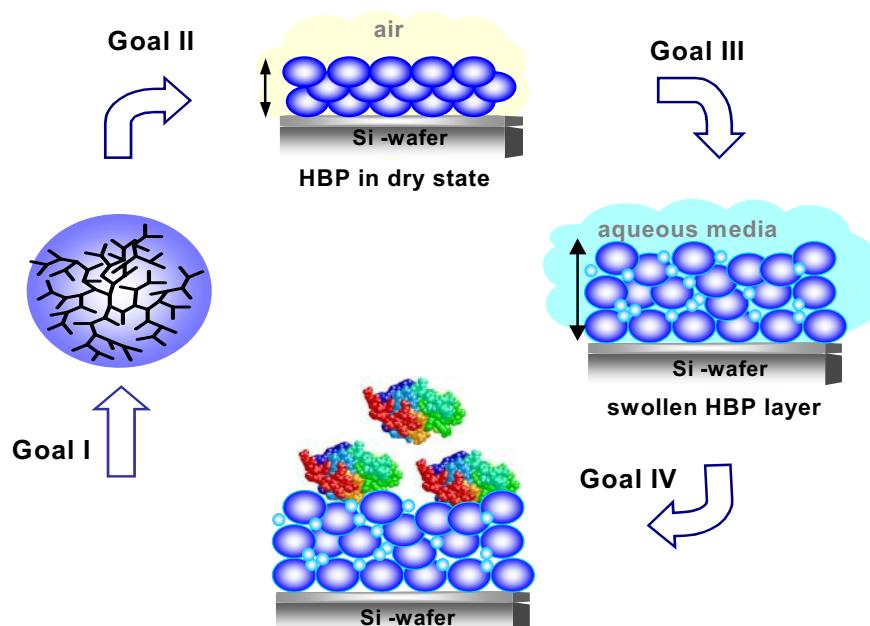
The chief goal of the present work is to investigate the adsorption of model proteins on hyperbranched aromatic polyester thin films from aqueous solution for practicable bio-applications. There were four main objectives in this doctoral research project:

Firstly, to determine the chemical and physical properties of hyperbranched aromatic polyesters having the same backbone structure and containing different functional groups in solution and in solid state (**Goal I**).

Secondly, to clarify the surface properties of the coatings in dependence on the type of functional groups and the influence of the self-organisation of HBPs due to hydrogen bonded network on these properties (**Goal II**).

Thirdly, to study the behaviour of HBP thin films in an electrolyte solution. These studies are expected to contribute to a better understanding of the interplay of functional groups on the film stability and swelling behaviour (**Goal III**).

Fourthly, to study the adsorption of proteins on HBP surfaces that can be considered to serve as model surfaces of biomaterials or/and biosensors (**Goal IV**).



Outline

The dissertation work focuses on the whole route of material development starting from the investigations of properties of the initial (raw) HBPs to their applications. Each research step is given in a separate chapter to enhance attention to various aspects of the aim of the work. Thus, every chapter is started with an introduction. After that, the methods applied and experimental procedure are described. Next part tries to give the comprehensive description of the results obtained. At the end of the chapter, the main points are summarized.

The **Chapter 1** gives the theoretical description of the main experimental techniques used in this work.

In **Chapter 2** the chemical (chemical composition, purity, typical structure elements) and physical (glass transition temperature, the temperature of the maximum decomposition, the thermal stability at the high temperatures, molar mass, polydispersity and possible aggregation in solution) properties examined by different techniques of polymer analysis are described.

The **Chapter 3** is divided into three separate parts:

In **Chapter 3.1** the description of the formation and modification of inter- and intramolecular hydrogen bonds of hydroxyl terminated HBP is presented to reveal the information of hydroxyl groups re- and/or association due to the high temperatures applied.

In **Chapter 3.2** the nature of the solid-liquid interface of HBP thin films have been studied by different surface sensitive techniques with respect to further protein adsorption investigations.

In **Chapter 3.3** the strategy for the fabrication of surface attached carboxyl terminated HBP using “grafting to” technique is developed.

The **Chapter 4** consists of two parts:

The first (theoretic) part outlines the basic principles of protein chemistry, factors influencing on the protein molecule stability in aqueous medium, the mechanism of protein adsorption and forces involved in the adsorption process. In the second part the combination of different *in situ* techniques was applied to obtain a comprehensive description of complex adsorption processes of protein molecules on different polymer surfaces.

Chapter 1. Theoretical background for the experimental techniques

Abstract

The aim of this chapter is to give a theoretical description of the main experimental techniques used in this work to characterise the hyperbranched aromatic polyester (HBP) thin films in dry state as well as the adsorption-relevant surface properties.

1.1. Ellipsometry

Principles of ellipsometry

Ellipsometry is a very sensitive, non-destructive, label-free optical method for the characterisation of thin films, surfaces, and material microstructures. Ellipsometry measures the change in the state of polarisation of light reflected from a surface. The state of polarisation of the polarised light beam is characterised by the phase and amplitude relations of two components into which the total electric field vector E of the light wave can be resolved (**Figure 1.1**). These two components p - and s - (parallel and perpendicular in the plane of incidence) are orthogonal to each other, and orthogonal to the direction of the beam propagation [Azz87, Sty99].

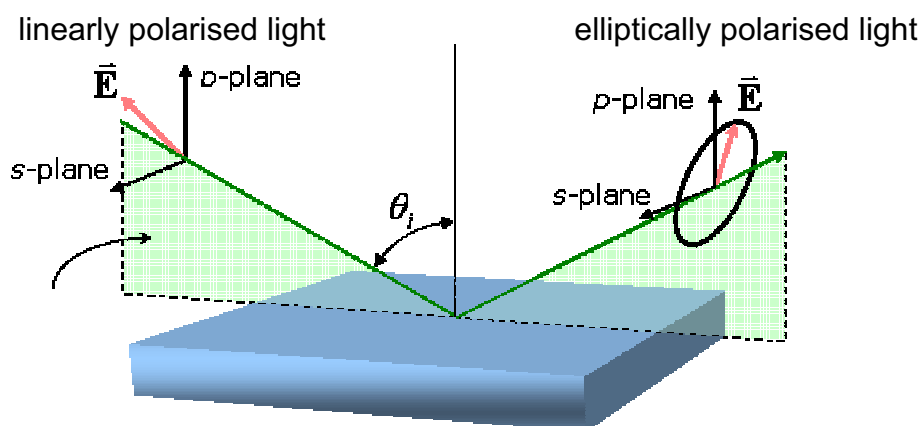


Fig. 1.1. Reflection of polarized light [Htt1].

Ellipsometry measures two ellipsometric angles Ψ and Δ in order to describe the changes in the state of polarisation. Prior to reflection, the polarisation of light is characterised by an amplitude ratio, E_p / E_s , and phase difference $(\delta_p - \delta_s)$, of the p - and s - components. Upon reflection, both the amplitude ratio and phase difference change. The angle Δ is the change in relative phase difference caused by the reflection [Azz87, Sty99]:

$$\Delta = (\delta_p^r - \delta_s^r) - (\delta_p^i - \delta_s^i) \quad (1.1)$$

where r and i represent the reflected and incident light.

The angle Ψ is defined by the ratio of the relative amplitude ratios before and after the reflection:

$$\tan \Psi = \frac{\overrightarrow{E}_p^r / \overrightarrow{E}_s^r}{\overrightarrow{E}_p^i / \overrightarrow{E}_s^i} \quad (1.2)$$

The ellipsometric angles can be related to the optical constants by using the **Fresnel reflection coefficients** which are dependent on the angle of incidence Φ_0 , wavelength λ , refractive index of an ambient medium n_0 , complex refractive index of a pure substrate N_s , complex refractive index of a layer N_j and thickness of a layer d_j ($j = 0, 1, 2, \dots$ number of layer). The ratio of the *Fresnel reflection coefficients*, R_p and R_s corresponding to the p - and s -planes, defines the ellipticity ρ (complex number).

This definition is the **fundamental equation of ellipsometry**:

$$\tan(\Psi) \cdot e^{i\Delta} = \frac{R_p}{R_s} = \rho(\Phi_0, \lambda, n_0, N_s, N_j, d_j) \quad (1.3)$$

The **complex refractive index** N is a presentation of the optical constants of a material and can be represented by following equation:

$$N = n + ik \quad (1.4)$$

where n is the refractive index (real part), i the complex number and k is the extinction coefficient (imaginary part).

The extinction coefficient is directly related to the absorption of a material and to the absorption coefficient α by:

$$\alpha = \frac{4\pi k}{\lambda} \quad (1.5)$$

where λ is the wavelength of light.

The optical constants can also be expressed as complex dielectric function ε by:

$$\varepsilon = \varepsilon_1 + i\varepsilon_2 \quad \text{and} \quad N = \varepsilon^{1/2} \quad (1.6)$$

Although the complex index of refraction is often seen as constant for a given material, one has to remember that both n and k vary with the wavelength of the light and the temperature of the medium.

Ellipsometer configurations

All ellipsometer arrangements start with a light source and end with a detector. The differences are in the arrangement of optical components between the source and detector that defines the type of ellipsometer being used (**Figure 1.2**) [Woo, Wooo, Woo99].

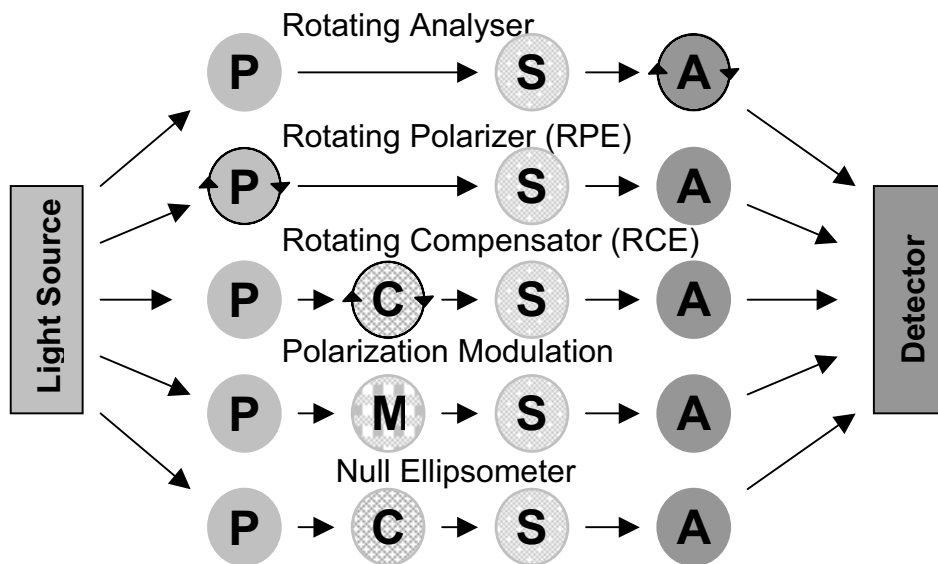


Fig. 1.2. Scheme of ellipsometer configurations: P - polarizer, C – compensator, S – sample, M – modulator, A – analyzer [Wooo].

Null-Ellipsometry configuration operates by adjusting the orientation of the polarizer, compensator, and analyzer so that the light incident on the detector is extinguished or "nulled". The main components of a common null ellipsometer are a light source (e.g. He-Ne laser), optical components that are used to manipulate the polarization of the light prior to and after reflection and a light detector. Generally, the measurements are done at a single wavelength and at one angle of incidence. Thus, only one pair Ψ and Δ is obtained from single measurement to describe a surface.

Nevertheless, the obtained experimental ellipsometric data Ψ and Δ can be detected very sensitive, i.e. submonolayer precision [Azz87, Arw93].

Rotating analyzer vs. rotating polarizer ellipsometers. There are some discussions regarding the place of the monochromator for setting the measurement wavelength in the rotating polarizer/analyzer system. The monochromator can be incorporated into either the detector or the source side. If it is incorporated in to the detector, than ambient light is easily rejected. On the other hand, if the monochromator is part of the source, the probe beam is monochromatic and there is no wavelength splitting element in the detector [Woo].

The **M-44**[®] (J. A. Woollam, USA) ellipsometer used in this work has a broad band light source and places the monochromator in the detector unit [Woo, Woo99]. The light source is a xenon lamp, which gives unpolarized light with a broad light spectrum. After the light passes the filter (option), which select a narrow light spectrum ($\lambda > 400$ nm), it goes through a prism polarizer. The diameter of the light beam hitting the sample is about 2 mm. After reflection at the sample the polarization of the light is measured. The rotating analyzer is identical with the polarizer but rotating with the frequency of $\omega=2\pi\nu$. When the analyzer rotates it tracks the polarization and the detector signal will be a sine curve with frequency 2ν . The detector is a photodiode-array.

Rotating compensator ellipsometer. The rotating compensator ellipsometer configuration compensates for most of the disadvantages of the rotating analyzer configuration. These advantages include: accurate measurements of the ellipsometric Ψ and Δ parameters over the complete measurement range, no residual input or output polarizations sensitivity, and the capability to directly measure depolarization effects. The ellipsometer **M-2000**[®] (J. A. Woollam, USA) used in this work also employs a CCD array detector making simultaneous acquisition of spectroscopic ellipsometric data. In addition, by switching the light source and/or diode array detector, it is possible to cover a variety of spectral ranges, from 371 nm to 1679 nm [Woo, Wooa].

1.2. Contact angle method

When a liquid drop is placed on a solid surface it will normally not only be in contact with the solid surface, but also with a gas (air). Contact angle measurements are widely used to characterise the particular solid/liquid interaction. Therefore, the contact angle serves as an indication of wettability of a solid by a liquid. Classically, the contact angle is described with in two ways: firstly, a force balance method and secondly, the energetic description. When in static equilibrium the line delimits the wetted and the dry part of the surface, the contact line has to remain fixed. In the horizontal direction this is fulfilled by a simple force balance illustrated in **Figure 1.3**. Therefore, drop of a liquid forming such angle may be considered as resting in equilibrium by balancing three forces which are correlated by Young's equation [Kwo99]:

$$\gamma_{lv} \cos \theta = \gamma_{sv} - \gamma_{sl} \quad (1.7)$$

where θ is the contact angle of a liquid droplet on a solid surface. γ_{lv} , γ_{sv} and γ_{sl} are the liquid/vapour, solid/vapour and solid/liquid interfacial tensions, respectively.

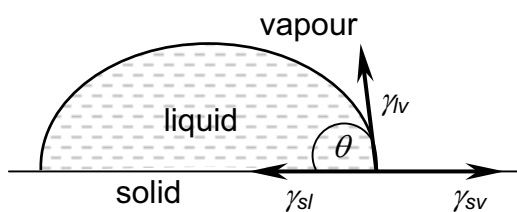


Fig. 1.3. Scheme of three-phase contact.

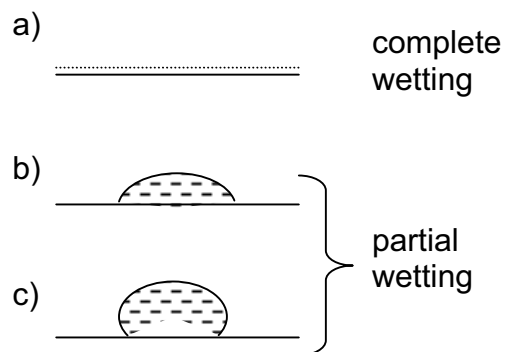


Fig. 1.4. Different wetting situations of a droplet in contact with a solid surface.

There are two distinct equilibrium regimes often described in the literature: complete and partial wetting [Gru01]. In the case of partial wetting (**Figure 1.4**), the contact angle is finite ($\theta > 0$) and liquid droplet deposited on a solid forms an equilibrium shape. The low values of θ indicate that the liquid spreads, or wets well, while high values indicate poor wetting. If the angle is less than 90° the liquid wets the solid (**Figure 1.4b**).

If the angle is more than 90°, the term “non-wetting” is used (**Figure 1.4c**). The contact angle value of zero represents complete wetting when liquid forms very thin film on a solid surface.

Equation of State approach

Several approaches have been developed to calculate the surface tension components from the contact angle measurements [Fow64, Owe69, Oss88, Goo92]. In this work, a combination of Young’s equation (Eq. 1.7) and the equation-of-state approach for the interfacial tensions proposed by *Neumann* [Kwo99] has been used to calculate the solid/vapour interfacial tension (γ_{sv}):

$$\gamma_{sl} = \gamma_{lv} + \gamma_{sv} - 2\sqrt{\gamma_{lv} \cdot \gamma_{sv}} \cdot e^{-\beta(\gamma_{lv} - \gamma_{sv})^2} \quad (1.8)$$

where γ_{lv} and γ_{sl} are the liquid/vapour and solid/liquid interfacial tensions. β is an empirical constant (0.0001247) [Kwo99]. Combining Eq. 1.7 and Eq. 1.8 one yields the following relation:

$$\cos \theta = -1 + 2\sqrt{\frac{\gamma_{sv}}{\gamma_{lv}}} e^{-\beta(\gamma_{lv} - \gamma_{sv})^2} \quad (1.9)$$

According to Eq. 1.9 the solid surface tension γ_{sv} can be calculated from the experimentally measured advancing contact angle θ and the known γ_{lv} of liquid, mostly water.

Contact Angle Hysteresis

The difference between the advancing θ_a and receding θ_r contact angle values is called the *contact angle hysteresis* H . A great deal of research has gone into analysis of the significance of hysteresis:

$$H = \theta_a - \theta_r \quad (1.10)$$

It should be noted that the advancing contact angle is more reproducible and less sensitive to surface roughness and heterogeneity than the receding one. Therefore, advancing angle data is commonly used to calculate surface and interfacial tension components (except rough surfaces) [Goo92, Kwo99]. Generally, contact angle hysteresis has been attributed to solid surface roughness, surface chemical heterogeneity, swelling, penetration of liquid into the solid surface, and surface reorientation of functional groups [Goo92, Yas94, Mar94, Mar98a, Haz93, Hen04].

Axisymmetric Drop Shape Analysis by Profile

Axisymmetric Drop Shape Analysis by Profile (ADSA-P) is a method often used to assess time-dependent changes in the contact angle and liquid/vapour interfacial tensions from a sessile or pendant drop. The strategy employed is to fit the shape of an experimental drop to a theoretical drop profile according to the *Laplace* equation of capillarity, which represents a relationship between the curvature of a liquid meniscus and the surface tension γ [Kwo99]:

$$\Delta P = \gamma \left(\frac{1}{R_1} + \frac{1}{R_2} \right) = \Delta P_0 + \Delta \rho g h \quad (1.11)$$

where ΔP is the pressure difference across the curved interface, R_1 and R_2 are the principal radii of curvature of a drop and γ is the liquid surface tension. ΔP_0 is the pressure difference in a reference plane, $\Delta \rho$ is the density difference, g is the acceleration due to gravity, and h is the vertical height of the drop measured from the reference plane.

ADSA-P is based on the minimisation of an error function expressing the difference between a measured experimental droplet contour and the theoretical curve. The software also provides the drop volume, surface area and the radius of curvature at the apex. The program requires several randomly chosen coordinate points along the drop profile, the value of the density difference across the interface, and the magnitude of the local gravitational constant as input. Each single image of a drop is

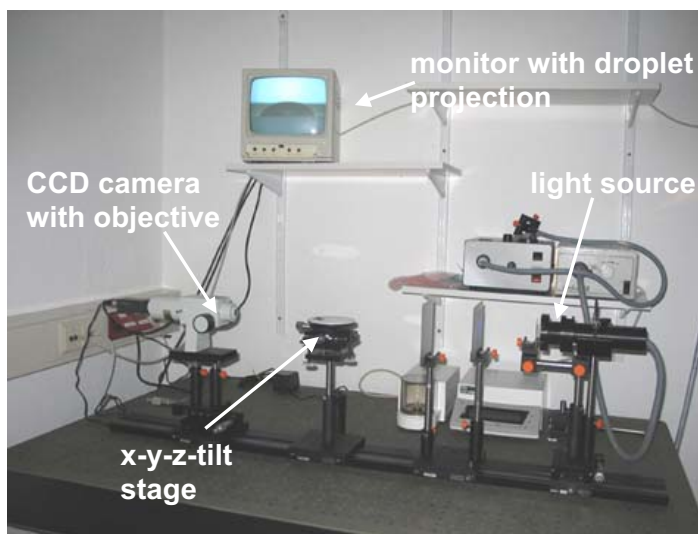


Fig. 1.5. Experimental ADSA-P set-up.

analysed ten times with twenty different, arbitrary profile coordinate points each time [Gru96,Gru96a,Gru99]. **Figure 1.5** shows the experimental ADSA-P set-up used in this work which consists of CCD camera with objective, light source, x-y-z-tilt manipulation stage, monitor and computer system with a frame grabber and ADSA-P software.

1.3. Electrokinetic method

The development of a net charge at the surface due to ions adsorption from the solution and/or dissociation of surface groups affects the distribution of ions in the surrounding interfacial region, resulting in an increased concentration of ions closed to the surface. Thus an *electrical double layer* arises at the solid-liquid interface (**Figure 1.6**). Generally, description of the charge distribution at the surface is based on the model developed by *Gouy* and *Chapman* and completed by *Stern* and *Grahame* [Hun86, Ste24, Bel02a]. The liquid layer surrounding a solid exists as two parts. The first one is an inner region (*Stern layer*) where the ions are strongly bound. The outer or diffuse region is less strongly attached. Within the diffuse layer there is a boundary inside which the ions and solid form a stable entity. This boundary situated between *Stern* and diffuse layers is called the plane of hydrodynamic shear or slipping plane. The potential that exists at this boundary is known as the **Zeta potential**.

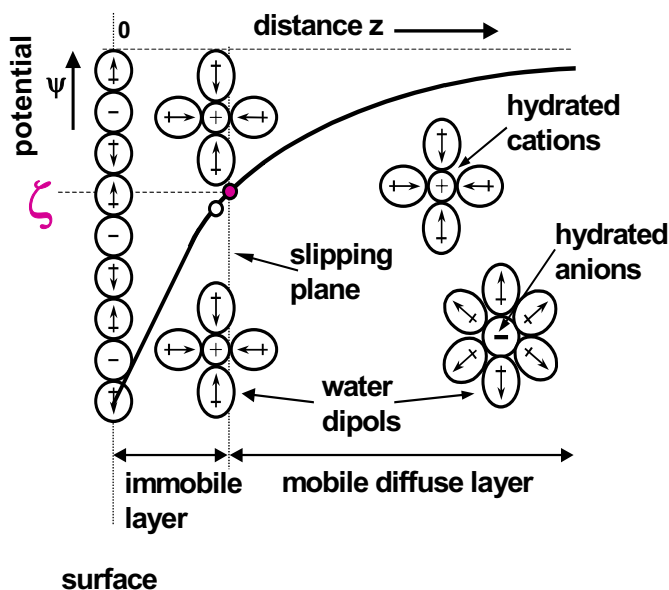


Fig. 1.6. Schematic representation of the electrochemical double layer at the interface [Jac96].

The zeta potential depends on the surface charge density and the double layer thickness. The surface charge density, in turn, depends on the concentration of “potential-determining ions” in the aqueous media that have a particular affinity for the surface. Generally, the zeta potential is positive for low pH values and negative for higher pH values. The point where the plot passes through zero zeta potential is called the **Isoelectric point** which is very important for a surface analysis. A typical plot of zeta potential versus pH is shown below (**Figure 1.7**).

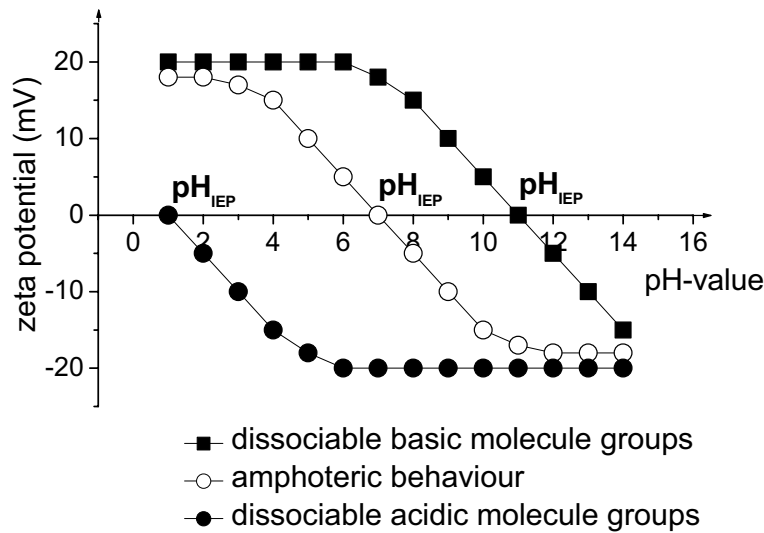


Fig.1.7. Schematic representation of zeta potential vs. pH plots of solids [Bel02a].

Several techniques can be used to determine the zeta potential of surfaces. Among these techniques, the streaming potential technique is the most suitable for different kind of solids (fibres, wafers, etc.). There are four distinct effects depending on the way in which the motion is induced. These are:

Electrophoresis: The movement of charged particles relative to the liquid under the influence of an applied electric field.

Electroosmosis: The movement of a liquid relative to a stationary charged surface under the influence of an electric field.

Sedimentation potential : The electric field generated when charged particles move relative to a stationary liquid under influenced gravity.

Streaming potential is the potential induced when an electrolyte solution flows across a stationary, charged surface. Streaming potential quantifies an electrokinetic effect which reflects the properties of the surface, the flow characteristics, and the chemistry and thermodynamics of the electrolyte solution in the experiment. Streaming potential is generated when an electrolyte solution is forced (by means of hydraulic pressure) to flow through a channel formed by two plates. The liquid carries a net charge. Its flow, caused by hydraulic pressure, generates a potential separation and with it a streaming current [Sha69, Hun81, Bel04].

Zeta potential can be derived from the experimentally measured streaming potential. The relationship between the measurable streaming potential and the electrokinetic potential of a cell is given by well-known *Helmholtz-Smoluchowski* equation:

$$\zeta = \frac{\Delta U_s}{\Delta p} \cdot \frac{\eta \kappa}{\varepsilon \varepsilon_0} \quad (1.12)$$

where U_s is the streaming potential, p is the hydrodynamic pressure difference across the channel, η is the viscosity of the solution and ε is the permittivity of the solution, ε_0 is the permittivity of free space, κ is the conductivity of a solution.

1.4. Infrared Spectroscopy

Infrared (IR) spectroscopy is one type of *vibrational spectroscopy* and used as the most common analytical technique in organic and inorganic chemistry. The covered range of wavelength of the IR spectroscopy is the wavenumber range from 10 000 (near-IR) to about 10 cm^{-1} (far-IR). In practice, the wavenumber range which are commonly used is corresponded to 4000 to 400 cm^{-1} (mid-IR). The principal of IR spectroscopy is that small molecules and macromolecules in different environments can absorb varying light intensities and at varying frequencies. Thus IR spectroscopy involves collecting absorption information and analysing it in a form of spectrum.

The characteristic frequencies for a particular molecule or segments are determined by its vibrations, dependent upon the masses of the atoms of the molecule, their spatial geometry, and the strengths of the connecting bonds. Usually, the IR spectrum is divided on two main regions. The absorption bands of the region lies above 1500 cm^{-1} can be assigned to the individual functional groups, whereas the region below 1500 cm^{-1} contains much more bands and characteristics of the molecule as a whole [Hes97]. The *Fourier transform (FTIR) technique* was the development of IR spectroscopy using the possibility of a simultaneous and almost instantaneous recording of the whole spectrum in the different regions.

The application of IR spectroscopy to investigate the structural elements of biological systems is limited by the presence of water. In biological molecules the interesting resonance frequencies of the C=N, C=O, N-H or O-H vibrations are often hidden by the strong IR absorption of the solvent water at around 3400 and 1600 cm^{-1} .

Experiments in aqueous systems are therefore possible only with very thin water layers and with high concentrations of the molecules of interest.

Therefore, a significant improvement of the sensitivity of IR spectroscopy might be achieved using the *Attenuated Total Internal Reflection Fourier Transform (ATR-FTIR) spectroscopy*. The concept of the internal reflection spectroscopy originates from the fact that a beam of radiation enters from a more optical dense (ATR crystal with higher refractive index) into a less optical dense medium (sample with lower refractive index). The fraction of the incident beam reflected increases when the angle of incidence increases. All incident radiation is completely reflected at the interface when an angle of incidence is greater than the critical angle of total reflection (a function of refractive index). But, the beam or so-called *evanescent wave* penetrates a very short distance beyond the interface and into the less-dense medium. This penetration is typically at a depth of a few micrometers. As a result, the reflected light intensity is reduced by the sample in regions of the IR spectrum where the sample absorbs. **Figure 1.8** illustrates the basic ATR principles.

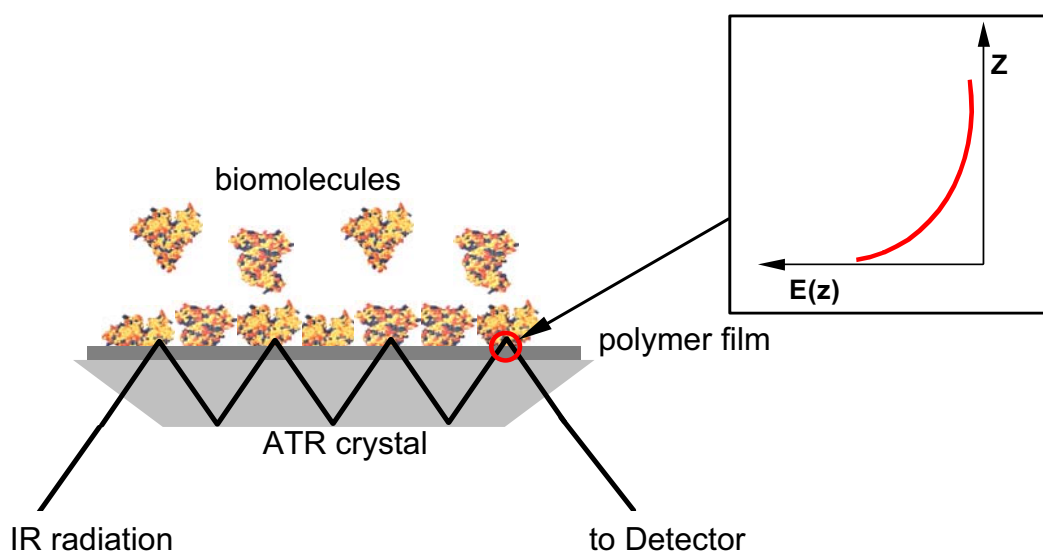


Fig. 1.8. Principle of attenuated total internal reflection (ATR) spectroscopy in the system “ATR crystal(reflection element)/polymer film/adsorbed biomolecule layer”.

1.5. Atomic Force Microscopy

The *atomic force microscope (AFM)* is one kind of a scanning probe microscope (SPM). SPMs are designed to measure local properties, such as height, friction, magnetism with a probe. To acquire an image, the SPM scans the probe over a small area of the sample, measuring the local property simultaneously.

AFMs operate by measuring force between a probe and the sample. Normally, the probe is a sharp tip, which is a tall pyramid with 15-40 nm end radius. Though the lateral resolution of AFM is low (~ 30 nm) due to the convolution, the vertical resolution can be up to 0.1 nm. To acquire the image resolution, AFMs can generally measure the vertical and lateral deflections of the cantilever. The optical lever operates by reflecting a laser beam off the cantilever. The reflected laser beam strikes a position-sensitive photo-detector consisting of four-segment photo-detector. The differences between the segments of photo-detector of signals indicate the position of the laser spot on the detector and thus the angular deflections of the cantilever (**Figure 1.9**). In *contact mode*, AFMs use feedback to regulate the force on the sample. The AFM not only measures the force on the sample but also regulates it, allowing acquisition of images at very low forces. The feedback loop consists of the tube scanner that controls the height of the tip; the cantilever and optical lever,

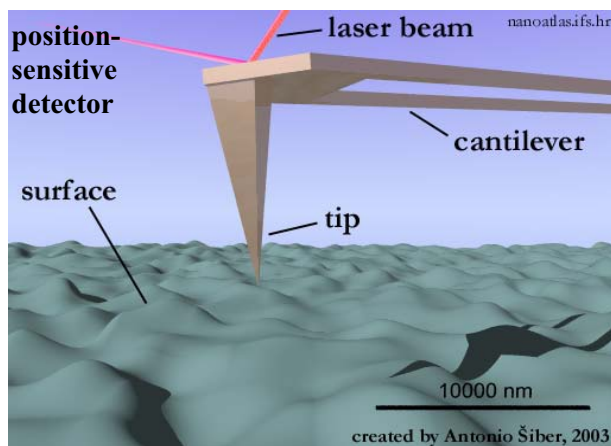


Fig. 1.9. Scheme of AFM [Htt3].

which measures the local height of the sample; and a feedback circuit that attempts to keep the cantilever deflection constant by adjusting the voltage applied to the scanner. A well-constructed feedback loop is essential to microscope performance. *Tapping mode* works by vibrating a tip which is at the end of a cantilever and bringing the tip into intermittent contact with a sample surface. When the tip interacts with a surface feature, its amplitude is decreased from its previous amplitude of oscillation. The AFM senses this decrease, and the tip is raised away from the sample in order to re-attain the previous amplitude of oscillation. In this way, the tip can be rastered across the sample to generate topographical images [Mir04, Htt2]. However, the resolution of tapping mode AFM is arguable though it is certainly less than contact mode.

Chapter 2. Characterisation of hyperbranched aromatic polyesters

Abstract

This Chapter focused on the determination of the chemical and physical properties of hyperbranched aromatic polyesters (HPB) having the same backbone structure and containing different functional groups. Nuclear Magnetic Resonance (NMR) was used to determine the chemical composition and purity of the HBPs in solution. Additionally, Fourier Transform Infrared (FTIR) spectroscopy was applied to reveal the typical structure elements of the HBPs in solid state (films). The glass transition (T_g) temperature, the temperature of the maximum decomposition T_{DTG} and the thermal stability of HBPs at the temperature above their T_g were characterised by Differential Scanning Calorimetry (DSC) and Thermo-Gravimetric Analysis (TGA). The determination of molar mass and polydispersity of the HBPs was done by Size Exclusion Chromatography (SEC). The results obtained with SEC using linear poly(2-vinyl pyridine) as a standard show too low molar masses due to the very compact structure of HBPs in a dissolved state. Therefore, the SEC coupled with the refractive index (RI) and the light scattering detector (MALLS) was applied to achieve absolute molar masses along the separation process and taking into account the actual compactness of dissolved HBP molecules. Moreover, the second method is able to give the information regarding the aggregation of HBP molecules in solution due to hydrogen bonding which is very important for the formation of smooth and homogeneous thin HBP films produced by the spin coating of the HBP solution.

2.1. Hyperbranched polymers (HBP): a promising class of materials

Dendritic polymers, including dendrimers and hyperbranched polymers, represent an important class of polymeric materials which attracted an increasing interest during recent years. Contrary to linear polymers, HBPs contain a large number of branching points and functional end groups, which result in their unique physical and chemical properties such as low intrinsic viscosity, high solubility, less flexibility, different

relationship between hydrodynamic volume and molar mass, and different origin of the glass transition temperatures. A large number of reviews concerning the synthesis, modification, and application of HBPs has been published during last years [Voi00, Jik01, Mor03, Gao04, Voi05].

Hyperbranched polymers (HBPs) do not have a perfect three-dimensional globular molecular structure. They exhibit a random branched structure including linear, dendritic and terminal units (**Figure 2.1**). In 1952, *Flory* described a concept of polycondensation of AB_x monomers which allows to obtain the hyperbranched architecture of the macromolecules [Flo52]. He gave in detail the theory behind the polycondensation of monomers with excess **B** functional groups and one **A** functional group arranged on a molecule. He showed that branched polymeric products begin to appear after the polymerisation had progressed to a definite extent. In 1982, *Kricheldorf* reported the copolymerisation of **AB** and AB_2 monomers to form highly branched polyesters [Kri82]. The name “Hyperbranched polymer” was applied for the first time by *Kim* and *Webster* and published in 1988 [Kim88]. Their report described the homopolymerisation of AB_x type monomers to form hyperbranched polyphenylenes as irregular analogue to dendrimers of high functionality [Kim90].

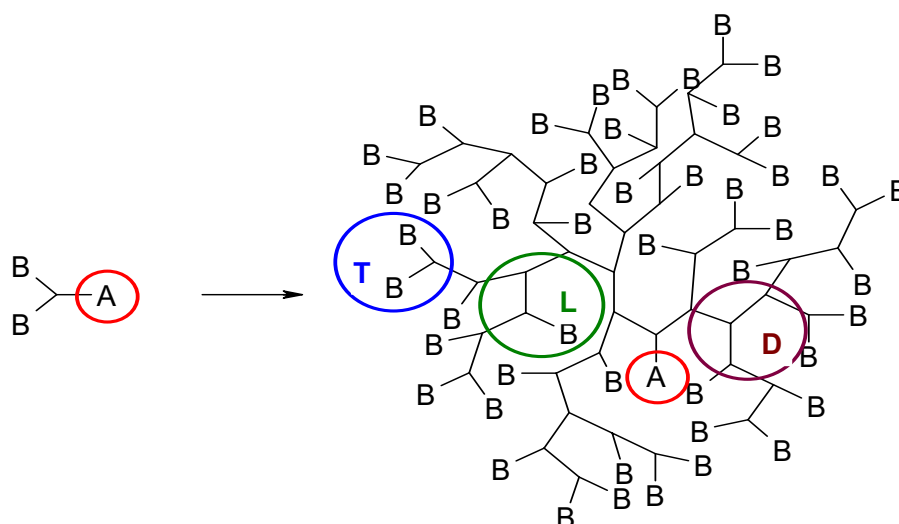


Fig. 2.1. Schematic representation of branched polymer architecture by AB_2 type monomers exhibiting linear (L), dendritic (D), terminal (T) units and one unreacted focal unit (A) based on the classic branched polycondensation approach by Flory [Flo52, Voi00].

The branching perfection of **AB₂** systems is characterised by the average degree of branching (*DB*), which was defined by *Frechet* [Haw91] as

$$DB = \frac{D + T}{D + T + L} \quad (2.1)$$

where *D*, *T* and *L* are the number of dendritic, terminal and linear units, respectively, (*DB* = 1 for a perfect dendrimers and *DB* < 1 for HBPs). *Frey at al.* [Höl97] have proposed another definition, where the number of actually existing growth directions is compared to the maximum possible number of growth directions in **AB₂** systems:

$$DB = \frac{2D}{2D + L} \quad (2.2)$$

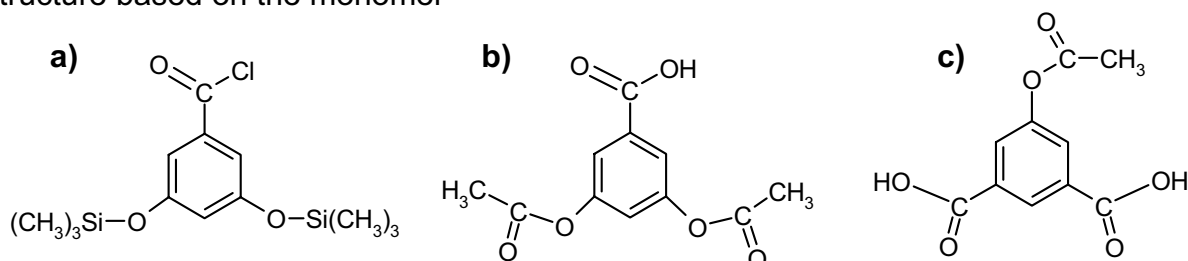
According to the later definition, the *DB* value range was assumed between 0 for the linear polymer and 1 for the dendrimers. The *DB* of HBPs formed by a random polymerisation of **AB₂** monomers or by co-condensation of a core molecules **B_f** (*f* is the core functionality) with **AB₂** monomers may not exceed a value of 0.5 [Zag02]. There are many different factors influencing the *DB* of HBPs, e.g. activation of the second **B** group of **AB₂** monomers after the reaction of the first **B** group, the synthetic procedure where **AB_x** monomers are slowly added to the core molecules **B_f** in solution and other [Zag02].

The most studies of the HBPs are focused on their synthesis. However, since the physical properties of HBPs under application crucially depend on the purity, the average molar mass, polydispersity, and thermal stability, the aim of the work described in this **Chapter** was to determine these parameters for the hyperbranched aromatic polyesters with the same backbone structure and different terminal groups. The chemical composition (in dissolved state) and typical structure elements (in solid state) of HBPs were checked by Nuclear Magnetic Resonance (NMR) and Fourier Transform Infrared (FTIR) spectroscopy. The Size Exclusion Chromatography (SEC) was used to characterise the molar mass and polydispersity of the polymers. Additionally, the SEC coupled with refractive index (RI) and a light scattering detection (MALLS) was applied to achieve absolute molar masses along the separation process. The glass transition temperature (*T_g*) and thermal stability of HBPs at the temperature above *T_g* were characterised by Differential Scanning Calorimetry (DSC) and Thermo Gravimetric Analysis (TGA).

2.2. Characterisation of hyperbranched aromatic polyesters with different functional groups: Materials and Methods

2.2.1. Polymers

Hyperbranched aromatic polyesters (HBP) (Figure 2.2) with the same backbone structure based on the monomer



3,5-bis(trimethylsilyloxy)benzoyl chloride (a), 3,5-diacetoxy benzoic acid (b) and 5-acetoxypthalic acid (c) were synthesized by Schmaljohann and Pospiech using melt polycondensation [Sch98, Sch03, Voi93].

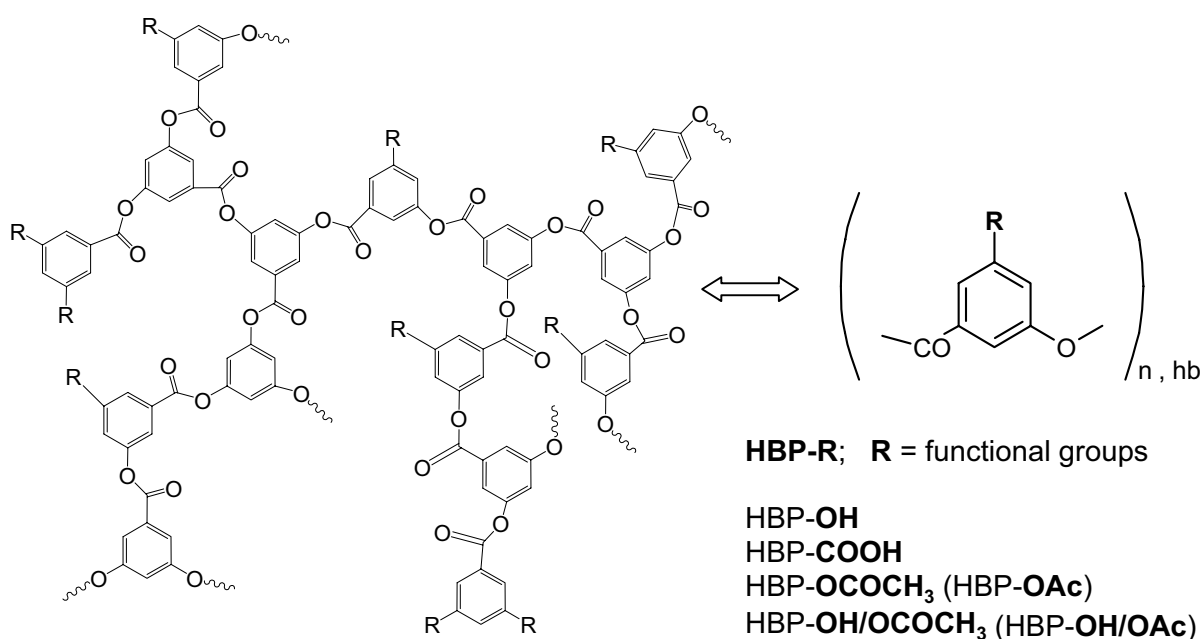


Fig. 2.2. Schematic representation of the hyperbranched aromatic polyesters, based on the classic branched polycondensation approach according to Flory [Voi05, Flo52].

2.2.2. Nuclear Magnetic Resonance (NMR)

The ¹H-NMR spectra were obtained on a Bruker DRX 500 (Germany) spectrometer operating at 500.13 MHz. The spectra were measured from the HBP solution in [²H₆]dimethyl sulfoxide (DMSO-*d*₆, δ(¹H) = 2.50 ppm, δ(¹³C) = 39.70 ppm, Merck, Germany) using 5 mm diameter tubes.

2.2.3. Fourier Transform Infrared (FTIR) spectroscopy

The FTIR spectroscopy was performed for the transmission measurements using a Bruker spectrometer IFS 66v/S (Germany). All spectra were recorded in the spectral range of 4000 - 600 cm^{-1} with a resolution of 2 cm^{-1} and an accumulation of 16 scans. The spectra were recorded in the steady state under vacuum of 3 mbar. All HBP samples were prepared as a thick film on KBr substrate by solvent casting from tetrahydrofuran solution (THF, Merck, Germany). After that the samples were carefully placed in an oven and dried at 40 °C under vacuum to remove the residual solvent.

2.2.4. Liquid Chromatography

The Size Exclusion Chromatography (SEC) measurements were performed on different types of chromatographic system.

System I: The chromatographic system was Agilent HP Series 1100 with the refractive index (RI) detector (Agilent Technologies, Germany). The molar mass was calculated using a calibration relationship determined with the linear polymer standard poly(2-vinyl pyridine) (PVP, Polymer Standard Service, Germany). The eluent was a mixture of N,N-dimethylacetamide (DMAc, Merck, Germany), 2 vol.% water and 3 g/l LiCl (Fluka, Germany). The column set was ZORBAX PSM 60 Trimodale-S, 250mm x 6.2 mm (Agilent Technologies, Germany). The sample was passed through the column at a flow rate of 0.5 ml/min.

System II: Modular builded SEC-system (KNAUER, Germany) with UV- and refractive index (RI) detector, and multi angle laser light scattering detector (MALLS) (DAWN-EOS, Wyatt Technologies, USA) was used to determine the molar mass and any formed associations arising in the system. The refractive index increment dn/dc was determined from RI-response for each HBP assuming a complete mass recovery of a sample from the column and was used for the calculation of M_w from SEC-MALLS. The eluent was THF. The measurements were carried out at a flow rate of 1.0 ml/min on a 2-PL-Mixed B-LS column, 300 mm x 7.5 mm (Polymer Labs., UK).

2.2.5. Differential Scanning Calorimetry (DSC)

The measurements were performed under nitrogen using a DSC 7 (Perkin Elmer, USA) and DSC Q 1000 (TA Instruments, USA) to determine the glass transition temperature (T_g) of the polymers used. The samples were subjected to a heating-cooling-heating cycle between 10 and 200°C for HBP-OAc and HBP-OH/OAc, 10 and 280 °C for HBP-COOH, -50 and 260°C for HBP-OH with a heating and cooling rate of 20 K/min. On the basis of the DSC results, Thermo Gravimetric Analysis (TGA Q 500, TA Instruments, USA) was applied to prove the thermal stability of the HBPs at high temperatures which were used for the annealing procedure (see Chapter 3). The samples were heated under nitrogen up to 180°C (HBP-OAc, HBP-OH/OAc) and up to 240°C (HBP-OH, HBP-COOH) with heating rate of 20 K/min.

2.3. Molecular structure analysis of HBPs in the liquid and solid state

The $^1\text{H-NMR}$ spectra of hydroxyl terminated hyperbranched aromatic polyester (HBP-OH) used in this study are shown in **Figure 2.3**.

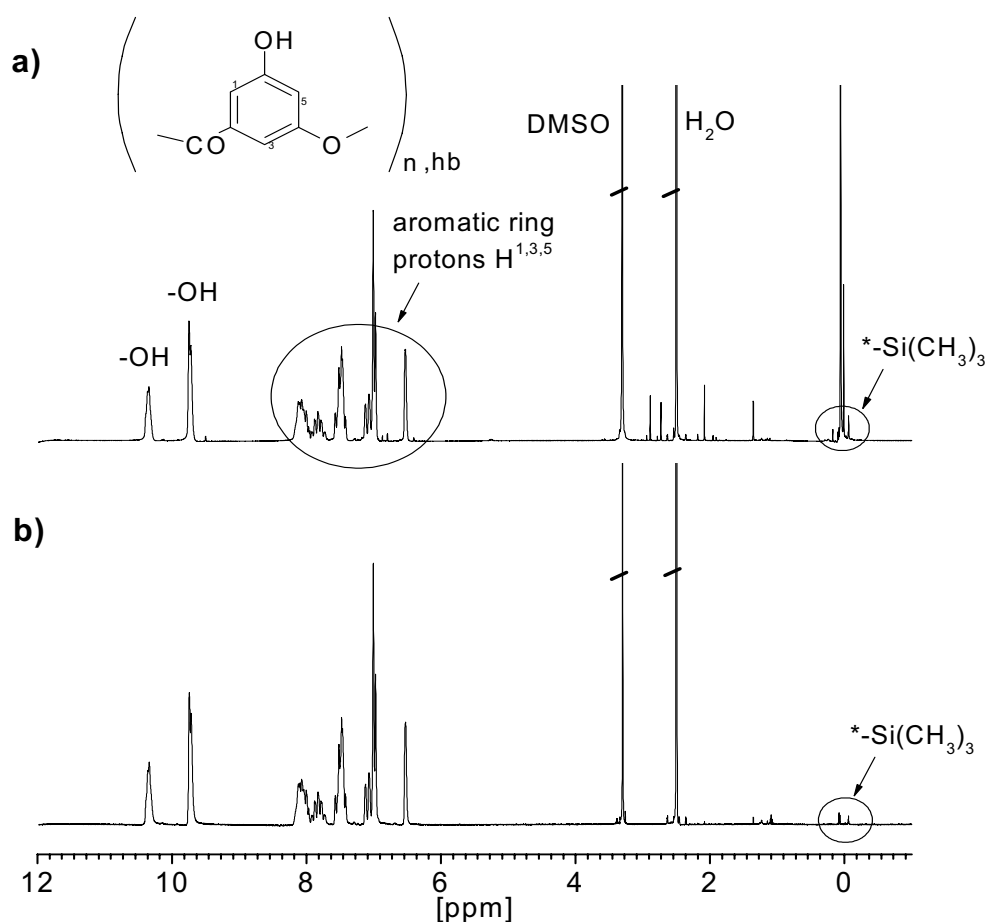


Fig. 2.3. $^1\text{H-NMR}$ spectra of HBP-OH before (a) and after purification (b) measured in DMSO-d_6 .

From the spectrum (**Figure 2.3a**) the contamination of the received bulk polymer with trimethylsiloxy (TMS) groups resulting from the synthesis using 3,5-bis(trimethylsiloxy) benzoyl chloride was calculated to be 14.8 mol-%. Since these groups can affect the surface properties of films prepared from this polymer, it was dissolved in THF containing 2.5 N hydrochloric acid and kept under nitrogen overnight in order to hydrolyse the TMS groups. A decrease of the TMS amount to 0.3 mol-% was determined. The $^1\text{H-NMR}$ spectrum of the purified HBP-OH bulk polymer is shown in **Figure 2.3b**. Proton signals of the aromatic region were found between 7 and 9 ppm confirming the expected chemical composition and branched structure of the compound. The degree of branching of 0.6 was calculated from the $^{13}\text{C-NMR}$ spectrum [Sch03].

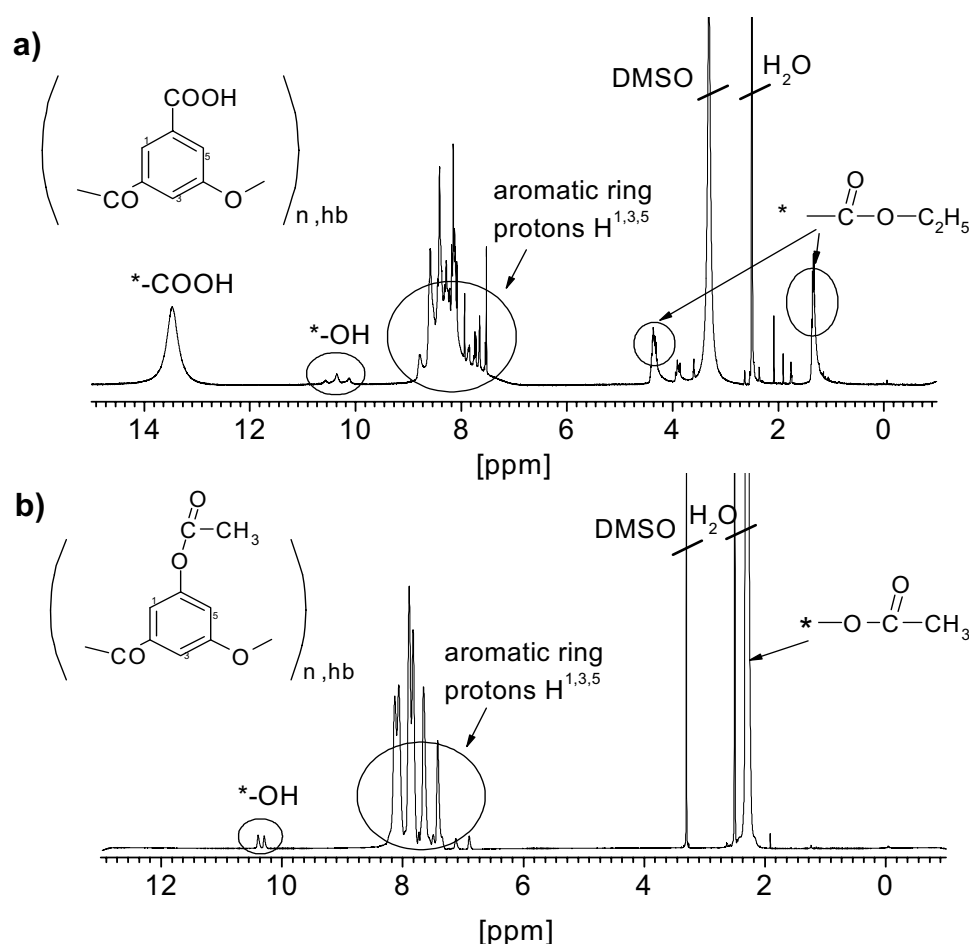


Fig. 2.4. $^1\text{H-NMR}$ spectra of HBP-COOH (a) and HBP-OAc (b) measured in DMSO-d_6 .

The $^1\text{H-NMR}$ spectrum (**Figure 2.4a**) of purified carboxyl terminated hyperbranched aromatic polyester (HBP-COOH) shows the typical signals of the hyperbranched core between 7 and 9 ppm. The intensive signal at 13.5 ppm is attributed to the carboxyl

end groups. The content of the ethyl ester groups coming from the precipitation of THF solution in diethyl ether was calculated from two proton signals at 1.3 (-CH₃) and 4.4 (-CH₂-) ppm as 12.8 mol-%. The peaks in the range from 10 to 11 ppm correspond to hydroxyl groups of non reacted monomer and the focal unit (7.7mol-%).

After synthesis the acetate terminated hyperbranched aromatic polyester (HBP-OAc) was purified two times by the precipitation from THF solution in water. Then the sample was dried in an oven at 60 °C under vacuum for 24 hours to remove the residual water. The chemical structure of purified HBP-OAc was controlled by ¹H-NMR (**Figure 2.4b**). As just mentioned above, the peaks between 7 and 9 ppm correspond to the branched structure of HBP. The intensive peak of the acetate end groups was detected at 2.2 ppm. The small amount of hydroxyl groups (10.2 - 10.5 ppm) due to non full conversion or hydrolysis was calculated to be about 5.0 mol-%.

For the preparation of the hydroxyl/acetate terminated hyperbranched aromatic polyester (HBP-OH/OAc), the HBP-OAc was hydrolysed at room temperature in humid air to obtain the hydroxyl terminal groups. Then the HBP-OH/OAc was purified and dried at 60 °C under vacuum for 24 hours. The amount of the hydroxyl groups after hydrolysis calculated from ¹H-NMR spectrum was found to be 22.5 mol-%.

In addition to the NMR measurements on dissolved HBPs, the typical structure elements of the HBPs in solid state were proved by FTIR spectroscopy. The IR transmission spectra of HBP films on KBr substrates are shown in **Figure 2.5**. As expected, the spectra are similar to the spectra of thin HBP films on silicon wafers measured by *Beyerlein* [Bey02]. Characteristic bands of the 1,3,5-trisubstituted aromatic ring were detected between 1050-1000 cm⁻¹ (δ CH in-plane) and 920-810 cm⁻¹ (δ CH out-off-plane) for all used polymers. Other typical aromatic bands can be observed at 3100 cm⁻¹ (ν C-H arom.), 1599 and 1449 cm⁻¹ (ν C=C arom.), 1084 cm⁻¹ (δ C-H arom.).

The hydroxyl groups of HBP-OH were identified by their complex band around 3415 cm⁻¹ (ν OH) indicating the existence of different types of hydrogen bonds. Additionally, the phenolic OH associated groups and the ester groups gave widely structured bands at 1323 cm⁻¹ and 1290 cm⁻¹ (ν C-O with δ OH), 1190 cm⁻¹ (δ C-O with δ OH), 1135 cm⁻¹ (δ C-O in C-OH). The ester carbonyl stretching vibrations (ν C=O) at about 1745 cm⁻¹ influenced by hydrogen bonds which are responsible for the low frequency shoulder of the band.

The wide band of hydroxyl vibration region (νOH) corresponding to the associated carboxyl groups of the HBP-COOH was detected between 2600 and 3500 cm^{-1} . The bands at 1436, 1205 cm^{-1} ($\delta\text{C-O}$) and 1415 cm^{-1} (δOH) were attributed to the complex vibration of carboxyl and ester groups of the HBP-COOH. The broad band of the carbonyl region is formed by the ester carbonyl ($\nu\text{C=O}$, 1744 cm^{-1}) and the complex band of hydrogen bonded carboxyl groups ($\nu\text{C=O}$ in $-\text{COOH}$, 1704 cm^{-1}) [Bey01].

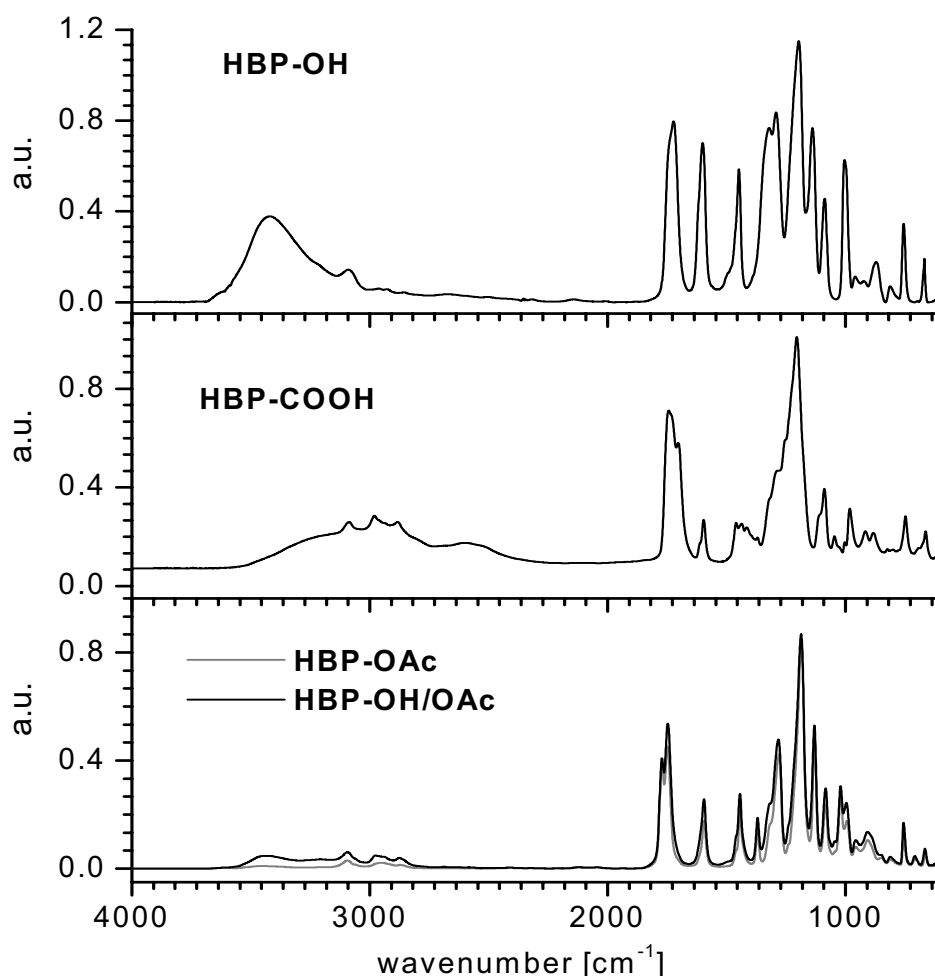


Fig. 2.5. IR spectra of HBP films casted from THF solution on KBr substrate and annealed at 40 °C for 30 minutes.

The weak broad absorption centred near 3432 cm^{-1} comes from the phenolic OH groups (νOH) of the HBP-OH/OAc. Two bands of the carbonyl region come from the stretching vibrations of the backbone (1747 cm^{-1}) and terminal (1772 cm^{-1}) ester groups. The observed peaks at 1280 and 1130 cm^{-1} correspond to the vibrations of ester groups in aromatic acid ($\delta -\text{COOC}_{-\text{as}}$).

Additionally, the most important vibration modes of HBP-OAc and HBP-OH/OAc can be assigned from the spectra: 1443 cm^{-1} (δCH_3 as in $\text{CH}_3\text{-C=O}$), 1369 cm^{-1} ($\delta\text{-OCOCH}_3$), 1325 cm^{-1} ($\delta\text{C-OH}$) and 996 cm^{-1} ($\delta\text{CH}_3\text{COO-}$ acetate).

2.4. Comparison of molar masses of HBPs determined by different type of chromatographic systems

The physical properties of polymeric materials depend not only on molecular composition and architecture but also on molar mass average and molar mass distribution. Moreover, the molar mass average and molar mass distribution of hyperbranched polymers obtained by polycondensation also depend on the conversion and monomer functionality. Generally, for AB_2 monomers at high conversion the molar mass distribution of the product is extremely broad and the polydispersity index ($\text{PDI}=\text{M}_w/\text{M}_n$) is predicted to approach infinity. Significant deviations from the expected molar mass growth are caused by side reactions, e.g. intramolecular interaction of A and B groups and intra- or intermolecular interactions between B groups [Zag02, Zag04]. There are several methods for the determination of polymer molar masses and their polydispersity.

The Size Exclusion Chromatography (SEC) is a relative method using the calibration with defined linear polymer standards and it was applied to characterise the molar mass and polydispersity of the polymers used.

SEC with calibration mode was used at first to characterise the molar mass and polydispersity of hyperbranched aromatic polyesters with different end groups. The molar mass determination by SEC is based on the fact that polymer coils migrate into the pores of the stationary phase (**Figure 2.6**). Smaller coils with lower hydrodynamic volume will penetrate deeper into the pores than larger coils and this elute later (entropic interactions). Therefore, polymers with a larger size than the pore sizes are excluded from penetration and elute at the beginning of the separation process [Htt4]. However, exist several problems to determine the “real” molar mass of the hyperbranched systems. The first problem is the broad molar mass distribution of HBPs. The second one is the high molecular density of branched polymer molecules compared to linear polymers of the same molar mass. Therefore, the calculated values of the molar mass of HBPs using a linear polymer standard (e.g. polystyrene, PS) are usually much more smaller than the “real” ones. The third problem is the

large number of polar groups, which often leads to aggregation of the HBP molecules increasing their calculated molecular weight or to stronger interactions of the polymer with the material of a column leading to non-SEC separation mechanism (enthalpic interactions).

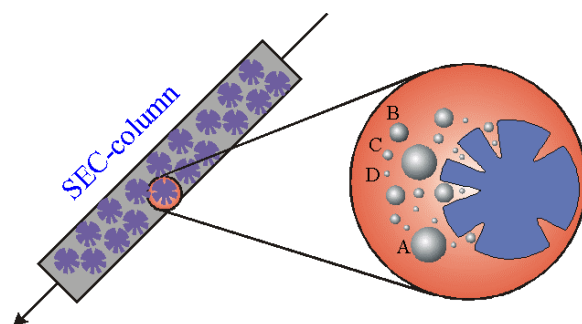


Fig. 2.6. Separation principle of size exclusion chromatography (SEC) [Htt4].

For our measurements PVP as a linear polymer standard was used to evaluate the molar mass (System I). However, due to factors mentioned above the obtained values carry a relative character and permit only a qualitative comparison between HBPs with a similar chemical composition and degree of branching. However, this comparison should be carried out very carefully due to different chemistry and/or polarity of the end groups of HBPs used. **Table 2.1** shows the evaluated relative values of molar masses and polydispersities of each polymer determined using a linear standard (PVP) calibration.

Table 2.1. System I: The molar masses and polydispersities of HBPs obtained by SEC with RI detector and PVP-calibration, solvent: DMAc–H₂O–LiCl.

N	polymer	M _n [g/mol]	M _w [g/mol]	PDI = M _w /M _n
1	HBP-OH	12 600	45 500	3.61
2	HBP-OH/OAc-1*	9 600	42 100	4.38
3	HBP-OH/OAc-2*	8 800	33 200	3.77
4	HBP-OAc	7 600	27 000	3.55
5	HBP-COOH	15 300	34 000	2.22

* HBP-OH/OAc-1 and -2 are the acetate terminated HBP with subsequent hydrolysis of two different synthetic series; ratio (OH/OAc // ~20/80).

However, the hydrodynamic volume of HBP molecules especially having terminal groups of high polarity can not be easily correlated to the volume of the linear polymers. Additionally, *Lederer et al.* [Led02] showed that the hyperbranched poly(etheramide) with molar mass on the top of the peak of about 60 000 g/mol corresponds to the volume of PS or PVP with a molar mass of about 20 000 g/mol. It means that the determination of the relative molar mass of HBPs obtained by a linear polymer standard is not optimal because of the significant difference of the backbone structure and solvation behaviour between HBPs and linear polymers.

The SEC coupled with refractive index (RI) and light scattering detection (MALLS) is a method which allows to achieve absolute molar masses along the separation process. After the separation of the sample the MALLS enables to receive the direct signal of the scattering intensity which is proportional to the weight-average molar mass and the polymer concentration. Additionally the light scattering detection gives an information about the size of the polymers in solution and/or their aggregates. Therefore, the investigation of the molar mass of HBPs dissolved in THF with SEC-MALLS was applied to exclude the influence of a linear polymer standard on the evaluation procedure. However, it was not possible to receive any RI- and LS-chromatograms of HBP-OH and HBP-COOH. One reason might be their irreversible adsorption to a column substrate. Therefore, all measurements using SEC-MALLS were performed only for HBP-OAc, HBP-OH/OAc-1 and -2. It is interesting to note the large difference of the intensity of the RI-signals between these three HBPs. The response of the RI-detector (**Figure 2.7**) and the value of the refractive index increment dn/dc (**Table 2.3**) increase from HBP-OH/OAc-2 to HBP-OH/OAc-1. Moreover, the RI- chromatogram of these HBPs demonstrates the order of their elution from the column, i.e. a decrease of the hydrodynamic volume:



The LS-response of HBP-OAc has a very intensive and well recognisable signal between 9 and 10 ml (**Figure 2.9**) indicating the broad molar mass distribution and possible aggregation. However, the LS detector is not particularly sensitive towards the low molar masses. The problem is the strong dependence of the LS response on molar mass and polymer concentration, i.e. only polymer molecules with a high molar masses are able to give a scattering signal of high intensity.

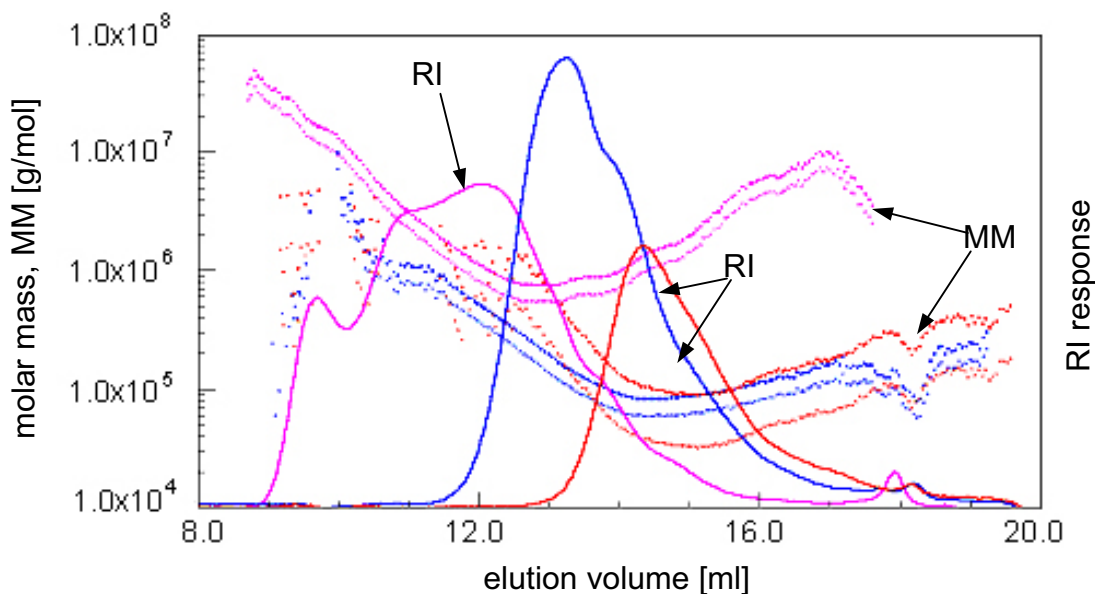


Fig. 2.7. System II: Calibration curves of the molar mass (MM) evaluated using the dn/dc of PS (bottom) and HBP (top) as a function of elution volume, together with the SEC-MALLS chromatogram of RI response (\rightarrow) of HBP-OAc (magenta), HBP-OH/OAc-1 (blue) and HBP-OH/OAc-2 (red).

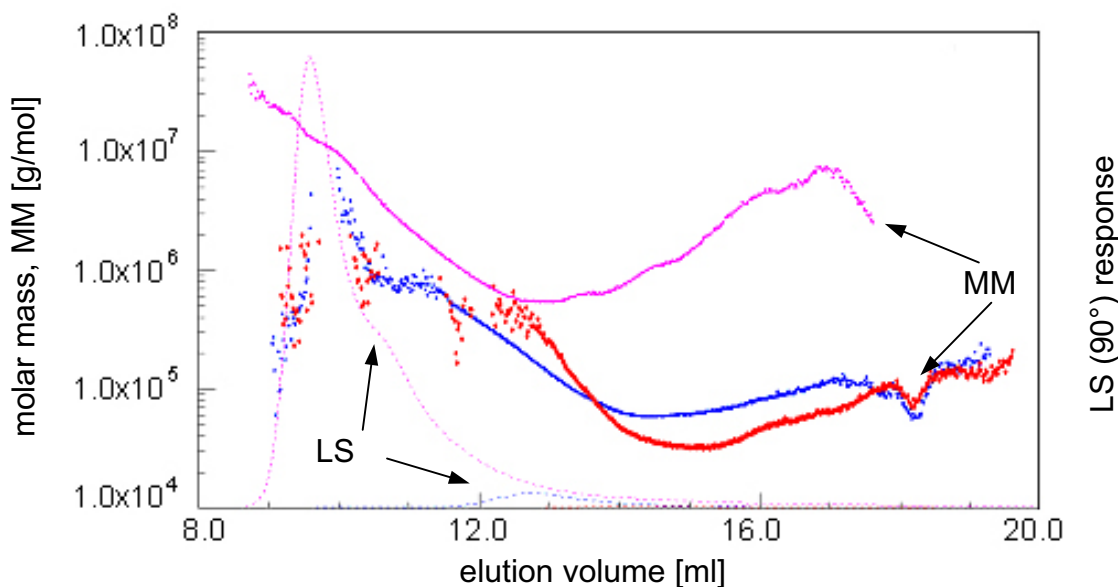


Fig. 2.8. System II: Calibration curves of the molar mass (MM) evaluated using the dn/dc of PS as a function of elution volume, and SEC-MALLS chromatograms of LS(90°)-response of HBP-OAc (magenta), HBP-OH/OAc-1 (blue) and HBP-OH/OAc-2 (red).

The RI-response of HBP-OAc having very broad elution range is also attributed to the high molecular mass and high polydispersity (**Figure 2.7 and 2.9**). **Table 2.2** shows the SEC-MALLS results of molar masses obtained from LS- and RI-detectors

(Figure 2.9) and evaluated using the dn/dc of a PS dissolved in THF. The similar trace of RI- and UV-signals obtained shows that there is no chemical heterogeneity in the system. However, the differences of the slope of the calibration curves (Figure 2.8) of the high area of the elution volume indicates the distinction in the separation mechanism: entropic (separation by size) and enthalpic (separation by interaction with column material). Therefore, the calculated average values of M_n were found to be too high and the index of polydispersity too small compared to the “real” molar mass distribution. Nevertheless, the proportionality of the UV-signal to the sequence of the UV activity and its connection to the RI-signal indicate the chemical heterogeneity of the HBP-OH/OAc-1 which could ascribed to the dependence of the degree of modification on molar mass. It should be also noted that only HBP-OAc shows this large difference between UV- and RI-signals compared to both HBP-OH/OAc.

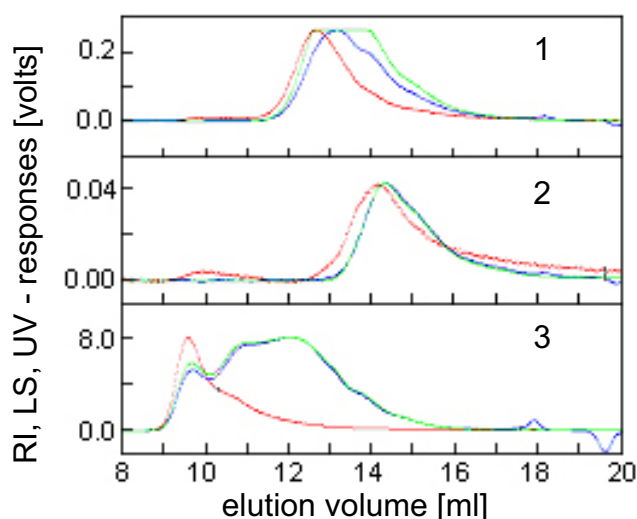


Fig. 2.9. System II: The LS- (red), RI- (blue) and UV_{254nm}- (green) chromatograms obtained from SEC-MALLS for HBP-OH/OAc-1 (1); HBP-OH/OAc-2 (2); HBP-OAc (3).

Table 2.2. System II: The molar masses obtained from LS- and RI- chromatograms using the refractive index increment of PS ($dn/dc = 0.184 \text{ ml/g}$), solvent: THF.

N	polymer	M_n [g/mol]	M_w [g/mol]	PDI
2	HBP-OH/OAc-1	90 700	119 700	1.32
3	HBP-OH/OAc-2	42 600	50 200	1.2
4	HBP-OAc	925 000	1 444 400	1.6

Moreover, the non linear calibration curves presented in **Figure 2.8** indicate a non uniform separation process consisting of the entropic (SEC) and enthalpic (adsorption) separation mechanisms in the chromatographic system. Therefore, the calculated values of M_w and M_w/M_n of the HBPs based on the dn/dc of PS carry only a relative character. The influence of the dn/dc on the values of the molar mass is presented in **Figure 2.7** and **Tables 2.2** and **2.3**. The difference between the results obtained using the dn/dc of PS and HBP can be clearly seen.

The differences of the molar mass averages obtained by the calibration and MALLS detection are presented in **Table 2.3**. The values of molar mass using SEC-MALLS were obtained using the calculated dn/dc of each HBP. There are two possible explanations of the large differences in the values of the molar mass determined by SEC and SEC-MALLS. The most probable one is the strong dependence of the hydrodynamic volume and coil density on the molar mass. The results obtained with SEC using linear PVP as a standard show too low molar masses due to very compact structure of HBPs in a dissolved state. On the other hand, SEC-MALLS allows the determination of the exact molar masses (M_w) of the HBP taking into account the actual compactness of dissolved HBP molecules near the concentration used. The second one is the aggregation of the molecules dissolved in THF (e.g. HBP-OAc), which can be influenced by the hydrogen bond formation. Differently, the SEC-measurements with PVP-calibration were carried out in mixed solvent with LiCl, which breaks eventual hydrogen bonds.

Table 2.3. The molar mass averages of HBPs obtained by the calibration (SEC) and MALLS detection (SEC-MALLS).

N	polymer	System I: SEC (DMAc-H ₂ O-LiCl)			System II: SEC-MALLS (THF)			
		M _n [g/mol]	M _w [g/mol]	PDI	M _n [g/mol]	M _w [g/mol]	PDI	dn/dc (HBP) [ml/g]
2	HBP-OH/OAc-1	9 600	42 100	4.38	128 000	168 000	1.31	0.131
3	HBP-OH/OAc-2	8 800	33 200	3.77	120 000	144 000	1.20	0.066
4	HBP-OAc*	7 600	27 000	3.55	1 500 000	4 500 000	3.00	0.133

* high molar mass due to aggregation, see text.

2.5. Thermal properties of HBPs

Differential scanning calorimetry (DSC) was applied to investigate the thermal behaviour of HBPs. There are many factors affecting the value of the glass transition temperature (T_g), e.g. molecular structure, molar mass, degree of branching in the case of HBP, nature of end groups, and interactions such as physical and chemical crosslinking (network formation). **Figure 2.10** shows the DSC thermograms of the first heating, the first cooling and the second heating scans of HBP-OH and HBP-COOH. The DSC curves of the first heating show a broad peak at 100°C caused by the vaporisation of the water absorbed within the polymers. The curves of the first and second heating of HBP-OH and HBP-COOH show clearly a step in the heat flow curves corresponding to the glass transition.

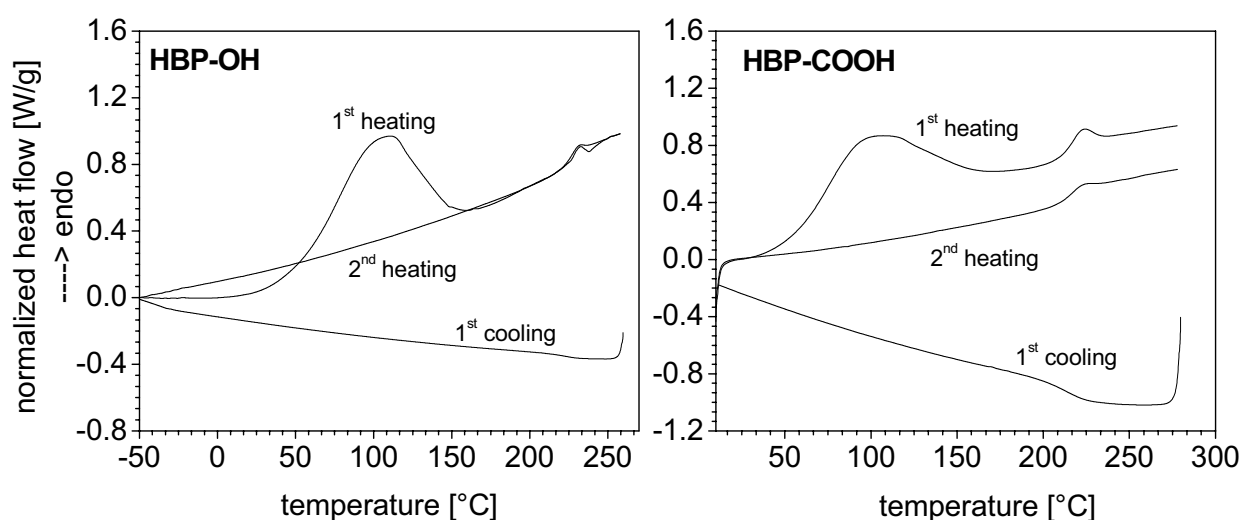


Fig. 2.10. DSC “heating-cooling-heating” cycle of HBP-OH and HBP-COOH.

The glass transition temperature of HBPs was evaluated from the second heating run for all polymers and presented in **Table 2.4**. As can be seen, the hydroxyl and carboxyl terminated HBPs gave the highest values of the T_g compared to the acetate terminated HBPs. Such high temperature can be attributed mainly to the formed network of intra- and especially inter-molecular hydrogen bonds within HBP-OH and HBP-COOH. Moreover, the high value of molar mass of HBP-OH/OAc-2 leads to a slight raise of the T_g .

Table 2.4. The glass transition (T_g) temperature and temperature of maximum decomposition (T_{DTG}) of HBPs determined from the second DSC scans and TGA data analysis, respectively.

polymer	HBP-OH	HBP-COOH	HBP-OAc	HBP-OH/OAc-1	HBP-OH/OAc-2
T_g [°C]	227	214	158	158	163
T_{DTG} [°C]	390	390/480/523	411	404	–

* HBP-OH/OAc-1 and -2 are the acetate terminated HBP with subsequent hydrolysis of two different synthetic series; ratio (OH/OAc // ~20/80)

The investigations of the thermal stability in terms of dynamic TGA measurements were performed in the temperature range from 20 to 800°C with a heating rate of 10 K/min and using nitrogen as inert gas. All HBPs showed good thermal stability up to 300°C before the degradation started. **Figure 2.11** and **Table 2.4** show thermograms and the temperature of maximum decomposition (T_{DTG}) of HBPs with different end groups. The decomposition behaviour with sharp degradation slope is very similar for HBP-OH, HBP-OAc and HBP-OH/OAc-1. The decomposition of HBP-COOH starts earlier at the temperature of about 280°C. However, the maximum temperature of the main decomposition of HBP-COOH occurs at 480°C.

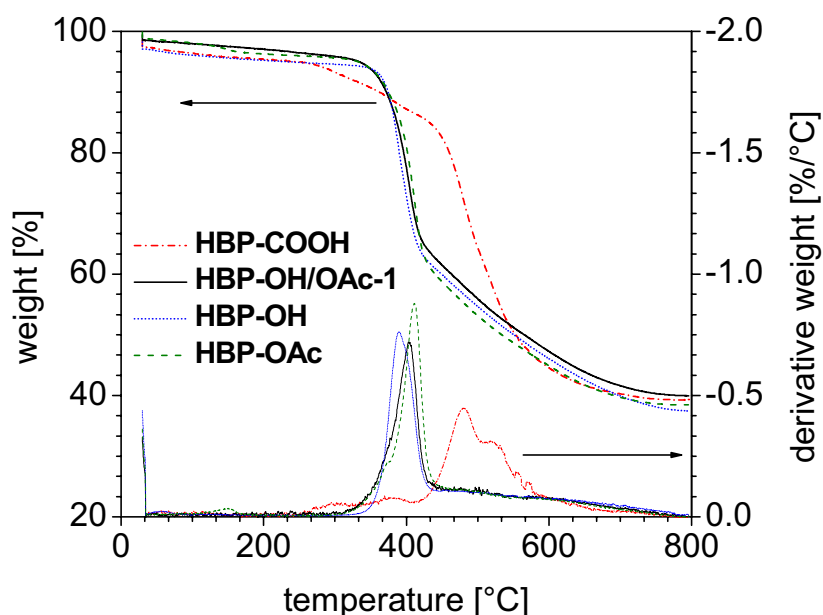


Fig. 2.11. Dynamic TGA curves obtained in nitrogen atmosphere.

Due to high temperatures applied for the annealing of HBP thin films during the preparation for the contact angle, zeta potential and ellipsometric experiments (see

Chapter 3), isothermal TGA measurements were performed for all HBPs (**Figure 2.12**). The HBP-OH and HBP-COOH were heated at 240°C for 8 hours. The temperature applied for the annealing of the HBP-OAc and HBP-OH/OAc-1 was 180°C. All HBPs showed good stability without any decomposition.

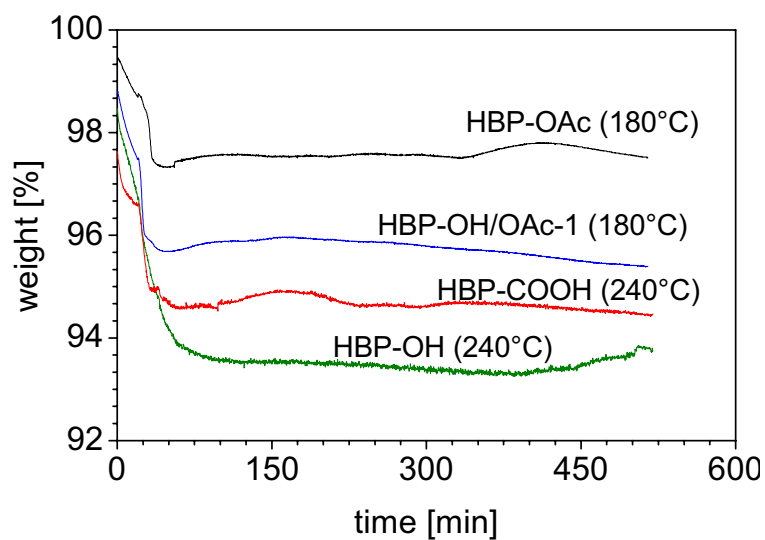


Fig. 2.12. Isothermal TGA curves obtained in nitrogen atmosphere.

Chapter 3. Characterisation of the film properties of hyperbranched aromatic polyesters

3.1. Temperature-dependent FTIR spectroscopic and thermoanalytic studies of hydrogen bonding of hydroxyl (phenolic group) terminated hyperbranched aromatic polyesters, HBP-OH

Abstract

The formation and modification of inter- and intramolecular hydrogen bonds of hydroxyl (phenolic group) terminated hyperbranched aromatic polyesters (HBP-OH) have been studied by temperature-dependent Fourier Transform Infrared (FTIR) spectroscopy. Three “heating-annealing-cooling” (HAC) cycles starting from room temperature to 235°C were measured.

The IR spectroscopic results indicate different types of hydrogen bond association. The weakening and breaking of hydrogen bonds with increasing temperature was observed. Additionally, a curve fitting procedure of the hydroxyl and carbonyl vibration regions has been done to gather additional information of the hydrogen bond association. On the basis of the band shifts and the changes of the normalised integral band intensity (NIBI) and halfwidth of a band (HWB), the formation of a network of hydrogen bonds was proposed. Four different interactions regarding hydroxyl (phenolic) groups association were detected. Several types of associated carbonyl groups existing within HBP-OH were revealed. The spectra and curve fitting results indicate the relative stability of formed bond structures with participation of the ester groups of the HBP rigid segments in the studied temperature region. Differential Scanning Calorimetry (DSC) was applied to reveal changes in thermal behaviour after the first, the second and the third HAC cycle. As expected, the aromatic ester backbone structure strongly influences the glass transition. Therefore, the performed measurements did not show any changes in glass transition related to the rearrangements in the hydrogen bonded network.

3.1.1. Role of supramolecular interactions in HBPs

Hyperbranched polymers (HBP) are an established class of polymeric materials, the growing interest to which is demonstrated by the increasing number of publications concerning their technological applications in different fields, e.g., sensors [Bel02, Vol05], additives and coatings [Joh93, Sid01, Sid02, Bey01, Voi02]. Therefore, their dynamics in films and possible self-organisation due to noncovalent interactions based on the chemical composition are of crucial importance. Physical properties such as thermal transitions, viscosity, surface tension and solubility are related to the strength of attractive forces between molecules. Hydrogen bonding is one of the most important non-covalent interactions playing a fundamental role in polymers in the interpretation of the various properties when it comes to interactions between macromolecules and macromolecules and substrate surfaces.

The hydrogen bond is not like a simple attraction between pointed charges. It possesses some degree of ordered preference and can have some of the characteristics of a covalent bond. Hydrogen bonding is a well-known phenomenon which plays a key role in biology, biochemistry and biophysics regarding interactions of proteins, nucleic acids and polysaccharides. This type of interactions is also of crucial importance in synthetic polymer science, e.g. in the blend formation and the mixing process of different polymers [Yhe01, Lee98, Ces93, Ces93a, Zie03, Kuo03]. Recently, the influence of hyperbranched polyesters based on the monomer 4,4-bis(4-hydroxyphenyl)valeric acid and the core molecule 2-ethyl-2-(hydroxymethyl)-1,3-propanediol on miscibility and formation of hydrogen-bonded complexes was studied [Zie03].

Painter et al. characterized hydrogen bonds in a hyperbranched, dendrimer-like polyester and its blends with poly(4-vinylphenol) by IR spectroscopy [Pai99]. They also discussed in detail the effect of hydrogen bonding and the “screening effect” on the carbonyl stretching region of IR spectra using different mixtures of a hyperbranched polyester with ethylphenol [Pru01].

Cesteros et al. applied IR spectroscopy to characterise the effect of hydrogen bonding in linear hydroxyl-containing polyesters [Ces93, Ces93a].

Furthermore, *Zagar et al.* [Zag03] applied temperature dependent IR measurements together with hydration and H/D exchange experiments for the determination of the hydrogen network of hydroxyl terminated hyperbranched aliphatic polyesters of the

fourth generation. The authors also employed difference spectroscopy, 2D generalized correlation infrared spectroscopy, and a band fitting procedure to study the main hydrogen bond interactions in the polymer.

This **Chapter** is focused on the investigation of changes of hydrogen bonding [Col99] in HBP-OH due to high temperatures and their influence on the glass transition temperature by Fourier Transform Infrared (FTIR) spectroscopy and Differential Scanning Calorimetry (DSC). In this contribution, the behaviour of hydrogen bonds in phenolic group terminated hyperbranched aromatic polyesters (HBP-OH) at different temperatures starting from room temperature to 235°C using three “heating-annealing-cooling” (HAC) cycles was studied. Considering the chemical structure of the polymer used, the existence of hydrogen bonding between the molecular segments of the same HBP molecule or between neighbouring HBP molecules was expected as a result of the interaction between the hydroxyl (phenolic) groups or carbonyl groups having a proton acceptor character and the phenolic end groups. DSC was applied to reveal changes in glass transition temperature of every cycle.

3.1.2. Application of “heating-annealing-cooling” cycles to study the hydrogen network formation in HBP-OH

3.1.2.1. *Temperature-dependent Fourier Transform Infrared (FTIR) spectroscopy*

The samples for IR measurements were prepared as films on KBr substrates by solvent casting of the HBP-OH from 5.0 wt% tetrahydrofuran solution (THF, Merck, Germany). After casting the solution, the solvent was evaporated during 3 minutes in the open air at relative humidity of $45 \pm 5\%$ and at a temperature of $24 \pm 1^\circ\text{C}$, both were kept constant. Then the samples were carefully placed in an oven and dried at 40°C for 5 minutes without vacuum and under vacuum at 40°C for 20 minutes to remove the residual solvent before the study.

A Variable Temperature Cell (SPECAC, UK) equipped with a temperature control unit (SPECAC, UK) was used for the temperature-dependent IR transmission measurements in a Bruker spectrometer Equinox 55 with DTGS detector (Germany). All spectra were recorded in the spectral range of $4000 - 600 \text{ cm}^{-1}$ with a resolution of 2 cm^{-1} and an accumulation of 16 scans. The heating runs (heating phase of the HAC cycle) were done stepwise (in steps of 10 K) from 25 to 235°C . The spectra were

recorded in the steady state under vacuum (5 mbar) and at the given temperature. After heating up the sample was annealed isothermally at 235°C for 2 hours (annealing phase of the HAC cycle). Eight spectra were measured with an interval of 15 minutes. After that, the sample was cooled down to 30°C and the spectra were recorded every 10 K during the cooling (cooling phase of the HAC cycle).

Curve fitting of the spectra in the O–H and C=O stretching vibration regions was performed using the curve analysis program of the Bruker software OPUS 5.0. The best fits were obtained using mixed Gauss-Lorentz profile and the Levenberg-Marquardt fit procedure.

The **normalised integral band intensity (NIBI)** of the separated band components **A, B, C, D, E** in the hydroxyl (ν O–H) and carbonyl (ν C=O) vibration regions (see **Figure 6**) was calculated according **Equations 3.1.1-3.1.4**:

For (ν O–H):

$$NIBI(A) = \frac{A(A)}{A(C)} \quad (3.1.1)$$

$$NIBI(B) = \frac{A(B)}{A(C)} \quad (3.1.2)$$

For (ν C=O):

$$NIBI(D) = \frac{A(D)}{A(D) + A(E)} \quad (3.1.3)$$

$$NIBI(E) = \frac{A(E)}{A(D) + A(E)} \quad (3.1.4)$$

where A is the integral absorbance determined from the curve fitting analysis. The band **C** (ν C–H arom.) was used as internal standard for the hydroxyl vibration region. **Band position** (in cm^{-1}) and **halfwidth of the band (HWB)** are the further fit results.

3.1.2.2. Differential scanning calorimetry (DSC) and Thermo Gravimetric Analysis (TGA)

A TGA Q 500 (TA Instruments, USA) was applied for the determination of the degradation temperature T_{DTG} of the HBP-OH. The measurements were performed in the temperature range from 20 to 800°C with a heating rate 10 K/min and using nitrogen as inert gas. Before measurement, the sample was heated at 30°C for 20 minutes. The changes in thermal behaviour of HBP-OH due to our HAC experiments were determined using a DSC Q1000 (TA Instruments, USA). The samples of about 5 mg were accurately weighted into aluminium pans, sealed and then measured under a nitrogen atmosphere at the heating scan rate of 20 K/min and at the temperature range of 30°C to 270°C. Calibration of temperature and heat flow was done using indium standard. According to the IR measurements the samples were heated up to 235°C, annealed for 2 hours and cooled down to room temperature. The resulting T_g of three samples was determined after the first, the second and the third HAC cycle, respectively.

3.1.3. Hydrogen bond formation and reorganisation during “heating-annealing-cooling” cycles

The temperature-dependent FTIR measurements were used to provide information regarding the formation, weakening, breaking and redistribution of hydrogen bonds [Yhe01, Zie03, Eic03]. The IR survey spectra of the initial and annealed HBP-OH in the full mid-infrared spectral region are given in **Figure 3.1.1**. The typical bands attributed to the hydroxyl (ν_{OH}), carbonyl ($\nu_{C=O}$) and aromatic vibration regions of the spectra are fully described in the Chapter 2.4. The solvent THF was removed complete only during heating above 180°C of the first HAC cycle (see heating1 of the first HAC cycle in **Figure 3.1.3** and **3.1.4**, bands in the range 3000 – 2800 cm^{-1} , **Figure 3.1.1**). The relative high temperatures needed to remove the solvent might be due the interactions via hydrogen bonding between HBP-OH and THF molecules. On the other hand, HBP molecules could form “ring-like” structure of hydrogen bonds and by these prevent the diffusion of THF molecules.

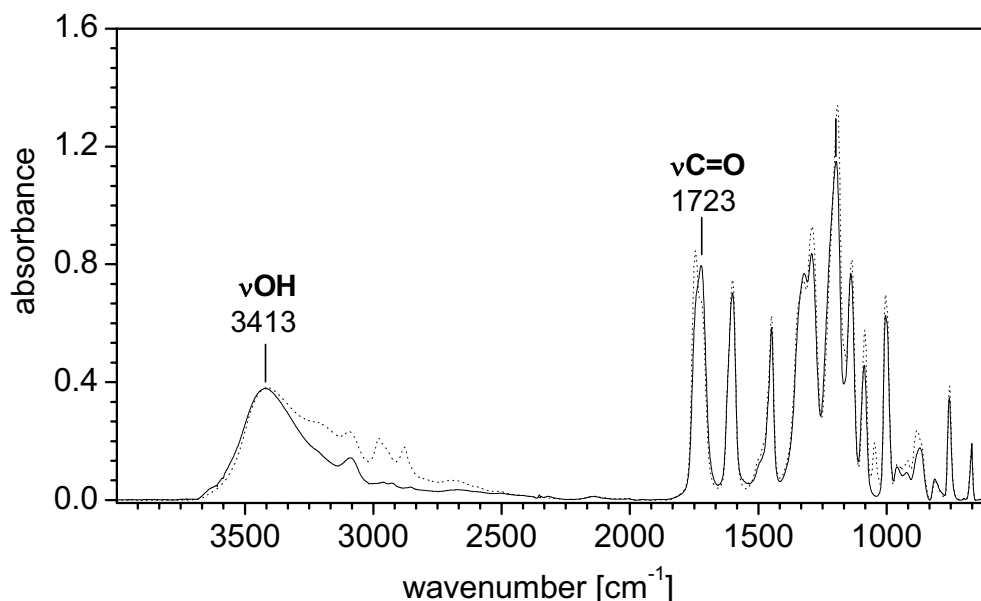


Fig. 3.1.1. FTIR spectra of the initial (.....) HBP-OH film and annealed for 2 hours / 235°C (—), casted from THF on KBr substrate.

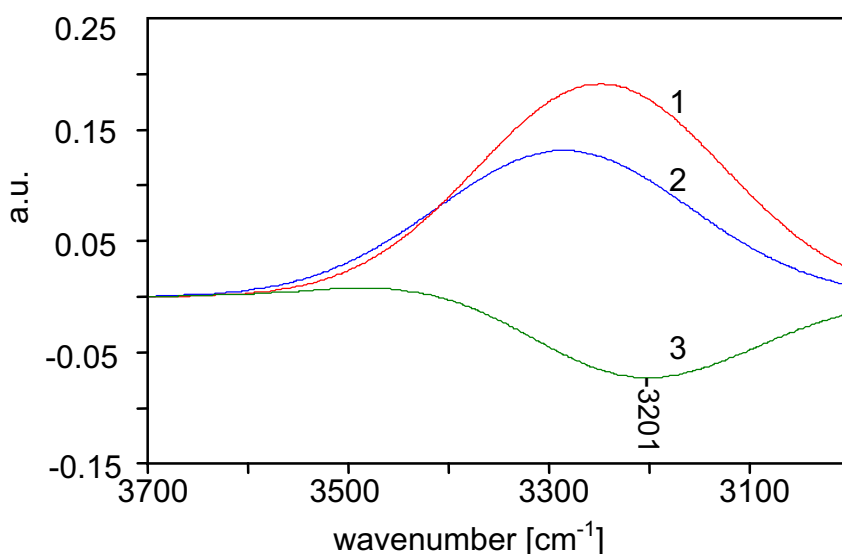


Fig. 3.1.2. The **B** components (see **Figure 3.1.6**) of the spectra in the (νO–H) region obtained by the curve fitting procedure (1 - before the first HAC cycle at 30°C, 2 – after the first HAC cycle at 30°C) and difference spectrum (3 = 2-1).

The content of the absorbed water within HBP-OH (from atmospheric humidity, r.h. ~ 55%) was examined by checking the presence of a band near 1640 cm⁻¹ belonging to the bending vibration (δOH) of water molecules [Zag03]. However, there was no visible band observed in this region of the survey spectrum (**Figure 3.1.1**). Moreover, the results obtained by the utilisation of the difference spectroscopy also

did not show the band assigned to the (δOH) of water molecules since the vicinity of the carbonyl stretching band ($\nu\text{C=O}$) screened the water (δOH) bending mode.

The broad complex band of the hydroxyl (νOH) vibration region at about 3410 cm^{-1} is attributed to the combined effect of the differently associated hydroxyl (phenolic) groups, i.e. hydrogen bonding between hydroxyl and hydroxyl/carbonyl groups of different strength and hydrogen bonding of water molecules. The difference spectrum presented in **Figure 3.1.2** clearly demonstrates this effect. Thus, the band at 3200 cm^{-1} of the difference spectrum is ascribed mostly to the (νOH) of the residual water molecules. These results showed a good agreement with the DSC data which indicate a negligible amount of the water absorbed in the polymer (chapter 3.1.3.2.).

The IR spectra of HBP-OH film in the hydroxyl and carbonyl vibration regions at different temperatures of three “heating-annealing-cooling” (HAC) cycles are shown in **Figures 3.1.3 – 3.1.5**. The annealing of the polymer film above T_g (see Chapter 3.1.3.2) indicated that an equilibrium condition for specific interaction is obtained. As expected, the hydrogen bonds in the HBP-OH were strongly influenced by heating and cooling. The spectra of the first heating cycle show two significant changes in the **OH stretching region** with an increase of the temperature: The absorbance decreases and bands shift to higher wavenumbers. This observed progressive shift of the ($\nu\text{O-H}$) band at about 3412 cm^{-1} toward higher wavenumbers can be attributed to a redistribution in the arrangement of hydroxyl group association. As described previously [Ces93a, Zie03, Mat67, Zag03], the wide band of the hydroxyl ($\nu\text{O-H}$) stretching region can be attributed to the summation of several contributions corresponding to the distribution of hydrogen bonded hydroxyl groups at different distances, geometry and with different force constants.

To gather additional information of the hydrogen bond rearrangement and/or association due to HAC cycles applied, a curve fitting of the hydroxyl vibration region in the range $3700 - 3000\text{ cm}^{-1}$ was performed (**Figure 3.1.6a**). The fitting results gave the band **A** at 3435 cm^{-1} which corresponds to “weakly” hydrogen bonded hydroxyl groups. The broad band **B** at around 3300 cm^{-1} is attributed to the cross effect of the “strongly” associated hydroxyl groups of HBP-OH. The position, the normalised integral band intensity (NIBI) and halfwidth of the band (HWB) of the **A** and **B** bands change during the three HAC cycles in a different matter (**Figure 3.1.7a,b,c**). The first position of the **B** band at 3250 cm^{-1} (**B₁**) is assigned to the

associated OH groups of HBP-OH and residual water molecules. The second position of the **B** band at 3300 cm^{-1} (**B**₂) and the third one at 3350 cm^{-1} (**B**₃) which were strongly influenced by the first HAC cycle, are due to association of hydroxyl groups and hydrogen bonding between hydroxyl and carbonyl groups of the polymer. The pronounced reduction of NIBI during the first HAC cycle corresponds to the breaking of **B**₁ H-bonds with following removal of the absorbed water molecules (curve B in **Figure 3.1.7b**). This is accompanied with a shift of **B** band position to higher wavenumbers (**B**₁ → **B**₂ → **B**₃, see curve B in **Figure 3.1.7a**) which resulted in an increase of the “weakly” associated hydrogen bonds (curve A in **Figure 3.1.7b**). The nearly invariable values of HWB of **A** and **B** bands (**Figure 3.1.7c**) indicate that the mean diversity of the “weakly” and “strongly” associated hydrogen bonds are almost constant during HAC cycles.

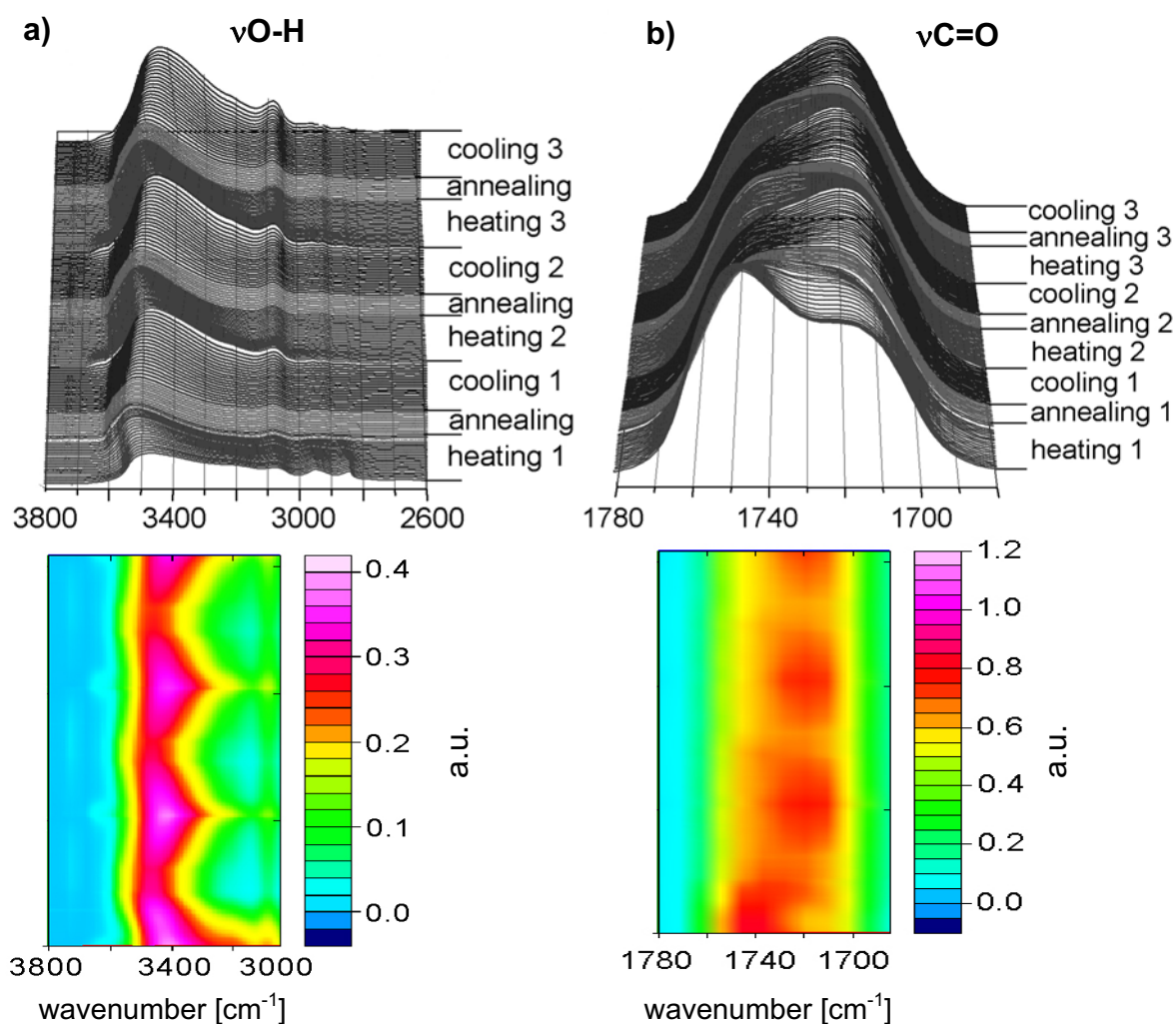


Fig. 3.1.3. 3-D and contour plots of hydroxyl ($\nu\text{O-H}$) and carbonyl ($\nu\text{C=O}$) stretching vibrations during the three HAC cycles.

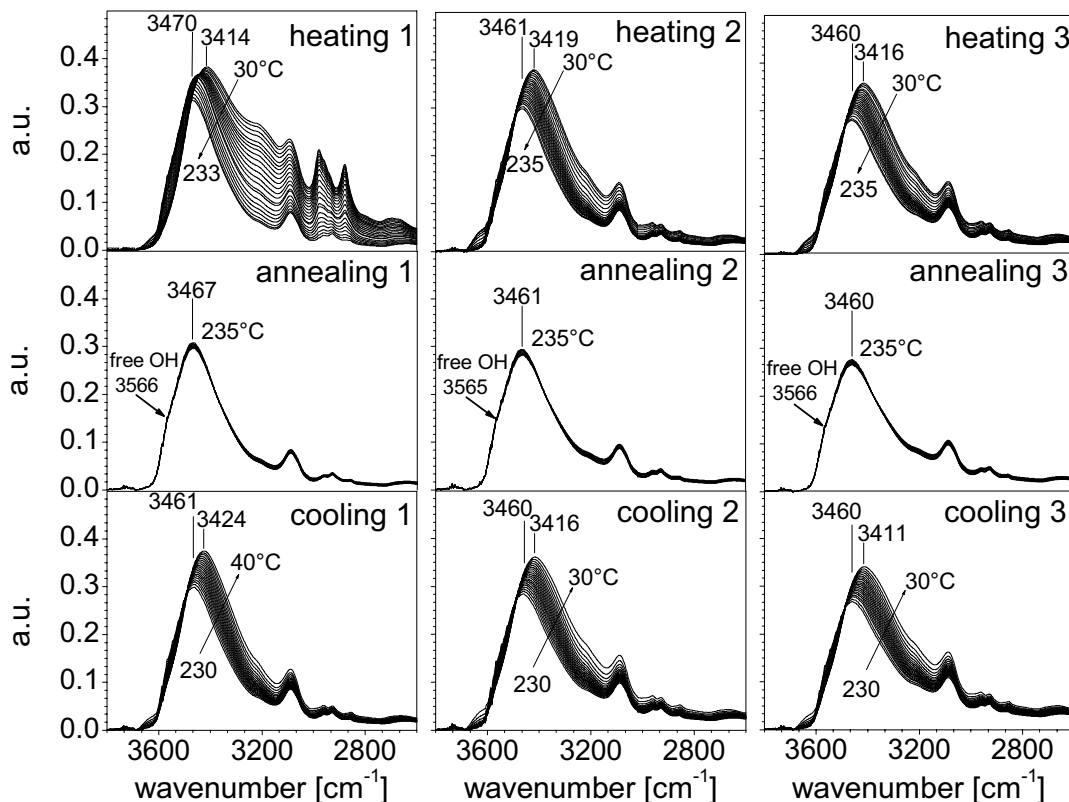


Fig. 3.1.4. The hydroxyl vibrations (ν_{O-H}) in the different HAC phases.

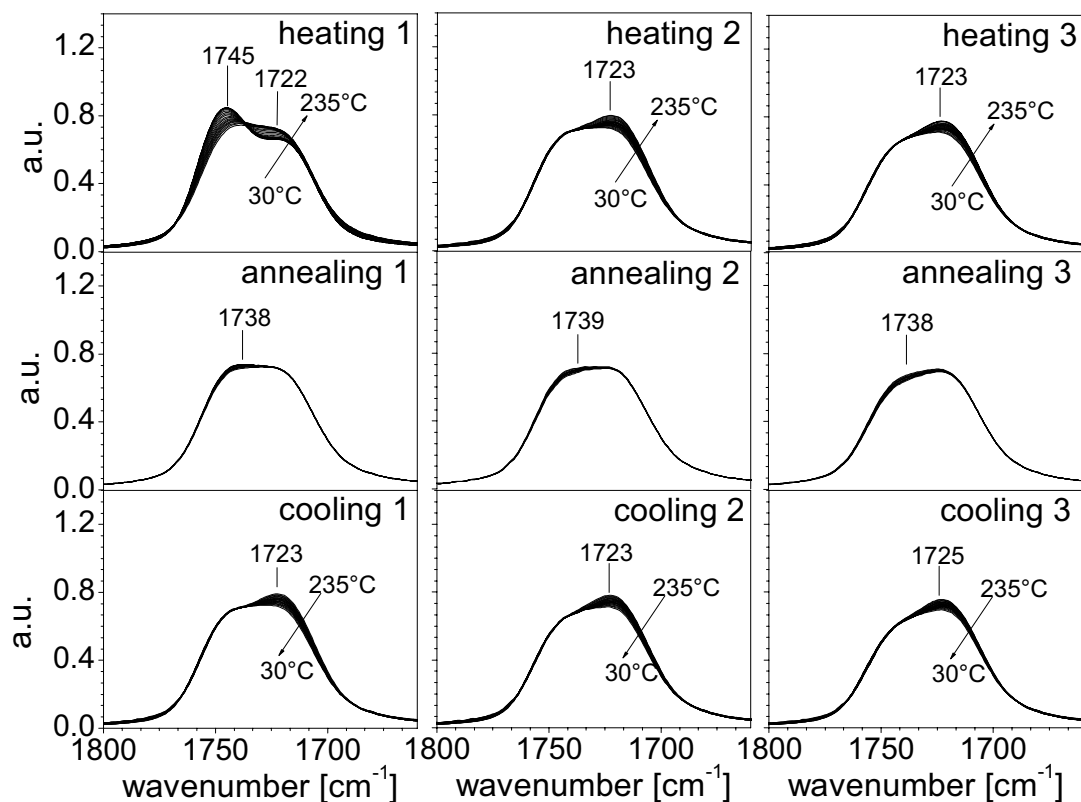


Fig. 3.1.5. The carbonyl vibrations ($\nu_{C=O}$) in the different HAC phases.

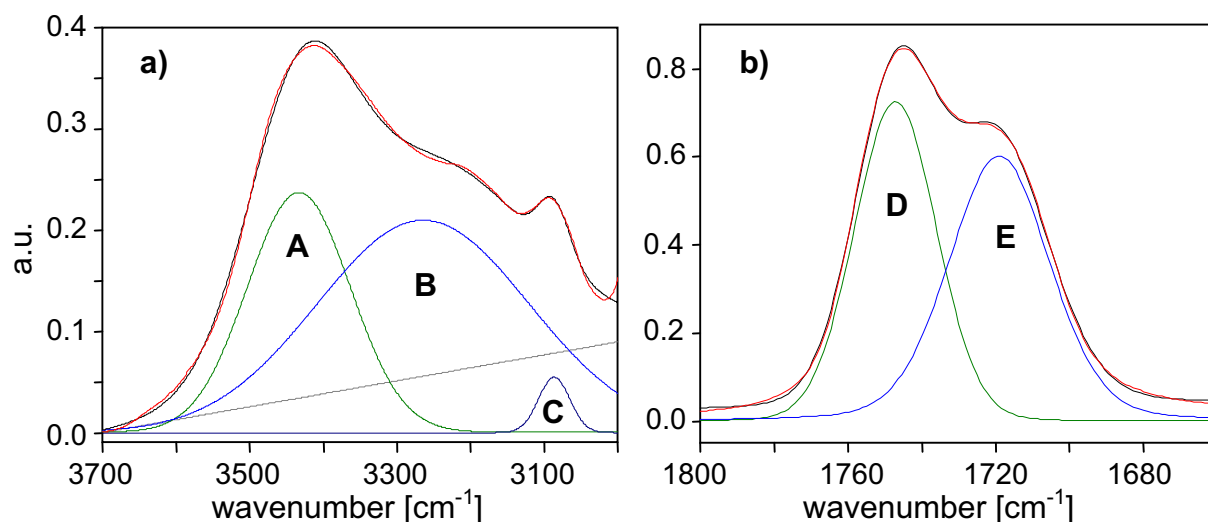


Fig. 3.1.6. Typical curve fitting results of the hydroxyl ($\nu\text{O-H}$) and carbonyl ($\nu\text{C=O}$) vibration regions at the beginning of the first HAC cycle (30 °C) of HBP-OH.

The spectra of the **carbonyl stretching region** (Figure 3.1.5) of the first HAC cycle showed a strong irreversible decrease of the relative absorbance of the carbonyl band at about 1745 cm^{-1} and pronounced increase of the relative absorbance at about 1722 cm^{-1} corresponding to the “free” and associated (**Z₁**, Figure 3.1.8) C=O groups. 3-D IR spectra (Figure 3.1.3b) clearly demonstrate these changes due to heating.

Two band components (Figure 3.1.6b) belonging to “free” (band **D**) and associated (band **E**) carbonyl groups were obtained from the curve fitting procedure. The significant changes of the NIBI of **E** and **D** bands (Figure 3.1.7e) were attributed mainly to the structural rearrangement of HBP molecules with weakening and breaking the existing network of hydrogen bonds between O–H groups and creation of a new one between O–H and the more electronegative ester groups. The small increase of NIBI of the **A** band (Figure 3.1.7b) during the second and the third HAC cycles indicates the relative high stability of the formed bond structures with the participation of the ester groups of the HBP rigid segments in the studied temperature region. Moreover, the consecutive increase of the HWB of the **E** band (Figure 3.1.7f) indicates the existence of several types of associated carbonyl groups within HBP-OH molecules, i.e. of carbonyl groups associated with OH of different strength (**A** and **B₂**) and re-associated **B₃**. This rearrangement and/or association of C=O comes from the more favourable C=O / OH interaction, which is a function of the binding strength and possible structural arrangements of HBP molecules.

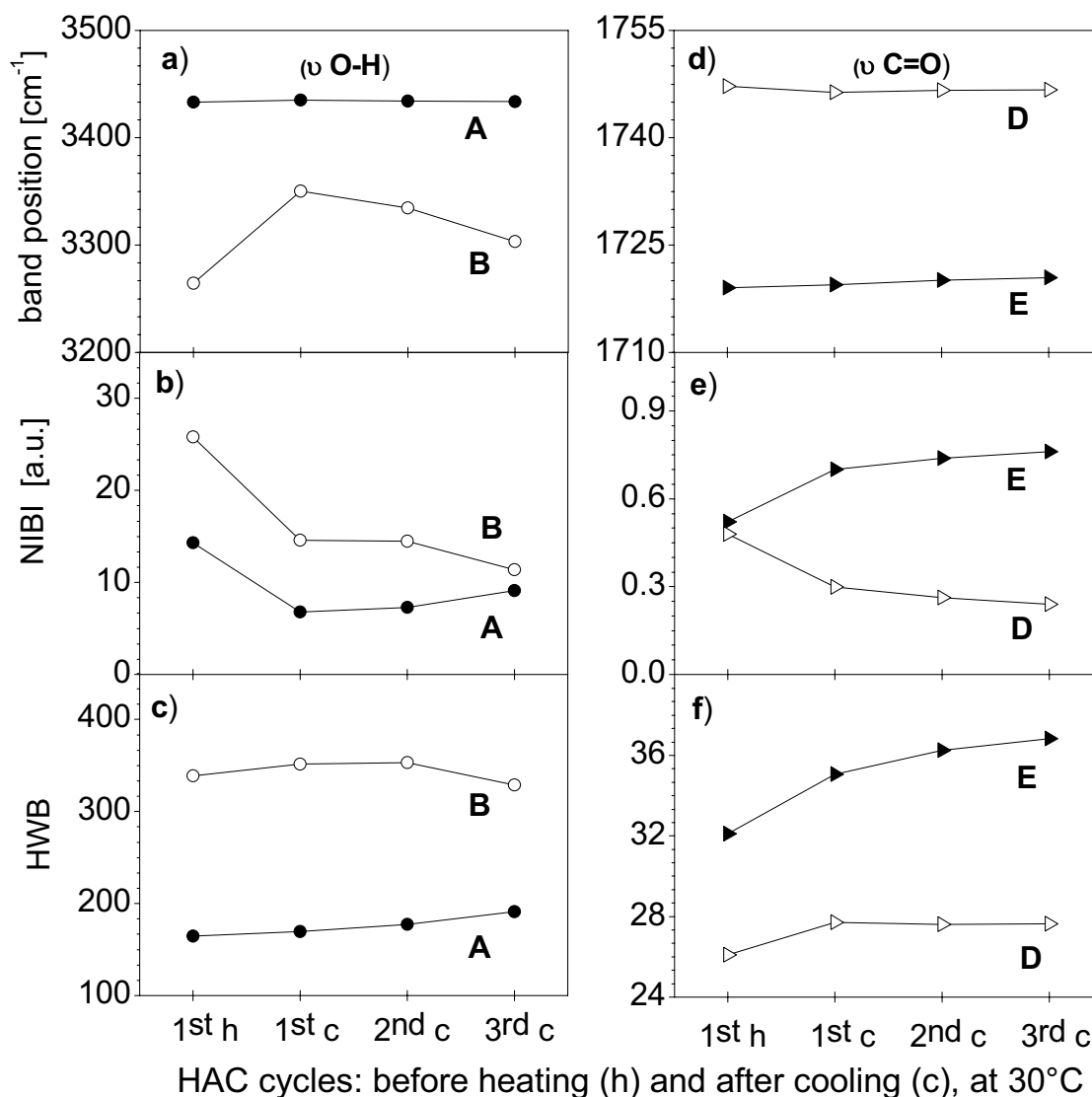


Fig. 3.1.7. Temperature-dependent changes in band position, normalised integral band intensity (NIBI) and halfwidth of a band (HWB) of hydroxyl (A, B) and carbonyl (D, E) band components: Band position: a) bands A and B; d) bands D and E, NIBI: b) bands A and B; e) bands D and E, HWB: c) bands A and B; f) bands D and E.

A schematic representation illustrating several types of hydrogen bonds which might be created in the polymer microstructure containing hydroxyl (phenolic) and ester groups and the supermolecular situation **during the most important first HAC cycle** from the point of view of FTIR results is shown in **Figure 3.1.8**. A significant part of the hydroxyl groups interacts via hydrogen bonds with each other or with ester groups to form single (Y, Z) or complex (X) H-bonding systems. The increase of the mobility of molecules due to heating leads to weakening of the existing network of hydrogen bonds, their rearrangement and creation of a new one (X₁, Z₁, Y₁) with

other O–H or ester groups involved of the same or neighbouring HBP-OH molecules during cooling. It should be mentioned that nearly “free” OH groups were observed only at 235 °C detected from the asymmetry of the band at the high frequency side at about 3565 cm^{-1} (**Figure 3.1.4**). Cooling down the system promotes the formation of new inter- and intramolecular hydrogen bonds between O–H groups (Y-types).

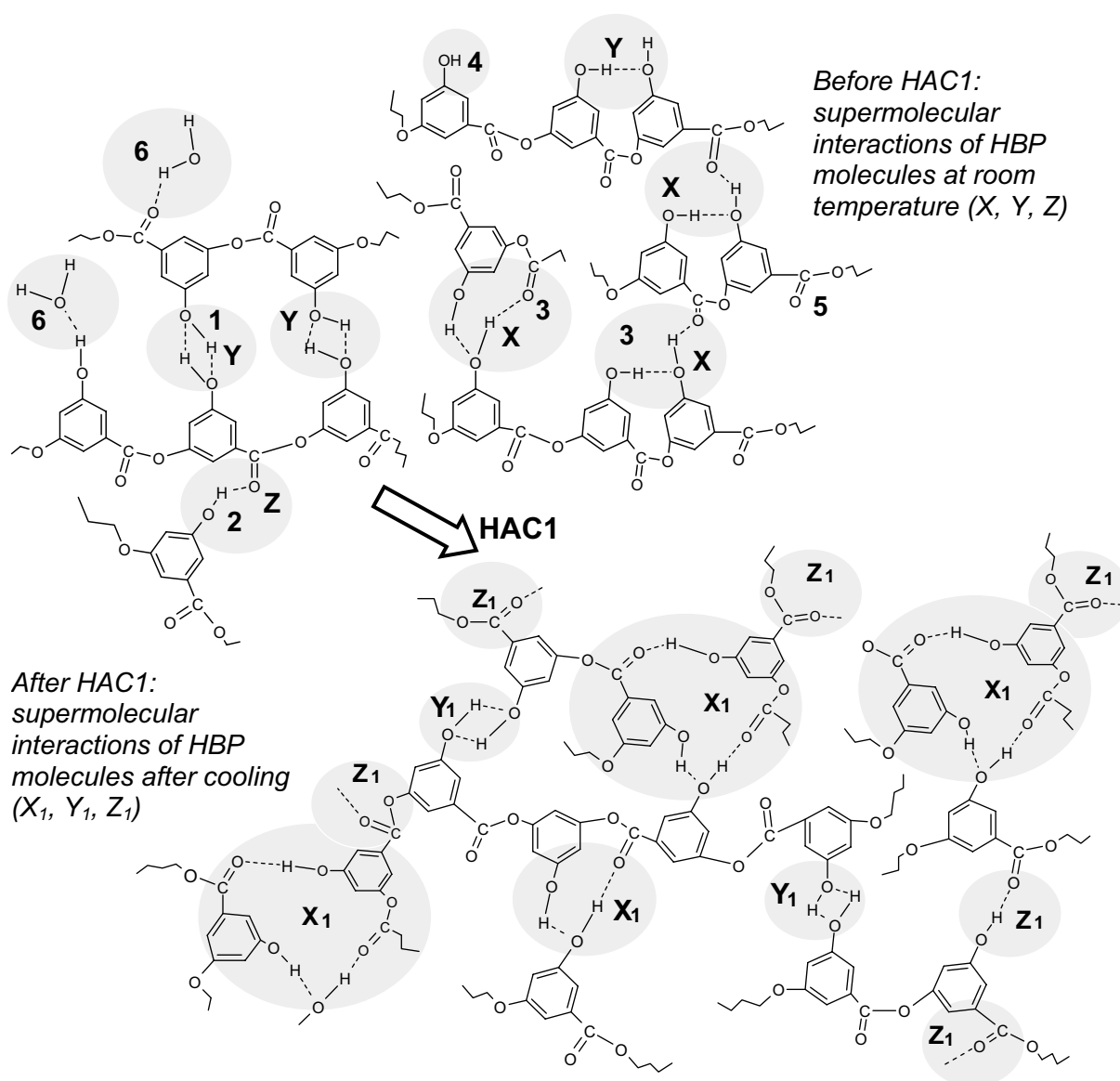


Fig. 3.1.8. Scheme illustrating the supermolecular interactions (X, Y, Z) occurring upon heating and different types of hydroxyl bond interactions during the first “heating-annealing-cooling” cycle (HAC1): **1** - hydroxyl groups hydrogen bonded with other hydroxyl groups in the same or neighbouring molecule, forming dimers, trimers, etc.; **2** - hydroxyl groups hydrogen bonded with ester groups in the same or neighbouring molecule; **3** - complex system containing **1** and **2** structures; **4** - non-hydrogen bonded hydroxyl groups; **5** - non-hydrogen bonded carbonyl groups.

To give a semi-quantitative estimation of the particularly H-bonded species, **Figure 3.1.9** combines and summarises the results of the changes in the normalised integral band intensity (NIBI) of the hydroxyl ($\nu\text{O-H}$) and carbonyl ($\nu\text{C=O}$) groups (NIBI is corresponding to the number of these groups) **during all HAC cycles**: As can be seen, the NIBI of the **B** band corresponding to the “strongly” hydrogen bonded OH groups is nearly constant during the first and the second HAC cycle. The pronounced decrease observed after the third HAC cycle can be attributed to the transformation of the “strongly” hydrogen bonded OH to “weakly” bonded ones (NIBI of the band **A**). The slight reduction of the NIBI of the **A** band after the first HAC cycle due to association with “free” carbonyl groups (band **D**), the breaking the bonds between OH groups of the HBP-OH and water molecules, and the destruction of the “strongly” bonded OH (band **B**) of the HBP-OH gave a large increase of the NIBI of the **E** band (associated C=O). Furthermore, the NIBI of the **E** band shows a subsequent increase during all HAC cycles which results from the association with OH groups transferred from the “strongly” hydrogen bonded OH (band **B**).

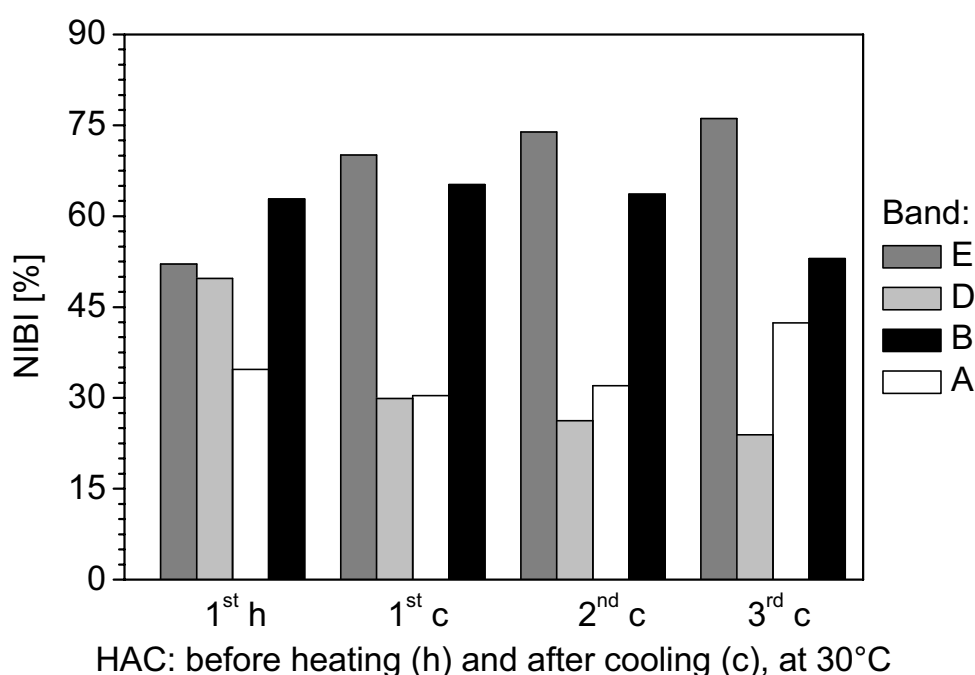


Fig. 3.1.9. Changes in normalised integral band intensity (NIBI) of hydroxyl ($\nu\text{O-H}$) and carbonyl ($\nu\text{C=O}$) vibration regions during HAC cycles.

3.1.4. Effect of the “heating-annealing-cooling” cycles on the glass transition temperature of HBP-OH

From the TGA measurements it was found that the HBP-OH is stable without decomposition up to 300°C. **Figure 2.11** (Chapter 2) shows the thermogram of the decomposition behaviour with a sharp degradation slope and the temperature of maximum decomposition $T_{DTG} = 390^{\circ}\text{C}$. The content of the water absorbed into the initial polymer was calculated to be about 2%. The DSC curves of the first heating (**Figures 2.10** and **3.1.10**) also show a broad peak at 100°C caused by the evaporation of the absorbed water.

Many factors affect the value of the glass transition temperature, e.g. molecular structure, molar mass, degree of branching in the case of HBP, nature of end groups, and further interactions such as physical and chemical crosslinking (network formation). **Figure 3.1.10** shows DSC thermograms of the HAC cycles during the first heating up to 235°C and the last heating up to 270°C to determine the resulting T_g . In contrast to the H-bonding sensitive IR spectroscopy, the DSC measurements of the samples prepared analogously as for the IR measurements did not show any changes in the glass transition. This can be attributed mainly to the predominant influence of the aromatic rings and formed network of hydrogen bonds independent of the groups involved in the association itself on the values of T_g .

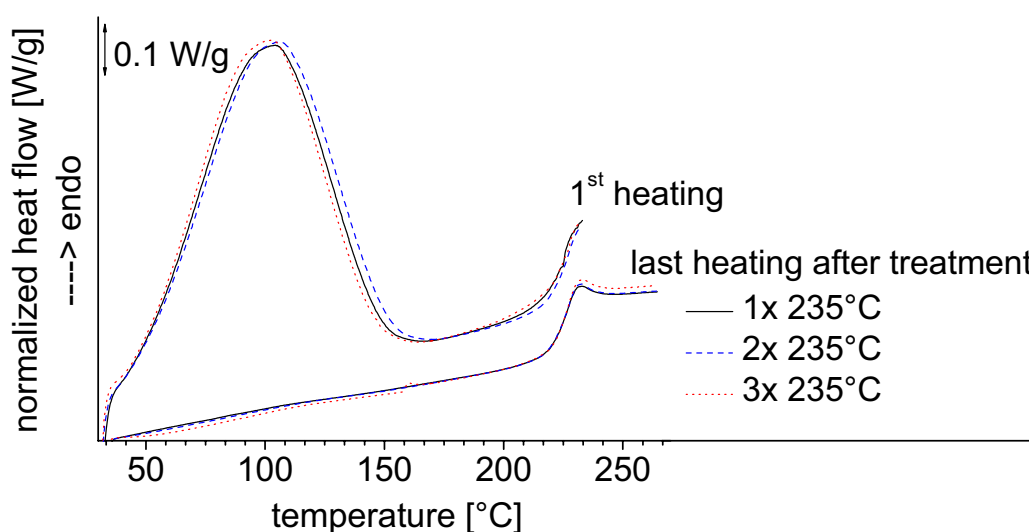


Fig. 3.1.10. DSC thermograms of the HBP-OH of the first and the last heating cycle.

3.1.5. Hydrogen bonding in HBP-OH: summary

Temperature-dependent IR measurements together with a curve fitting procedure allowed a complete analysis of the spectra obtained for HBP-OH as well as to determine hydrogen bond network organisation.

It was found that the HBP-OH forms a stable network of hydrogen bonds through the interactions between the hydroxyl groups or hydroxyl and ester groups of the same or neighbouring molecules. Thus, the irreversible changes of the carbonyl stretching region of the spectra especially during the first HAC cycle were obtained.

The changes in the association of hydrogen bonding with temperature were clarified. The formation of a better ordered and thermally more stable network of hydrogen bonds occurred after the first HAC cycle. Most of formed hydrogen bonds between OH and C=O groups showed high stability and withstood higher temperature.

The creation of new stable hydrogen bonds between OH groups during every cycle was observed.

Differential Scanning Calorimetry did not show any changes in glass transition related to the rearrangements in the hydrogen bonded network due to the strong influence of the aromatic ester backbone structure on T_g .

3.2. Characterisation of the properties and swelling behaviour of HBP thin films

Abstract

The nature of the solid-liquid interface of hyperbranched aromatic polyester (HPB) thin films has been studied with respect to further protein adsorption investigations. Contact angle measurements, atomic force microscopy, zeta potential measurements and spectroscopic ellipsometry were used to characterize the physical and chemical structure of the HBP thin films as well as the adsorption-relevant surface properties. It was shown that film properties such as the effective refractive index significantly depend on the thickness of HBP films whereas the water contact angle does not reveal any changes with thickness variations. All surface-sensitive methods used indicate marked swelling behaviour of HBP layers in aqueous buffer solutions. Moreover, the degree of swelling, zeta potential as well as surface free energy (in terms of water contact angle) strongly depend on the time the films had been annealed above their glass transition temperature.

3.2.1. Swelling of polymer films: why to study?

For the most of potential applications of HBPs (chemical sensors, multifunctional coatings, etc.) the surfaces of thin HBP films with predictable variable properties are of critical importance. There had been many different methods applied to characterise the properties of the surface of HBPs [Sid01, Sid02, Sid02a, Mac01, Bru97, Orl02]. During the last years polymer films and surfaces in contact with biomolecules are in focus of scientific and technological research activities. This is demonstrated by the increasing number of publications concerning the behaviour e.g. of complex multilayer systems formed by charged polymers in aqueous solution of different pH, which is the native medium for proteins, cells, enzymes and antibodies. Therefore, it is very important to clarify the dynamic properties of polymer thin films such as swelling, the interaction of polymer molecules with an electrolyte solution with further dissociation or hydration of polar groups, before the interaction with biomolecules can be studied and understood.

The swelling process disturbs and destructs the existed network of hydrogen bonds due to dynamic movements involving diffusion of small molecules and ions into existent voids, micro-pores or a free volume of polymers. Thus, swelling forces segmental motion within the polymer, resulting in an increased distance between polymer segments. This suggests that the film confinement tends to increase the mobility of small species with further segment relaxation. For example, the transport of ions through polyelectrolyte multilayers has been found to be enhanced with increase of film thickness [Far01]. Additionally, *McCormick et al.* [McC03] showed that the water absorption of polyelectrolytes increases the polymer mobility when confined in a multilayer system.

The kinetics of the absorption process of small molecules into the polymer matrixes and factors influencing this process have been a field of significant recent attention [Tan01, Tan02, Vre75, Vog04, Tan04]. The influence of the film thickness on the degree of swelling and swelling kinetics of water in thin poly(4-ammonium styrenesulfonic acid) films was examined using X-ray reflectivity and quartz crystal microbalance (QCM) measurements [Sch02]. Ellipsometry was applied to reveal the changes in film thickness of a grafted hyperbranched poly(acrylic acid) as a function of pH [Pee98]. The influence of chemical composition and annealing temperature of phosphorylcholine biocompatible polymer films on swelling mechanism characterised by diffusion and relaxation times was described by *Tang et al.* [Tan01, Tan02]. The authors also supposed that hydrophilic and hydrophobic fragments of a polymer may promote the formation of a structured morphology within the film which may influence the water sorption.

Previously [Bey01a], the surface properties of thin films of hyperbranched aromatic polyesters terminated by hydroxyl, carboxyl and acetoxy groups were studied. It was found that the surfaces of these polymers are hydrophilic caused by polar functional groups at the outermost surface. Using spectroscopic ellipsometry and reflectometric interference spectroscopy, at first the swelling behaviour of the HBP films was investigated at different atmospheric humidities. From the results it was concluded that these HBP films might be used as sensor materials. Based on the results obtained, HBP were studied in more details. Vapours of a homologous series of alcohols from methanol to pentanol were exposed in the gas phase to the thin films. It was demonstrated that a calibration and discrimination of the analytes is possible depending on the functional groups of the HBP, and the polarity of the analytes,

respectively [Bel02]. On the other hand, it was shown that the quantification of an unknown quaternary mixtures of methanol, ethanol, propanol and butanol in aqueous phase is possible using a combination of HBP and polyimide based sensors [Vol05]. Therefore, the main aim of this **Chapter** was to investigate the surface properties of HBPs in aqueous media using different surface-sensitive techniques. The morphology, thickness, and refractive indices of the initial HBP thin films were checked by scanning force microscopy and spectroscopic ellipsometry. The surface properties of HBPs controlled by the nature of terminal groups were determined by water contact angle and zeta potential measurements in aqueous solutions of different pH. The swelling behaviour of the films in the aqueous phase was monitored *in situ* by spectroscopic ellipsometry and zeta potential measurements.

3.2.2. Wafer cleaning technology

The objective of wafer cleaning is the removal of particulate and chemical impurities from the surface without damaging or deleteriously altering the substrate surface. The traditional approach of wafer cleaning is based on wet-chemical processes. There are a number of techniques employed for the wafer cleaning depending on the nature of the impurities that need to be removed from the surface. In general, the chemical cleaning is performed with a series of acid and rinse baths. Aqueous cleaning solutions are currently the most widely used due to their many advantages over alternative processes [Ker93].

To reveal the influence of the cleaning technology on the properties of the surface of polished silicon wafers covered by a thermally oxidized silicon dioxide of about 55 nm layer thickness used as substrates, two cleaning procedures were applied. As the first cleaning method (**M1**) only acetone (Merk, Germany) and reagent-grade water produced by Milli-Q filtration system were used to remove any impurities. After that the wafers were dried with argon stream.

In the second method (**M2**), the silicon wafers were cleaned at first using a dichloromethane of 99.5% purity (Acros, Germany) in an ultrasonic bath (2 times for 5 min). The ultrasonic shaking causes microscopic bubbles to form and collapse, creating shock waves that loosen and displace any particles. After that, a hydrogen-peroxide (HP) bath at 60 °C for 1 hour was applied. As a HP bath, a mixture of water, ammonia solution (25%, Merk, Germany) and hydrogen peroxide (30%, Merk,

Germany) in the volume ratio 1:1:1 was prepared [Min02]. After cleaning, the samples were rinsed with Milli-Q water and dried with argon. The HP bath slowly dissolves the outer surface oxide layer and forms a new one by oxidation of the surface. This oxide regeneration has a self-cleaning effect and helps the removal of particles by dislodging them.

Figure 3.2.1 shows the influence of the cleaning method on the charge of the wafer surface in the aqueous media measured by the zeta potential. The absolute value of the Isoelectric Point, *IEP*, that describes the chemical properties of the surface, of the cleaning method **M2** displaces on 0.4 pH units to the acid region. This difference

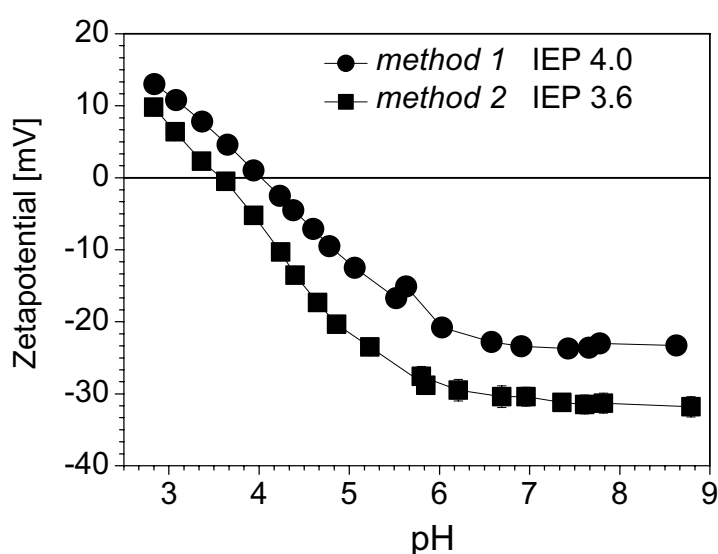


Fig. 3.2.1. Zeta potential for silicon wafers plotted as a function of pH: **M1** (●) and **M2** (■).

caused by the increased number of silanol groups (-Si-OH) available at the wafer surface. Moreover, the large difference between the values of the water contact angle corresponding to non cleaned wafers ($\sim 50^\circ$) and cleaned ones with method **M2** ($\sim 0^\circ$) was observed. AFM roughness analysis did not reveal any differences between these cleaning procedures.

3.2.3. Thin film preparation

HBP were spin coated (20 seconds, 3000 rpm, Model 6708D Desk-Top Precision Spin Coating System, Specialty Coating Systems, USA) as thin films from a 1.0 wt% tetrahydrofuran solution (THF, Merck, Germany). The thickness was ellipsometrically determined to be in the range from 30 to 40 nm. After preparation, the HBP films were annealed for different time above T_g in vacuum (at 240°C HBP-OH and HBP-COOH, at 180°C HBP-OAc and HBP-OH/OAc-1) to remove voids and inhomogeneities in the polymer films due to release of stress and to form a stable H-bonding network (checked for HBP-OH, see Chapter 3.1).

3.2.4. Methods applied to characterise HBP thin films in dry state and aqueous media

3.2.4.1. Contact Angle Method

The wettability of polymer films was investigated by advancing and receding contact angle measurements using a DSA 10 (Krüss, Germany) with deionized water (pH ~ 6.4). The measurements were performed in the open air at relative humidity of $40 \pm 2\%$ and at $24 \pm 1^\circ\text{C}$, which were kept constant. At least 9 separate measurements were used in averaging the contact angle. The solid surface tension (γ_{sv}) was calculated according **Eq. 1.8** and **Eq. 1.9**.

Dynamic contact angles were measured as a function of time by means of the Axisymmetric Drop Shape Analysis by Profile, ADSA-P (Chapter 1). The droplets of the water with a volume of 200 μl and a phosphate buffer saline (pH 7.4) with a volume of 50 μl were gently deposited onto the polymer surface. Small glass cell was used to prevent evaporation effects.

3.2.4.2. Atomic Force Microscopy (AFM)

Sample surface topography was examined using a scanning force microscope Nanoscope IIIa-D3100 (Digital Instruments, USA), operating in tapping mode. All images were taken for a dry surface under constant conditions at relative humidity of $50 \pm 5\%$ and at $24 \pm 1^\circ\text{C}$.

3.2.4.3. Electrokinetic measurements

Streaming potential measurements were carried out using an Elektrokinetic Analyser EKA (Anton Paar KG, Austria). Two wafers with the size of 10 x 20 mm each were inserted into the device between two measuring cell parts separated by a defined streaming channel. An electrolyte solution of 1×10^{-3} M KCl was pumped with increased pressure through the streaming channel. The streaming potential was measured for each pressure applied. The final value of the zeta potential was calculated from the slope of the experimental plot.

Changes in pH were achieved by addition of 0.1 M KOH or 0.1 M HCl. The streaming potential was detected using two Ag/AgCl electrodes. Due to the pressure difference, potential separation by shearing of the mobile parts of the electrochemical double layer takes place. Therefore, the streaming potential can be detected via electrodes

placed on the sample. Streaming potential was measured by the so-called tangential method, i.e. the electrolyte solution flows parallel to the polymer surface. The zeta potential was calculated from the *Helmholtz–Smoluchowski* equation (**Eq. 1.12**).

3.2.4.4. Ellipsometry

A rotating analyzer type variable angle multiwavelength ellipsometer M-44 (J.A. Woollam Co. Inc, USA) was used to determine the optical properties of substrates and thin films on these substrates in the wavelength range of 428 to 763 nm (see Chapter 1.2). Each ellipsometry measurement was started with determination of the thickness and refractive index of a dry film in air at 22°C and $45 \pm 5\%$ relative humidity. The refractive index of dry polymer films was measured using three angles of incidence 65, 70 and 75°.

The ellipsometric data were analysed using the *WVASE 32* software package. The refractive index n as well as the film thickness d were calculated from obtained ellipsometric data Ψ and Δ using the *Cauchy* layer optical model to describe the wavelength dependence of the refractive index:

$$n(\lambda) = A_n + \frac{B_n}{\lambda^2} \quad (3.1)$$

where n is the index of refraction, λ is the wavelength [μm], A_n and B_n are the *Cauchy* parameters.

Note, that the HBP films are non-absorbing ($k = 0$) in the used visible spectral range. The behaviour of the polymer thin films in aqueous media was investigated in a quartz cell in the central area of which a sample was positioned and held by a special holder (**Figure 3.2.2**). The light beam was directed to the middle of the sample surface at an incidence angle of 68°. To consider a possible influence of cell adjustment and window effects on the data the thickness of the polymer film being in the cell was re-examined before filling with buffer solution. Then, a buffer solution of 3.0 ml volume was introduced into the cell using an Eppendorf syringe. Immediately afterwards, subsequent time dependent ellipsometry autoscan was started to obtain the equilibrium swollen state of the polymer film for at least 300 minutes.

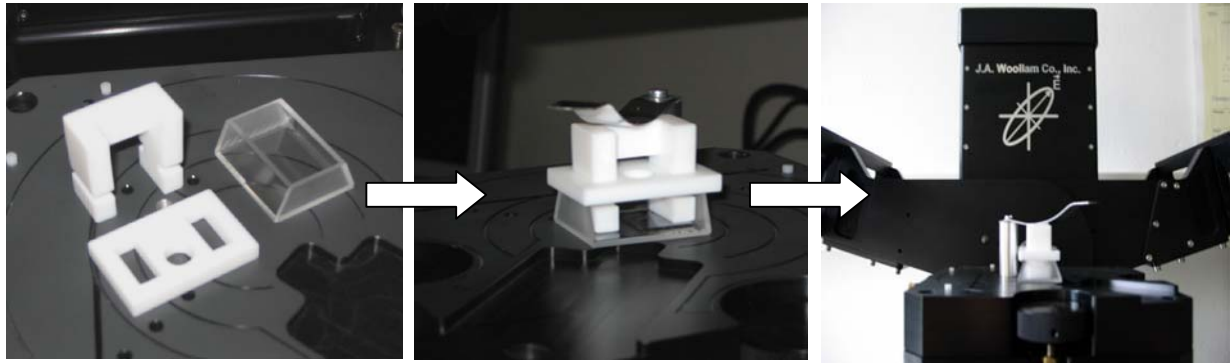


Fig. 3.2.2. Liquid cell for in situ ellipsometric measurements at solid-liquid interface.

For the evaluation of changes in the layer thickness and refractive index due to swelling of the polymer film the optical model illustrated in **Figure 3.2.3** was applied.

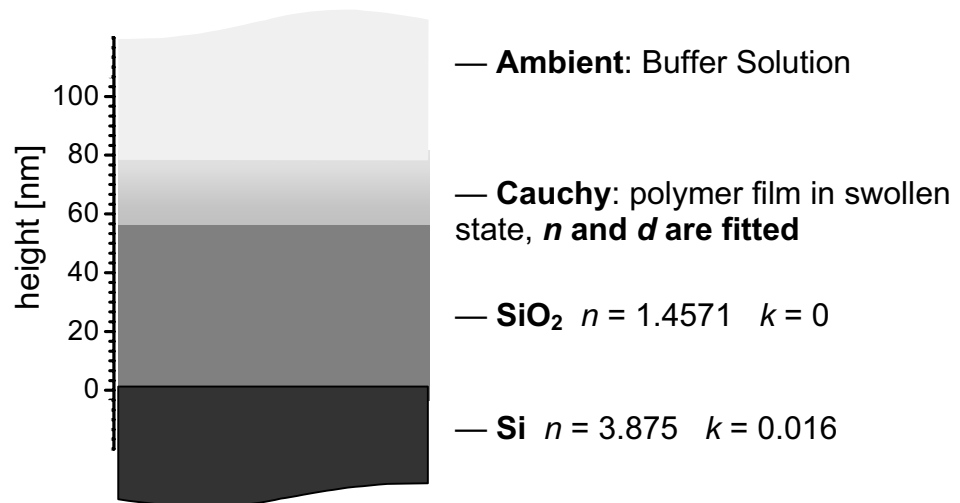


Fig. 3.2.3. Optical model, used for the fitting of the ellipsometric data to obtain the refractive index n and the thickness d of the swollen HBP films.

Again, a *Cauchy* layer model was used for the swollen polymer film. The equilibrium *out of plane* swelling degree (SD) was calculated as follows:

$$SD(\%) = \frac{D_{\infty} - D_0}{D_0} \times 100 \quad (3.2)$$

where D_{∞} and D_0 are equilibrium thickness values of the polymer film in swollen and dry state, respectively.

The actual refractive index of the pure buffer solution was separately determined from an independent spectroscopic ellipsometry scan under the same conditions in the solid-liquid cell using a well-known silicon wafer as inert reference sample:

$$n(PBS) = (1.321 \pm 0.0005) + \frac{(0.0023 \pm 0.0013)}{\lambda^2} \quad (3.3)$$

3.2.5. Role of end groups functionality on surface properties of HBP films: -OH, -COOH, -OH/OCOCH₃ and -OCOCH₃

Thin films of HBPs have been prepared by spin-coating from THF solution on silicon wafers. It is well known that the topology of polymer surfaces has a very strong influence on experimental data obtained by different surface sensitive techniques such as contact angle, zeta potential, ellipsometry and others. Therefore, an appropriate preparation of polymer films with a high reproducibility is very important. As it can be seen from the AFM images, (**Figure 3.2.4**), HBP films in the thickness range from 10 to 100 nm have very smooth and homogeneous surfaces with a resulting roughness (*rms*) of about 1 nm. From these results, we conclude that the subsequently obtained surface characteristics are controlled to a very large extent by the surface chemistry and not the topology.

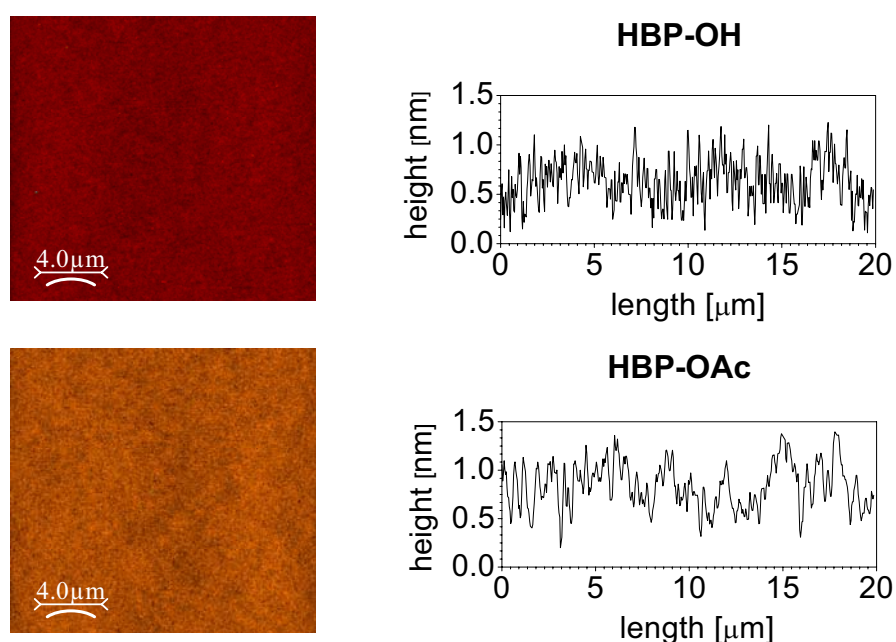


Fig. 3.2.4. Topographical and corresponding section AFM images of HBP-OH and HBP-OAc with scan size of 20 μm x 20 μm.

The results of the water contact angle measurements for HBP films are presented in **Figure 3.2.5**. Annealing of the thin films of HBPs having terminal groups of high polarity (HBP-OH and HBP-COOH) results in an increase of the advancing contact angle. The significant changes in the surface properties in terms of surface free energy (γ_{sv}) were obtained when the samples were annealed above T_g at least for one hour. Prolonged annealing did not further influence the surface free energy of HBP-OH and HBP-OAc remarkably. It is interesting to note that the annealed surfaces of different HBPs show the mean equilibrium value of about $38 \pm 1 \text{ mJ/m}^2$. These changes might be influenced by a structural reorganization of hydrophobic and hydrophilic segments, and hydrogen bonded network reorganisation due to temperature (see Chapter 3.1) in order to become better segregated within the film [Tan01, Tan02].

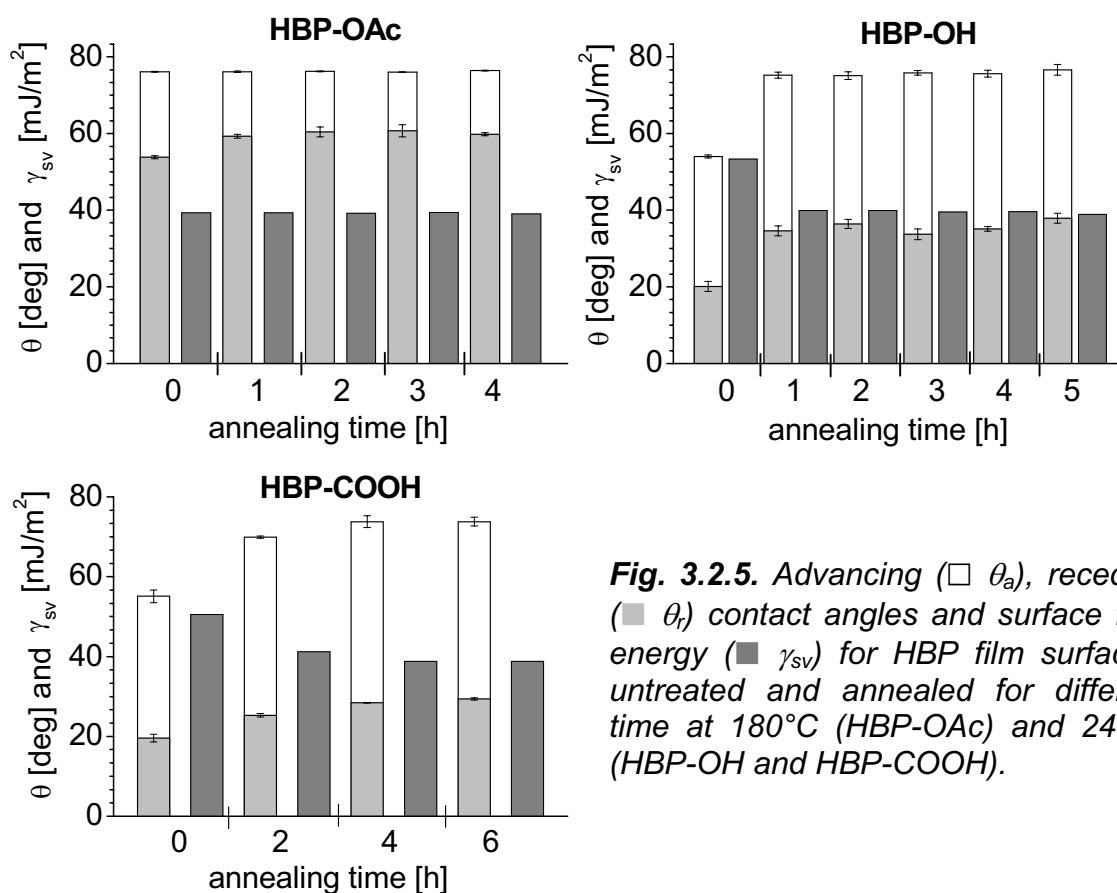


Fig. 3.2.5. Advancing ($\square \theta_a$), receding ($\blacksquare \theta_r$) contact angles and surface free energy ($\blacksquare \gamma_{sv}$) for HBP film surfaces, untreated and annealed for different time at 180°C (HBP-OAc) and 240°C (HBP-OH and HBP-COOH).

The surface-energetic properties of the HBP-COOH films were changed similarly to the HBP-OH films by the annealing. The originally hydrophilic HBP-COOH surface was changed into a surface with a lower surface free energy. In this case only after annealing time of 4 hours, no further change in the surface properties was observed. These changes in the surface hydrophobicity are attributed mainly to the inter- and

intramolecular re-association of hydrogen bonds between carboxylic groups of HBP-COOH which occur during annealing and lead to an increase of both contact angles (see Chapter 3.3).

After annealing of the polymer films for 1 hour, a decrease in the film thickness of 5.5, 9.1 and 2.6% and an increase in the refractive index of about 0.3, 0.2 and 0.1% for HBP-OH, HBP-COOH and HBP-OAc were revealed due to restructuring of the polymer molecules resulting in a closed and homogeneous film. Significant influence of the polymer film thickness on the value of the contact angle measurements was not observed. The influence of the varying thickness of untreated HBP films on the refractive index of the polymer film at $\lambda = 630$ nm is presented in **Figure 3.2.6**. It was found that the refractive index (which can be correlated to material density as well) decreases with increase of the film thickness. In the case of films with thickness between 30 and 40 nm, the values of the refractive index were measured to be 1.651 ± 0.002 for HBP-OH, 1.610 ± 0.003 for HBP-OH/OAc-1, 1.592 ± 0.001 for HBP-OAc and 1.630 ± 0.001 for HBP-COOH.

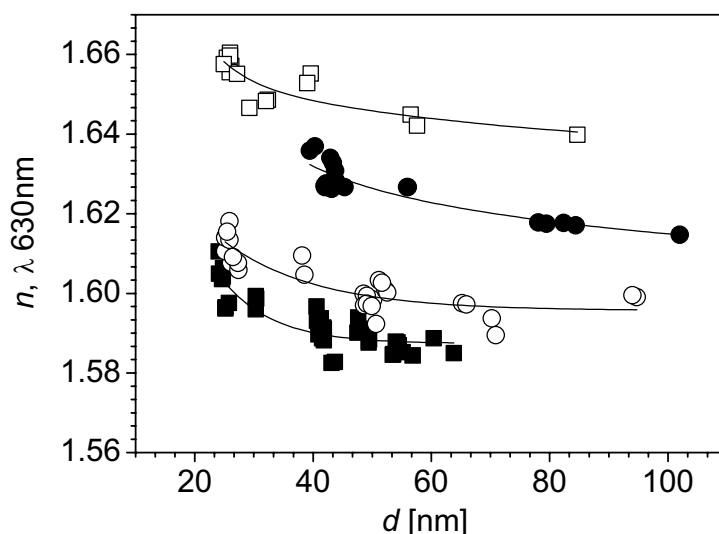


Fig. 3.2.6. Changes in the refractive index n at λ 630 nm of untreated HBP films as a function of layer thickness: HBP-OH (\square), HBP-COOH (\bullet), HBP-OH/OAc-1 (\circ), HBP-OAc (\blacksquare).

Interesting results were obtained on thin films of HBP-OH/OAc-1 (22.5 mol-% of phenolic groups, see Chapter 2.4.1) using broadband dielectric spectroscopy employed to investigate the molecular dynamics of these films [Ser05]. It was found that with decreasing film thickness and increasing refractive index, the slower relaxation modes of the dynamic glass transition are gradually suppressed, resulting

in an increase of the average relaxation rate and in a linear decrease of the dielectric strength. This behaviour was attributed to an immobilization of the polymeric segments at the periphery of the HBP molecules in the confinement of very thin films.

3.2.6. Stability, equilibrium swelling, kinetics and swelling degree of HBP thin films in aqueous media

Polymers containing a large fraction of hydrophilic groups are likely to swell when immersed into aqueous media, especially into electrolyte solutions. Therefore, the possible *self-organisation* or *self-cross linking* due to noncovalent interactions such as hydrogen bonding is of great importance in order to be able to understand the dynamics in films immersed in an aqueous medium.

As just mentioned, the results obtained by the temperature dependent FTIR spectroscopy (see Chapter 3.1) showed that HBP-OH forms a stable network of hydrogen bonds through the interactions between the hydroxyl groups or hydroxyl and ester groups of the same or neighbouring molecules. The applied cycles showed the changes in the association of hydrogen bonding and an increase of the fraction of strongly associated carbonyl groups due to heating up to a temperature above T_g . Furthermore, *Sun* and *Crooks* [Sun02] observed strong adhesion of dendrimer molecules of the sixth-generation poly(amido amine) to the mica surface. The authors supposed that the electrostatic attraction and especially, the formation of hydrogen bonds between functional groups of the dendrimers and the mica surface and also between neighbouring dendrimer molecules play a key role in the stability of the non-covalently attached layers in the liquid phase.

To investigate the stability and swelling behaviour of HBP-OH films in an aqueous medium (PBS, pH 7.4; phosphate buffered saline: Na_2HPO_4 , KH_2PO_4 , KCl, NaCl) as a function of annealing time of the initial samples, the variation of Ψ and Δ with time was monitored by ellipsometry at the solid-liquid (polymer-aqueous solution) interface. So, time-dependent data of the HBP-OH film thickness and refractive index were obtained. The swelling kinetics of the HBP-OH films (annealed for 3 hours before a swelling experiment) is plotted in **Figure 3.2.7**. Changes in refractive index and thickness of the films indicate a typical swelling process which can be described by a **two steps mechanism**:

During the first step, already about 90 % of the total amount of the soaked buffer is absorbed into the film within a few seconds. This can be classified by the Fickian moisture diffusion [Tan04]. Buffer molecules penetrate into micro-voids and free volume of HBP, interacting via hydrogen bonds. As a result of the corresponding out-of-plane expansion, an increase of the thickness is observed. At the same time, the uptake of the “optical thinner” buffer solution (n at 630 nm = 1.327) gives a decrease of the effective refractive index of the swollen “effective” layer consisting of polymer and penetrated buffer. The second, much slower step is due to relaxation processes within the layers. The changes in conformation of the polymer molecules allow the absorption of an additional amount of buffer by the layer [Tan01, Tan02].

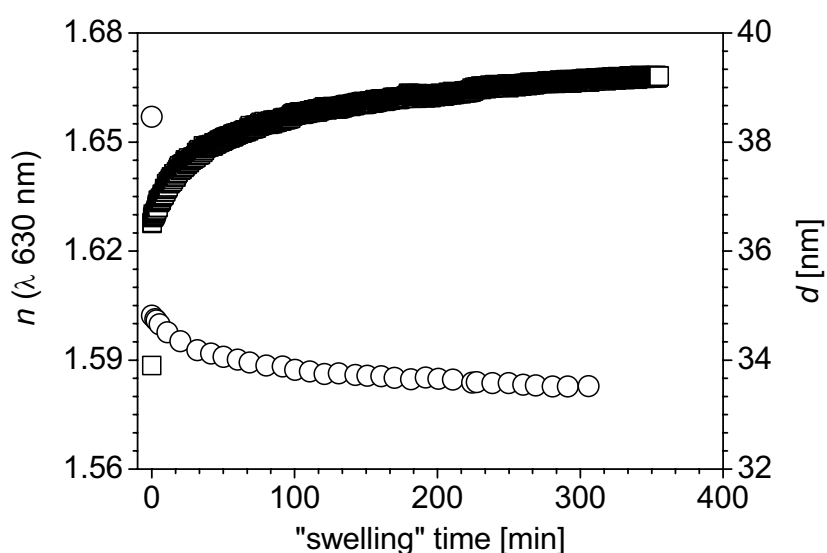


Fig. 3.2.7. Typical curves of changes in layer thickness d (□) and refractive index n at λ 630 nm (○) with time due to swelling of an HBP-OH film (annealed for 3 hours / 240°C).

The strong effect of annealing time of the initial HBP-OH films on the changes in refractive index and thickness of the films during swelling is illustrated in **Figure 3.2.8**. An increase of the annealing time leads to a decrease of the equilibrium swelling degree (SD) and an increase of the equilibrium refractive index n due to a lower buffer uptake. Similar SD values for HBP-OH annealed from 3 to 5 hours show that an annealing time of up to 3 hours is enough for complete segment reorganization within the polymer film. It was found that the values obtained for the HBP-OH films annealed from 2 to 5 hours are similar resulting in a refractive index of about 1.582. These results are in a good agreement with the data obtained by the temperature-dependent FTIR spectroscopy showing the formation of the better ordered and thermally stable network of hydrogen bonds after the first HAC cycle

(Chapter 3.1). Thus, an increase of the annealing time reduces the buffer solution uptake of the film due to increasing the polymer density by forming a stable network of inter- and intramolecular hydrogen bonds through the interactions between the hydroxyl groups or hydroxyl and ester groups of HBP-OH.

To examine the reversibility of swelling, the HBP-OH films were removed from the buffer solutions after reaching the swelling equilibrium, rinsed with deionised water, dried under an argon stream, and stored under constant conditions for three days. The HBP-OH layers were re-examined having a thickness variation upon swelling of about 4% from the initial state. Hence, a nearly complete reversible swelling process occurs.

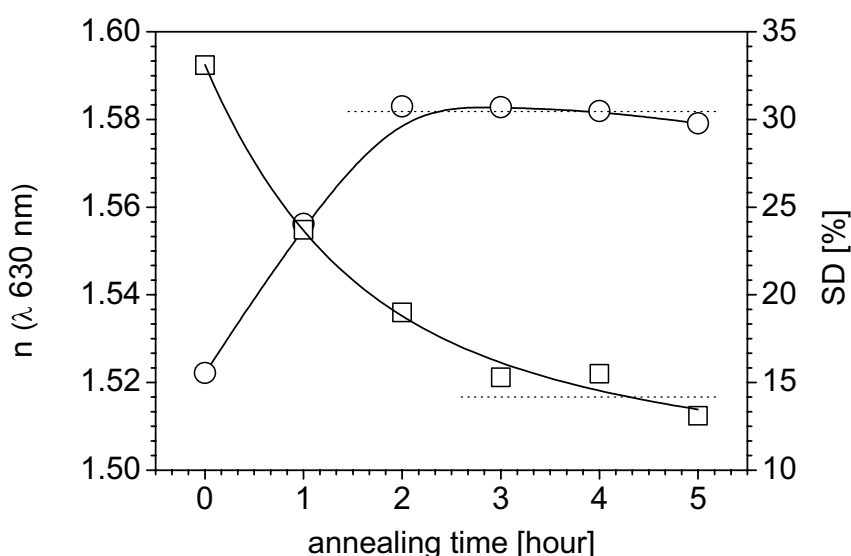


Fig. 3.2.8. Equilibrium swelling degree SD (\square) and equilibrium refractive index n (\circ) at $\lambda = 630$ nm of the HBP-OH films in the swollen state as function of the annealing time of the initial samples.

The stability of all HBP thin films untreated and annealed for 1 hour was examined using aqueous solutions of different pH. The HBP films immersed in buffer solution of pH 10.0 (buffer compounds: boric acid, KCl, NaOH; Bernd Kraft GmbH, Germany) were not stable and partly removed from a substrate. An apparent low level of SD of about ~15 % for untreated and annealed (240 °C) HBP-OH films using pH 4.0 (buffer compounds: citric acid, NaOH, HCl; Bernd Kraft GmbH, Germany) was obtained. The Milli-Q water (pH ~ 6.5) was applied to decrease the influence of buffer components on the results obtained. The values of SD for untreated and annealed HBP-OH thin films were found to be 25.1 and 19.6 %, which are lower compared to SD of about 33.1 and 23.7 % obtained for films swelled at pH 7.4.

The annealing of the HBP-OH/OAc-1 thin films (180 °C) did not reveal a significant influence on the values of SD obtained for different pH. The SD data obtained for the films immersed in water, buffer solutions of pH 4.0 and 7.4 were found in the range from 10 to 15 %. The HBP-COOH thin films showed strong dependence of the annealing procedure on the swelling behaviour. The SD data obtained for untreated and annealed (240 °C) HBP-COOH films were found to be 30.4 and 25.0 % for buffer solution of pH 4.0, 52.0 and 31.6 % for the Milli-Q water. Thus, it appears that the swelling properties of HBP thin films are governed not only by the annealing procedure but also by their environment.

The changes in wettability of an untreated and an annealed (for 3 hours at 240 °C) HBP-OH film during its contact with water was studied via measurements of advancing contact angles using ADSA-P (Figure 3.2.9). Since the buffer is a multicomponent solution, the water was used at first in order to minimise the number of influencing factors (ions) on the obtained results.

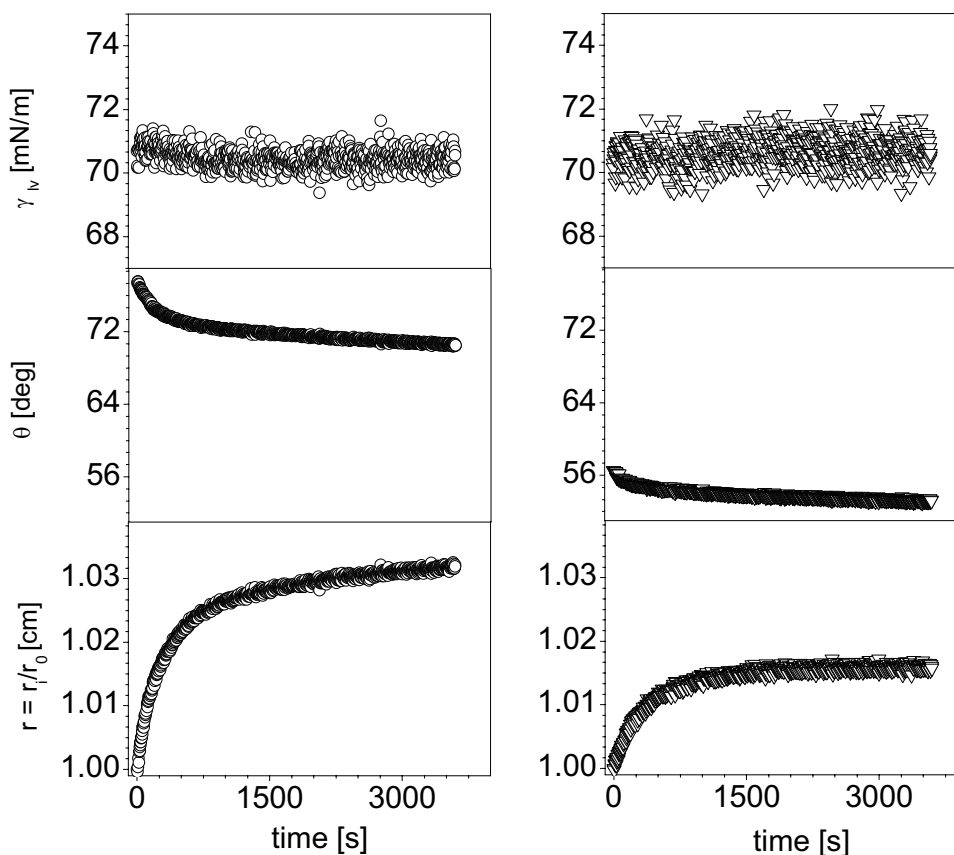


Fig. 3.2.9. Time-dependent changes in liquid/vapour interfacial tension γ_{lv} , advancing contact angle θ_a and contact radius r using water measured on untreated (∇ , right) and annealed (\circ , left) HBP-OH films.

It can be seen clearly that the contact angles decrease with time, i.e. the hydrophilicity of the surface increases. These significant changes in the contact radius r and advancing contact angle θ_a can be attributed mainly to the spreading of water droplet on the surface and a partial swelling, i.e., penetration of water molecules into the bulk phase of the polymer film [Sed96, Kis99, Hen04]. Both curves of θ_a and r of an untreated and an annealed HBP-OH film have similar kinetics and reached a plateau after 15 minutes. These results showed a good agreement with the data of the swelling kinetics (**Figure 3.2.7**) obtained using spectroscopic ellipsometer. The observed strong decrease in θ_a and r within the first 10 minutes (first step of the swelling kinetics) is due to water penetration within the film and also the relaxation of hydroxyl groups at the surface, i.e., weakening and destruction of the existent network of hydrogen bonds and creation of a new one.

To reveal the influence of the chemical composition of HBPs, the contact angle measurement with a limited number of components under the same conditions in order to follow the progress in the surface wettability by buffer was applied. **Figure 3.2.10** shows the changes of γ_{lv} , θ_a and r during the contact of the PBS (pH = 7.4) droplet with the untreated surfaces of HBP-OH and HBP-OAc. No changes in γ_{lv} for both HBPs were obtained during the time of the measurement (10 minutes). The similar character of the curves, i.e. a decrease of θ_a and an increase of r is indeed the direct consequence of the swelling of HBP films [Sed96]. The results presented in **Table 3.2.1** reflect the changes in θ_a during the measured time. There was no effect of the hydrophobicity of HBP surface on the spreading of the PBS or/and water droplets on the polymer film observed. Surprisingly, the untreated HBP-OH did not show any difference in the hydrophilic character of the surface due to contact with PBS solution compared to the water.

Table 3.2.1. Changes in θ_a due to contact PBS and water droplets with the surfaces of untreated HBP-OH and HBP-OAc during 10 minutes.

advancing contact angle	PBS		water
	HBP-OAc	HBP-OH	HBP-OH
θ_0	76.1	57.0	56.5
θ_{10}	73.6	55.0	54.6
$\Delta\theta = \theta_0 - \theta_{10}$	2.5	2.0	1.9

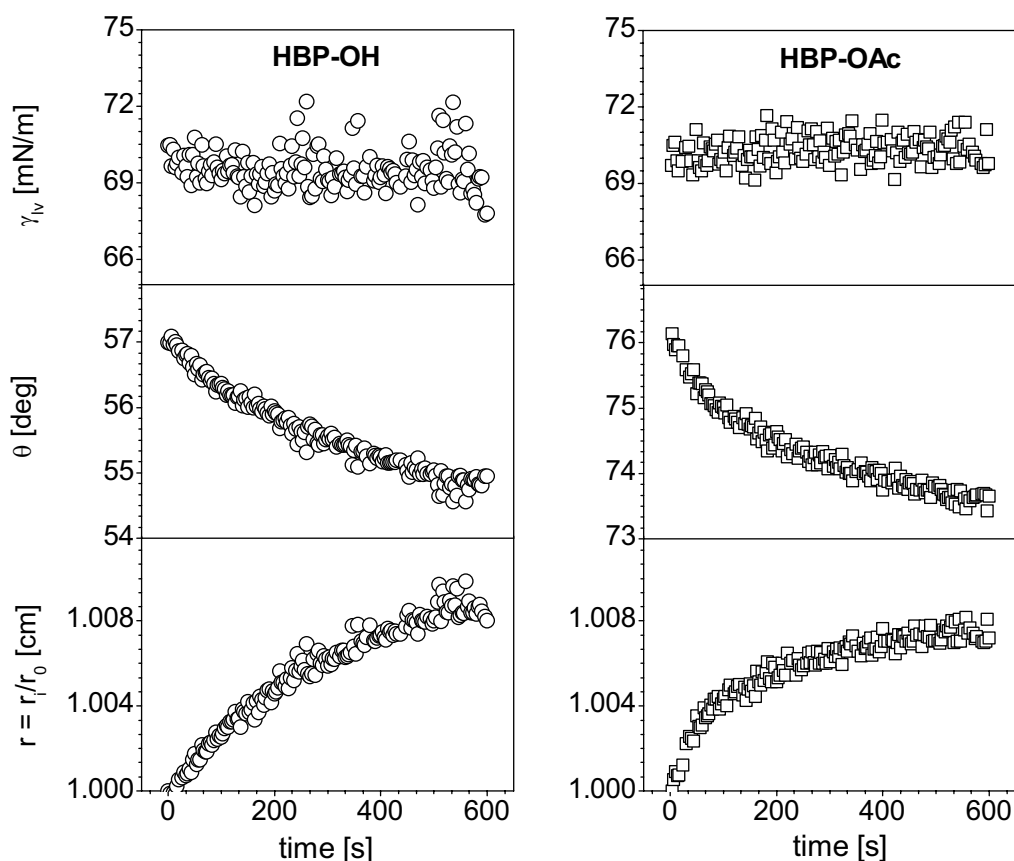


Fig. 3.2.10. Time-dependent changes in liquid/vapour interfacial tension γ_{lv} , advancing contact angle θ_a and contact radius r using PBS measured on HBP-OAc and HBP-OH) films.

Zeta potential measurements were performed to provide information on the stability and charging behaviour of polymer surface immersed in an electrolyte solution. The influence of annealing of thin films on the electrochemical double layer composition due to swelling process [Bel04] is shown in **Figure 3.2.11**. The surfaces of the untreated HBP-OH and HBP-OH/OAc-1 showed a strong decrease of the zeta potential vs. time. This can be attributed mainly to a higher number of an ionisable hydroxyl surface groups in a swollen layer compared to the surface of annealed films. In this case, the equilibrium swollen state was not reached whereas for the annealed HBP-OH and HBP-OH/OAc-1 surfaces a stable state was observed after a few minutes. The surface of HBP-COOH did not reveal significant changes of the annealing procedure on the film stability. As mentioned, annealing of thin films of HBP-COOH leads to an inter- and intramolecular hydrogen bond network formation of carboxyl groups of HBP-COOH and between HBP-COOH and hydroxyl surface groups of a silicon wafer [Bey01]. However, the formed network is not strong enough to withstand the influence of flowing electrolyte solution and dissociation of carboxyl

groups. There was no difference observed between annealed and untreated HBP-OAc films. These results agree well with the data obtained by the spectroscopic ellipsometer which showed relatively good stability of the HBP-OAc thin films in aqueous media of different pH.

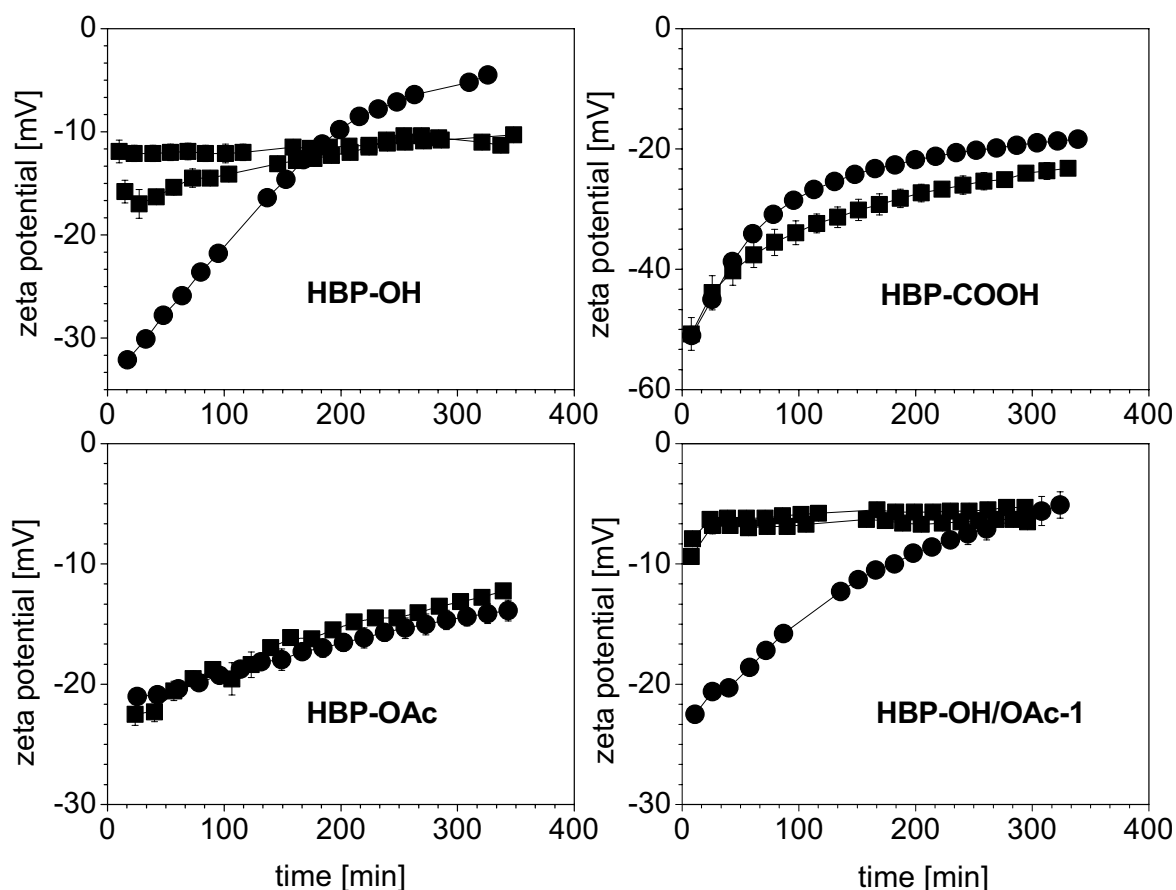


Fig 3.2.11. Zeta potential of untreated (●) and annealed for 1 hour (■) HBP films as a function of time: at 240°C HBP-OH and HBP-COOH, at 180°C HBP-OAc and HBP-OH/OAc-1.

To reveal the influence of the annealing process on the changes in the chemical composition of HBP surfaces in the liquid phase the zeta potential was measured as a function of pH (**Figure 3.2.12**). The pH value was varied between 2.5 and 6.0. It can be seen that the zeta potential as a function of pH is linear except the HBP-COOH. Moreover, the surface of HBP-OAc showed a lower values of Isoelectric Point (*IEP*) compared to the surfaces of the HBP-OH and HBP-OH/OAc-1 (**Table 3.2.2**). There are two potential factors influencing the values of the *IEP*: The first one is the adsorption of the simple electrolyte ions from the aqueous solution: K^+ , Cl^- , H_3O^+ , OH^- . For instance, *Zimmermann et al.* [Zim01] observed a high relevance of unsymmetrical (preferential) adsorption of ions as the origin of charge formation at

nonpolar polymer material (Teflon AF) in aqueous environment. The *IEP* was obtained at pH 4.0 at different KCl concentrations applied. They found that the preferential adsorption of hydroxyl ions (OH^-) is predominated as compared to the adsorption of hydronium ions (H_3O^+) at similar concentrations (neutral pH). The authors also showed that in this case there was no effect of the preferential adsorption induced by chloride and potassium ions. Furthermore, the *IEP* of the surface of photo-attached polystyrene ($\theta_a = 89.4$) was obtained at 4.4 pH units [Ger04].

The second influencing factor is the possible hydrolysis of the surface ester groups with subsequent dissociation of the acetic acid during the relatively long time of contact of the HBP-OAc with an electrolyte solution. Thus, the surface becomes more hydrophilic because of the formed hydroxyl surface groups and the dissociated carboxyl groups of the acetic acid located on the top of the surface of the HBP-OAc. Usually, these two processes, the adsorption of ions and the dissociation of surface groups, can exist parallel. However, one process can predominate over another one thereby determine the charge of a polymer surface.

Furthermore, only a slight difference was obtained between *IEP* belonging to the untreated and annealed HBP-OH and HBP-OH/OAc-1. The small displacement of *IEP* of annealed surface on 0.3 pH units to the basic region might be caused by the decreased number of the acidic OH surface groups on the top of the surface of annealed HBP-OH and HBP-OH/OAc-1 films due to segments rearrangement of molecules during heating above T_g , promoting low amount of adsorbed ions. The similar values of *IEP* of HBP-OH/OAc-1 compared to the HBP-OH can be effected by the strong influence of the hydroxyl surface groups of amount of 22.5 mol-% (see Chapter 2.4.1).

The charge of the HBP-COOH surface showed the lowest values of *IEP* which is promoted mostly by the dissociation of the carboxyl surface groups (pKa of benzoic acid is 4.20) due to their contact with an electrolyte solution.

Table 3.2.2. IEP for untreated and annealed for 1 hour at 240°C HBP-COOH and HBP-OH, at 180°C HBP-OAc and HBP-OH/OAc-1 films.

	surface	HBP-OH	HBP-OH/OAc-1	HBP-OAc	HBP-COOH
IEP	untreated	4.2	4.2	3.8	3.3
	annealed	4.5	4.6	4.1	3.5

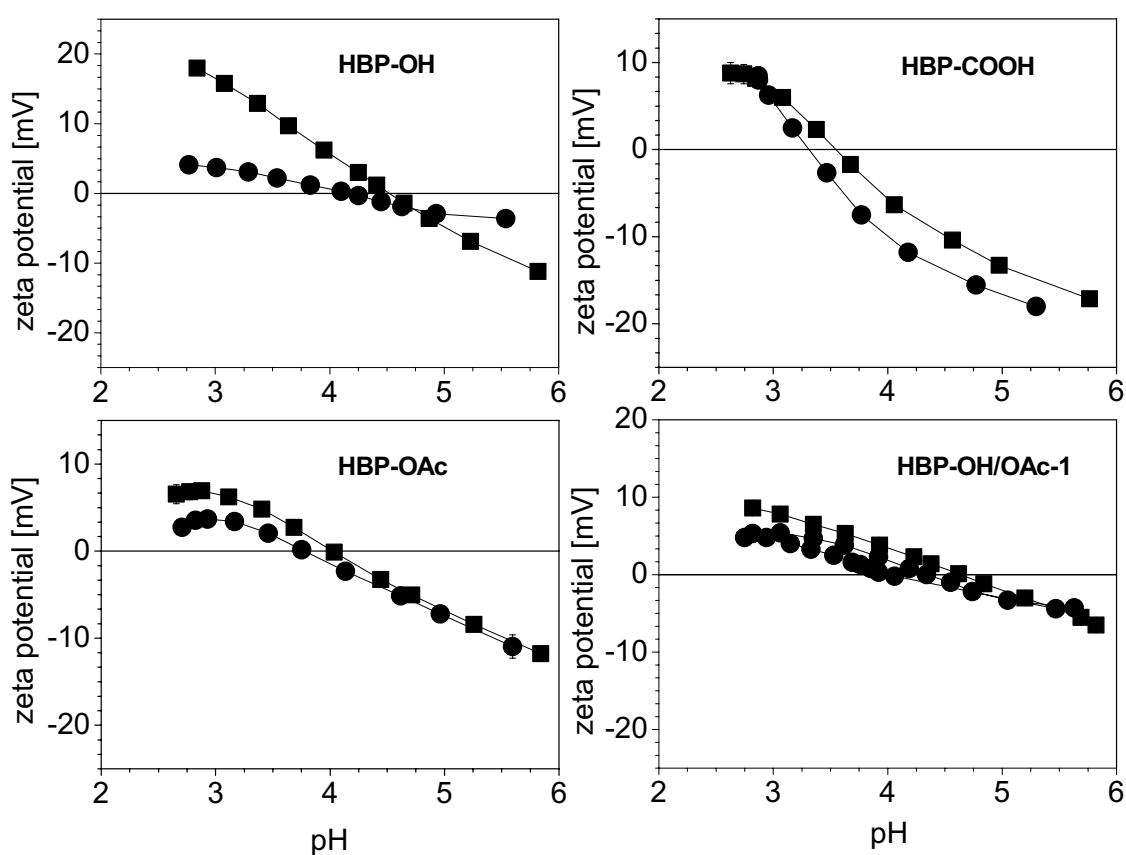


Fig 3.2.12. Zeta potential for HBP surfaces plotted as a function of pH: untreated (●) and annealed for 1 hour (■) at 240°C HBP-OH and HBP-COOH, at 180°C HBP-OAc and HBP-OH/OAc-1.

3.2.7. Conclusions

In conclusion, it has been found that the surface properties of very smooth aromatic HBP thin films depend on the annealing procedure. The difference in the water contact angles for differently treated HBP surfaces, untreated and annealed ones was observed. There is, however, after 1h annealing time no further significant effect of the annealing time on the contact angles measured and, consequently, on the surface free energy calculated for HBP-OH and HBP-OAc. Film thickness and annealing procedure were found to have a significant influence on the value of the refractive index which can be correlated to the film density.

Spectroscopic ellipsometry was applied *in situ* to study the swelling dynamics of HBP thin films in electrolyte solutions of pH 4.0 and 7.4, and water (pH~6.5). It was shown that all polymer films swell significantly, reversibly and had similar kinetics (very fast initial phase with reaching a plateau). However, thin films of HBP-COOH were not stable at pH above 7.

The *SD* data and equilibrium refractive index indicate that the formation of a compact and dense layer structure within HBP-OH films due to hydrogen bonding among terminal hydroxyl groups occurred after 3 hours of annealing.

The changes in the advancing contact angle due to contact of the polymer surface with water and PBS droplet depend on a combined effect of layer swelling and droplet spreading due to attraction of water molecules and electrolyte ions to the hydrophilic surface groups.

Therefore, for the application of HBP films as biofunctional materials, a control of the properties of HBP thin films immersed in an aqueous solution is necessary, when subsequent protein adsorption experiments will be carried out.

3.3. Preparation and characterisation of grafted films of carboxyl terminated hyperbranched aromatic polyester, HBP-COOH

Abstract

In this Chapter, the strategy for the fabrication of surface attached carboxyl terminated hyperbranched polyester HBP-COOH that is based on “grafting to” technique is presented. The branched chemical architecture with multiple carboxyl groups should provide an excellent grafting capability including surface functionality. Moreover, the high ageing temperature applied allows the formation of an inter- and intramolecular hydrogen bonded network (self-cross linking).

3.3.1. Hyperbranched polymers on solid surfaces

The control of the surface properties and the stability of polymer thin films is of a great importance in numerous technologies, such as biotechnology and advanced microelectronics (biosensors) [Bel02, Vol05]. The attachment of the polymers to a solid substrate is often necessary to enhance the stability of the films in different environments. The formation of the attached polymer layer is generally carried out using either of two techniques, namely physisorption or chemical bonding of polymer molecules to a substrate. Commonly, the choice of the attachment techniques is governed by the chemical composition of a polymer used.

The great advantage of hyperbranched polymers (HBPs) is that they usually demonstrate a high thermal stability and have large number of functional groups (Chapter 2). These polymers can form uniform layers with a significant fraction of functional groups located on the top of the surface. Several strategies were developed for the effective fabrication of the stable HBP layers. For instance, *Crooks et al.* [Bru97, Hie98, Wel96] observed fairly uniform layers of functional HBPs with controlled chemical composition and thickness obtained by the “grafting from” technique. Moreover, *Zhou et al.* [Zho96] reported the preparation of a highly branched poly(acrylic acid) films attached to a self-assembled monolayer of mercaptoundecanoic acid on gold using a series of repeated “grafting to” steps. The

fabrication of a molecular surface coating from an epoxy-functionalised hyperbranched polyester functionalised by secondary epoxy groups was studied by *Sidorenko et al.* [Sid02a]. The authors demonstrated the formation of a uniform monolayer with extremely robust and sustain high compression obtained by melt grafting of functionalised hyperbranched polymers to a bare silicon surface.

In the present **Chapter 3.3**, the fabrication of thin films from the carboxyl terminated hyperbranched polyester (HBP-COOH) chemically grafted to the surface of silicon wafers is described. Each step of the surface modification was controlled with ellipsometry, atomic force microscopy (AFM) and contact angle method.

3.3.2. Hyperbranched molecules with carboxyl terminal groups: Grafting to a solid surface (silicon wafer)

The grafted HBP-COOH films were prepared by two-step procedure using 3-glycidoxy-propyltrimethoxy silane (GPS, ABCR GmbH, Karlsruhe, Germany) as a coupling agent (**Figure 3.3.1**) [Min02]. For the chemisorption of GPS to the activated surface (see Chapter 3.2.2) of silicon wafers (Wacker Chemitronics, Germany) with native silicon dioxide of about 2 nm layer thickness a 1 wt% GPS solution in dry toluene (Merck, Germany) was used. The wafers were kept for 16 hours under argon atmosphere (<1 ppm H₂O) to avoid polymerisation of GPS. Then the wafers were washed two times in dry toluene in the argon box and three times in ethanol (Carl Roth GmbH&Co, Germany) to remove the non-attached GPS molecules. After that the wafers were dried under argon stream. HBP-COOH was dip coated (developed at IPF, Dresden, Germany) in 2 wt% tetrahydrofuran (THF, Merck, Germany) or methanol (Merck, Germany) solutions. Then the samples were annealed at 240 °C in vacuum oven (Transparent Drying Oven Buchi model T0-51, Jepson Bolton & Co Ltd, UK) for different time. The non-attached HBP-COOH was removed by THF or methanol Soxhlet extraction for 4 hours.

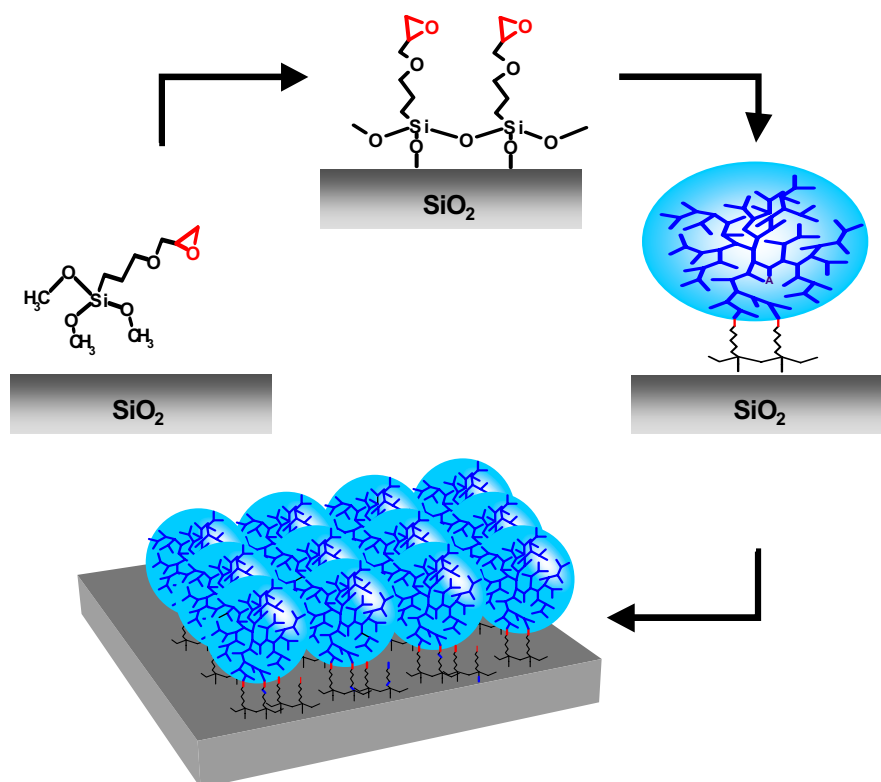


Fig. 3.3.1. Grafting of HBP-COOH to the silicon substrate.

3.3.3. Analytical methods

3.3.3.1. Investigation of hydrogen bonding formation during grafting reaction by temperature-dependent FTIR spectroscopy

Temperature-dependent IR transmission measurements were made analogously as described in Chapter 3.1. The samples were prepared as films on KBr substrates by solvent casting from 5.0 wt% THF solution as reported in Chapter 3.1.2.

3.3.3.2. Surface properties of attached HBP-COOH films

The advancing and receding contact angles of water were measured using DSA Krüss (Germany) as described in Chapter 3.2.3.

3.3.3.3. Ellipsometry

The Single Wavelength ellipsometer (SE402 Mapping ellipsometer, Sentech) with a He-Ne laser at $\lambda = 633$ nm and an angle of incidence 70° was used for the monitoring of each step of the “grafting to” process. The thickness of the native

silicon dioxide layer was calculated to be 1.7 ± 0.1 nm at refractive indices $n = 1.457$ ($k = 0$) for the silicon dioxide layer and $N = 3.875 - i0.016$ for the silicon substrate. The thickness of the GPS ($n = 1.429$) [Min02] monolayer was evaluated as 0.6 ± 0.2 nm using three layer model: Si/SiO₂/GPS. The thickness of HBP-COOH layer was calculated using the corresponding refractive indices of the polymer determined by spectroscopic ellipsometry (see Chapter 3.2.4).

3.3.4. Fabrication of surface attached HBP-COOH by “grafting to” technique

During the grafting of the HBP-COOH ($T_g = 214^\circ\text{C}$) to the GPS layer at the temperature above T_g (240°C), two parallel processes may occur. The first is the reaction between the carboxylic groups of the HBP-COOH and the epoxy groups of GPS. However, the nature of GPS molecules gave rise to several types of surface functionalities due to hydrolysis of the epoxy rings by traces of water (**Figure 3.3.2**) [Min02, Luz00]. For instance, *Minko et al.* [Min02] applied X-ray photoelectron spectroscopy (XPS) and ATR-FTIR spectroscopy for the analysis of the chemisorbed GPS layer. They showed that grafted GPS contains only a small fraction of epoxy groups of about 5-10 %. Most of them have undergone a ring-opening reaction and isomerization to carbonyl groups or even oxidation. However, the hydrolysis of the epoxy rings produces also the hydroxyl groups which can be used for the further attachment of the polymer.

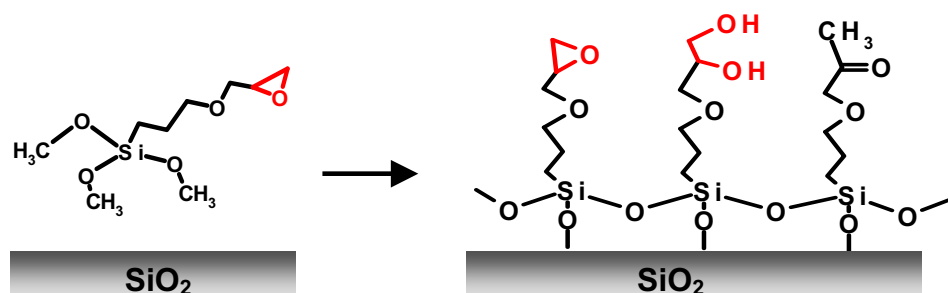


Fig. 3.3.2. Schematic representation of GPS chemisorbed layer [Min02].

The second process is the “self-cross linking” of the HBP-COOH with the formation of the inter- and intramolecular hydrogen bonds due to treatment using high temperature. The latter can influence the subsequent extraction of non-attached polymer molecules.

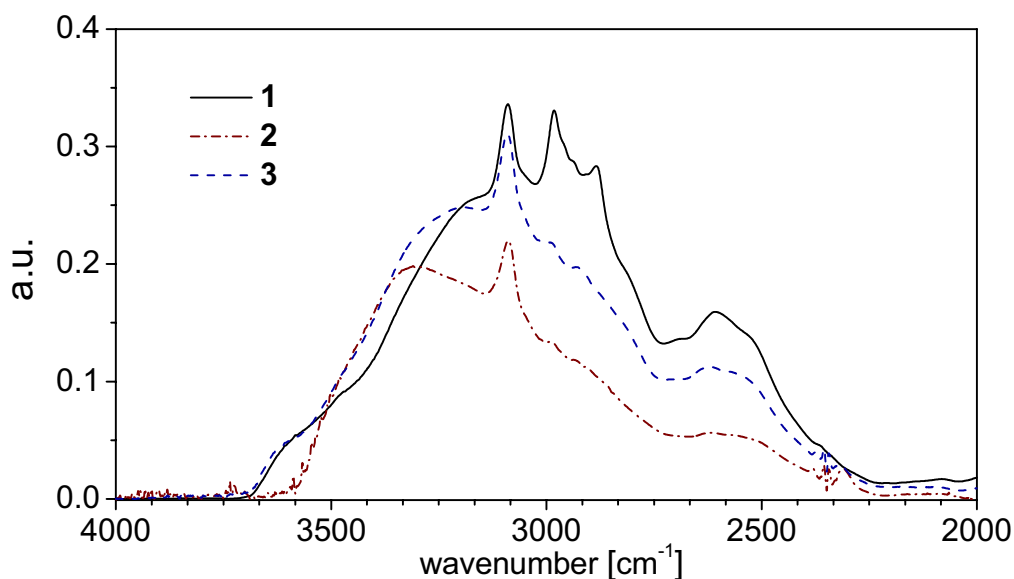


Fig. 3.3.3. The hydroxyl vibrations ($\nu\text{O-H}$) of HBP-COOH: (1) before heating up at 25°C; (2) after 6 hours of annealing at 235 °C; (3) after cooling down at 26 °C.

The IR spectrum of the initial HBP-COOH in the full mid-infrared spectral region is given in **Figure 2.5**. The broad band of the carbonyl region is attributed to the combined effect of the ester carbonyl ($\nu\text{C=O}$, 1744 cm^{-1}) and the complex band (weak and strong bonded -COOH) [Bey01] of hydrogen bonded carboxyl groups ($\nu\text{C=O}$ in -COOH, 1704 cm^{-1}). Therefore for the interpretation of the hydrogen bond network re- and/or association due to “heating-annealing-cooling” (HAC) cycle applied only the O-H stretching region (3700 – 3100 cm^{-1}) was used. Note, the bands of the initial IR spectrum between 2982 and 2500 cm^{-1} belong to the non removed THF (see part 3.1.3.1). **Figure 3.3.3** shows the IR spectra of HBP-COOH film in the hydroxyl vibration regions at different temperatures of the HAC cycle: before heating up at 25°C, after 6 hours of annealing at 235°C ($T_g = 214^\circ\text{C}$) and after cooling down at 26°C. As in the case of HBP-OH (Chapter 3.1), the hydrogen bonds in the HBP-COOH also displayed strong influence by heating and cooling. The ($\nu\text{O-H}$) band of the spectrum **3** shows progressive shift to higher wavenumbers indicating the re-association of the hydrogen bonds with formation of the better ordered H-bonded network.

Generally, the grafting conditions such as polymer solution concentration, the solvent used, the thickness of the initial film, grafting time and the temperature have strong influence on the quality of the obtained films. Therefore, it is very important to optimise the conditions of the grafting reaction and to control each step of the grafting process. The initially prepared films of HBP-COOH from methanol and THF solutions

(~ 30 nm) showed very smooth and homogeneous surface coverage (**Figure 3.3.4**). The thickness of attached HBP-COOH was measured as function of ageing time and the extraction solvent (**Figure 3.3.5, left**). As can be seen, the thickness of the HBP-COOH layer increases with the reaction time for both solvents and reaches approximately 12 nm after 6 hours of annealing.

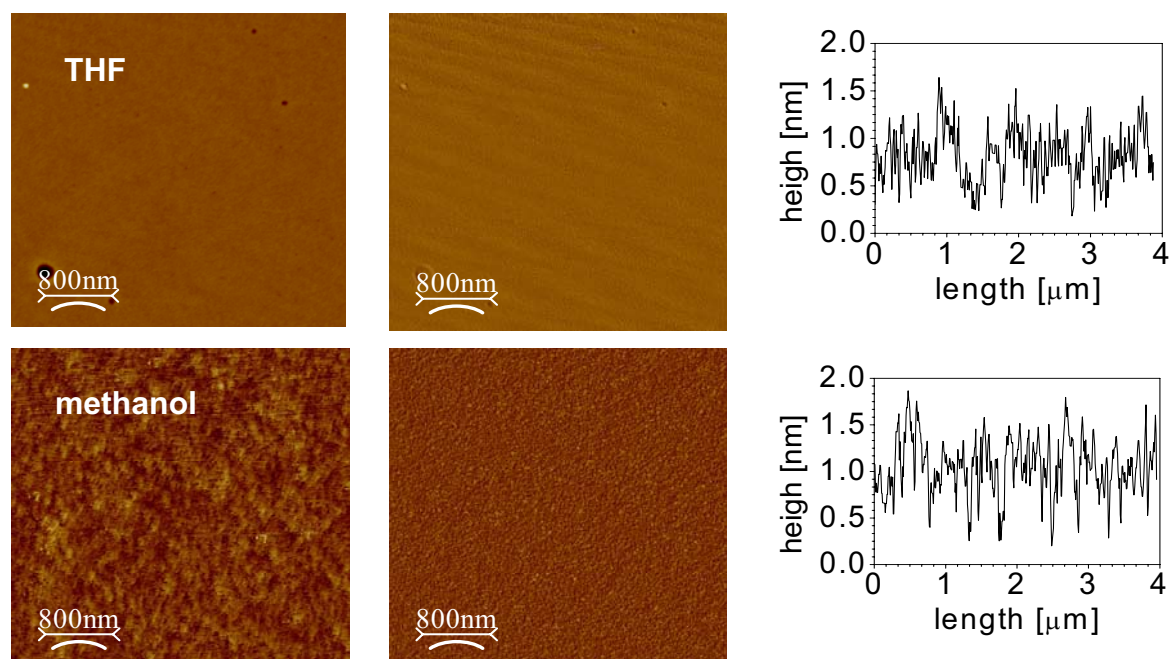


Fig. 3.3.4. AFM images of initial coated HBP-COOH obtained from different solutions with scan size of $4 \mu\text{m} \times 4 \mu\text{m}$: topography, left; phase, middle; corresponding sections, right.

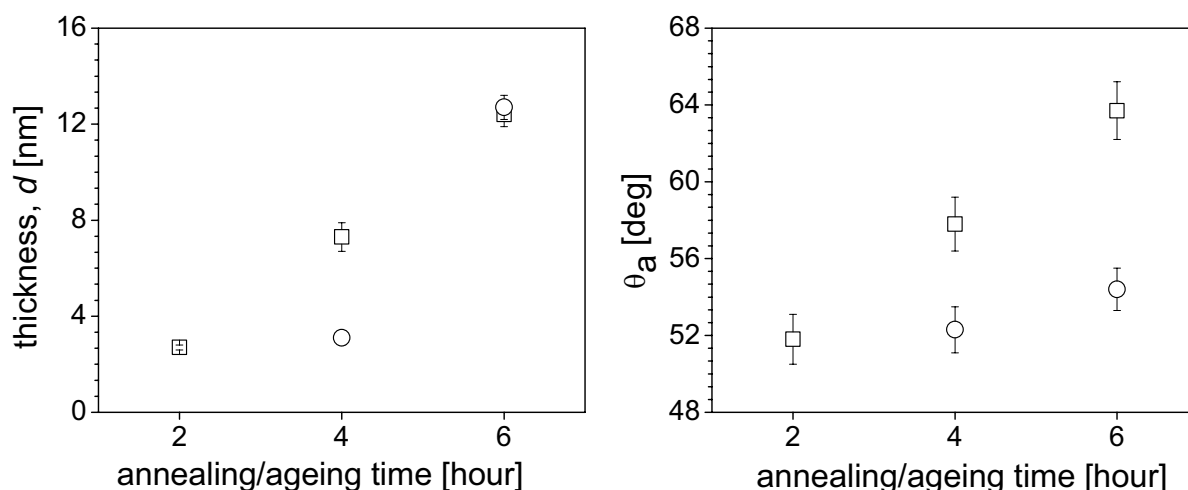


Fig. 3.3.5. Kinetics of grafting of the HBP-COOH from THF and methanol solutions with subsequent extraction monitored with ellipsometer (left) and contact angle measurements (right): THF (□) and methanol (○) extraction.

The results of the ellipsometric mapping of the surface of a silicon wafer which followed each step of grafting of the HBP-COOH with the utilization of four-layer model (Si/SiO₂/GPS/polymer), are presented in **Figure 3.3.6**. The mapping was performed with a step of 1 mm in two orthogonal directions. The Z-axis illustrates the increase of the layer thickness starting from the substrate (silicon). The entire thickness of the HBP-COOH is nearly constant and about 12 nm.

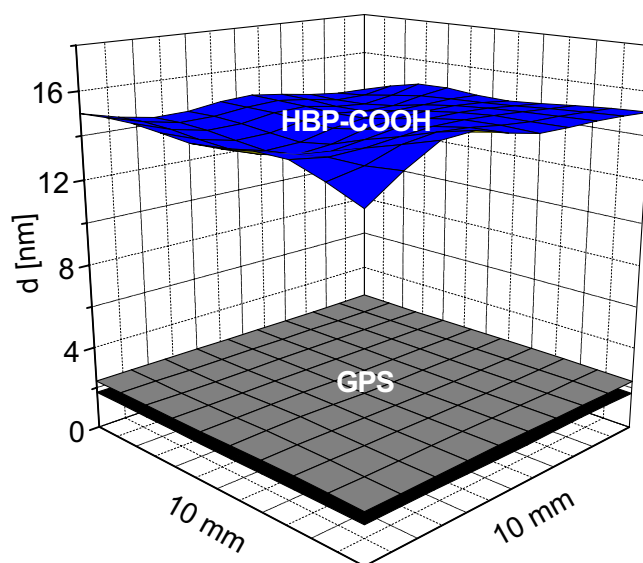


Fig. 3.3.6. Ellipsometric mapping of sample used after each step of surface modification (silicon dioxide, black).

The AFM analysis of the grafted layer of the HBP-COOH after THF extraction showed very smooth surface, without any dewetting and aggregates (**Figure 3.3.7**). The advancing contact angle θ_a of the HBP-COOH layer with reaction time of 6 hours (**Figure 3.3.5, right**) was found in the range between contact angles of untreated ($55.1 \pm 1.6^\circ$) and for 2 hours annealed non-grafted HBP-COOH. The methanol extraction showed lower values of θ_a compared to the values obtained after THF extraction. The obtained data of the contact angle allow estimation of how the surface is screened with the HBP-COOH deposited on the substrate. The θ_a of the silicon dioxide surface covered with the chemisorbed GPS (**Figure 3.3.8**) was measured as $47.1 \pm 1.3^\circ$. The receding contact angles θ_r of the grafted HBP-COOH show independence on the extracting solvent compared to the advancing ones. Moreover, the low values of θ_r with the initial contact angle of $29.0 \pm 3.0^\circ$ (GPS) allow the conclusion that the surface is completely covered by the HBP-COOH.

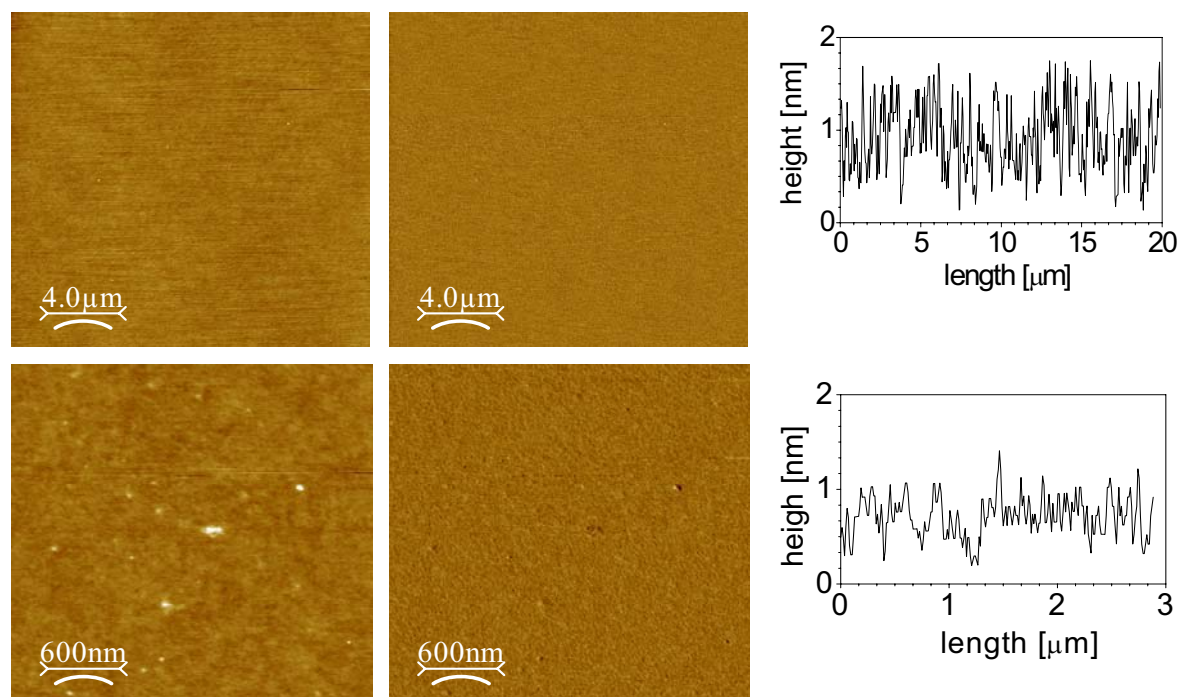


Fig. 3.3.7. Topographical (left), phase (middle) and corresponding section (right) AFM images of grafted HBP-COOH (~ 12 nm) with scan size of 20 μm x 20 μm and 3 μm x 3 μm .

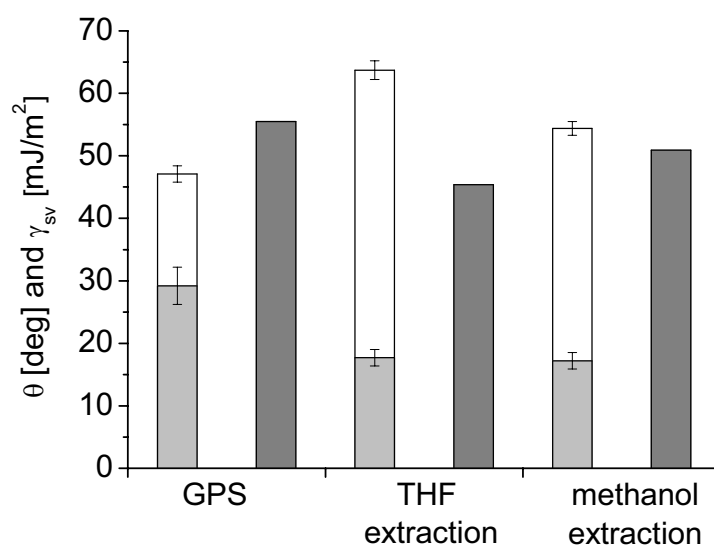


Fig. 3.3.8. Comparison of advancing (\square θ_a), receding (\blacksquare θ_r) contact angles and surface free energy (\blacksquare γ_{sv}) for GPS and grafted HBP-COOH (~ 12 nm, 6 hours of annealing) films.

To investigate the stability of HBP-COOH/GPS reactive layers in phosphate buffered saline (PBS, pH 7.4) the spectroscopic ellipsometry was applied (**Figure 3.3.9**). Several differently annealed samples to initiate the thermal grafting process were

used. The films with 2 and 4 hours of annealing were not stable enough in the buffer solution. The six hours annealed film was not removed from the substrate. However, a equilibrium swollen state was not obtained.

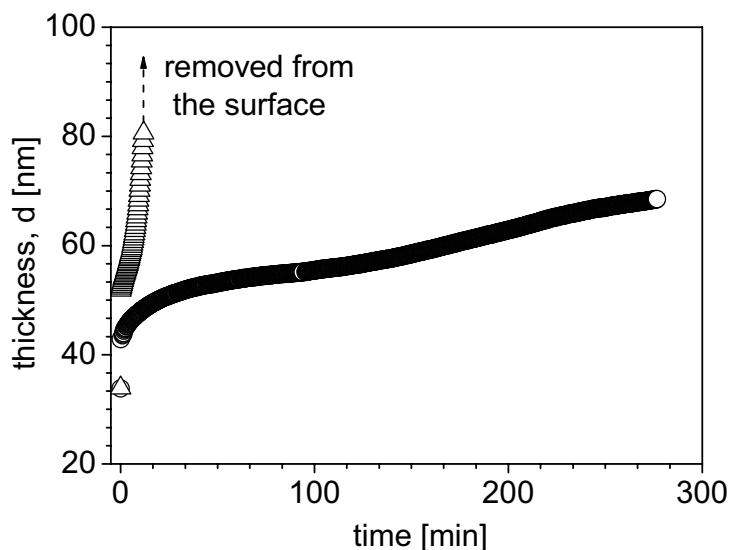


Fig.3.3.9. Time dependent swelling of non-extracted HBP-COOH/GPS samples with different times of annealing to proceed the grafting reaction: 4 (Δ) and 6 (\circ) hours.

3.3.5. Summary

It was demonstrated that immobilised uniform layer with the thickness of about 12 nm can be fabricated by chemical grafting of carboxyl functionalised hyperbranched polyesters to silicon wafer surface.

The dependence of the ageing time on the thickness and contact angle of attached HBP-COOH layer was also studied.

Strong dependence of the thickness of the HBP-COOH layer on the data of the advancing contact angle was found.

It suggests that these layers are monolayers (after solvent extraction) composed of densely packed hyperbranched molecules.

The non-extracted HBP-COOH annealed for 6 hours showed instability in aqueous electrolyte solution, although it was not removed from the substrate.

Chapter 4. Adsorption of model proteins

Abstract

A combination of different surface-sensitive techniques was applied to obtain a better understanding of adsorption processes of model proteins on hydrophilic surfaces of hydroxyl (phenolic group), hydroxyl/acetate and acetate terminated hyperbranched aromatic polyesters (HBP) in comparison to a hydrophobic polystyrene (PS) surface. Surprisingly, the adsorbed amount of lysozyme (LSZ) and human serum albumin (HSA) on the hydrophilic surface of HBPs having a weak negative surface charge was larger than on the hydrophobic PS surface. The adsorption kinetics of both proteins on the surface of HBP films was investigated in situ by spectroscopic ellipsometry and compared to the results obtained for PS surface. The adsorption kinetics of both proteins on all types of surfaces showed a very fast adsorption process. The adsorbed amount indicates the differences between LSZ and HSA adsorption on the polar surface of HBPs.

Furthermore, the irreversible adsorption of HSA on HBP-OH was examined by the formation of Amid-I and Amid-II bands using in situ Attenuated Total Reflection Fourier Transform Infrared (ATR-FTIR) Spectroscopy.

Axisymmetric drop shape analysis by profile (ADSA-P) was applied to measure in situ the changes in the contact angle and interfacial tensions as a result of the adsorption of protein molecules from a sessile solution droplet. The observed effects are very complex since not only the presence of proteins, including the arrangement and conformation of the adsorbed molecules, but also the properties of the polymer surfaces play a role.

Therefore this Chapter begins with a review of protein chemistry, factors influenced on the protein molecule stability in aqueous medium, the mechanism of protein adsorption and forces involved in the adsorption process.

4.1. Theory of protein adsorption

The interfacial behaviour of proteins is of crucial importance in biochemical and biophysical processes, especially in biomedical and biotechnological applications such as drug delivery, biomaterials, biosensors, biotechnical separation methods. Adsorption of proteins from an aqueous solution on a surface is the net result of various types of interactions that simultaneously occur between all the components in the system: the protein molecules, the initial state of the surface, the solvent (water), the low molecular weight ions (buffer components), pH and temperature.

4.1.1. Structure of protein molecule

Proteins are copolymers of different amino acids which are linked to each other to form linear polypeptide chain (**Figure 4.1**). The C-N bond is fixed in a plane because of its partial double-bond character due to mesomerism. In a random structure of a polypeptide chain rotational mobility exists around the ψ and ϕ bonds. The amino acid side groups R^1 , R^2 , ... are positioned in trans configuration to minimise steric barrier [Nor91]. The amino acids have varying polarity, resulting in a more or less amphipolar protein molecule. Furthermore, some amino acid residues containing an ionised group and can adopt positive or negative electric charge after protonation or deprotonation. This makes the protein an amphoteric polyelectrolyte. Moreover, if a polypeptide chain organises in secondary structures as helices or β -sheets, hydrogen bonding between peptide units (**Figure 4.1 and 4.2**) strongly restricts the rotational freedom along the polypeptide chain [NorX, Nor86, Nor98].

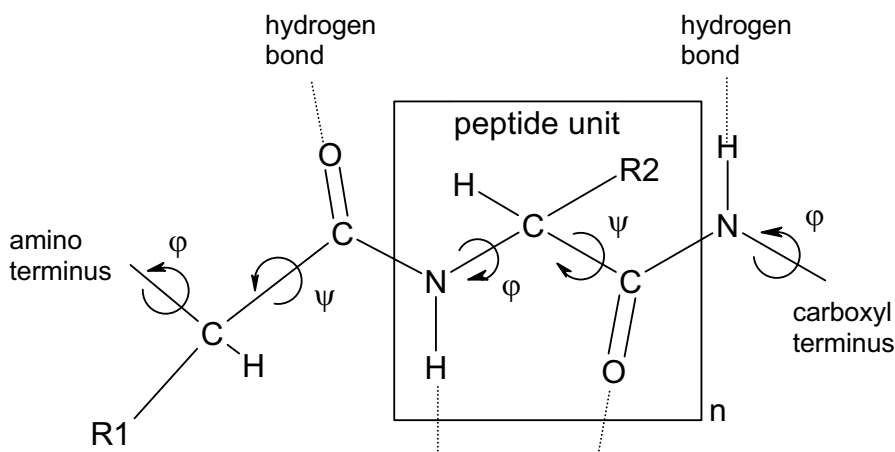


Fig. 4.1. Schematic representation of a polypeptide molecule.

4.1.2. Factors affecting protein folding and stability in aqueous medium

The complex internal and surface architectures of proteins (especially for globular protein) make it difficult to characterise their organisation in aqueous medium which is of primary importance in their adsorption behaviour. This indicates that protein unfolding is a highly cooperative process. The distraction of any significant portion of the folded structure leads to unfolding of all the rest. Thus, although conformational entropy and hydrophobic effects dominate the folding process, no type of molecular interaction is unimportant [Nor98, Nor91, Hay94].

Hydrophobic interaction

The term *hydrophobic interaction* refers to the subsequent aggregation of non-polar components in an aqueous environment (**Figure 4.2**). The dehydration originates from the fact that contacts between water molecules are much more favourable than contacts between non-polar groups or between non-polar groups and water. Hence, non-polar groups tend to be rejected from an aqueous environment rather than being attracted to one another. Hydrophobic interaction is characterised by a large entropy increase and a relatively small enthalpy effect. Moreover, it is considered as the primary driving force for the folding process [Nor86, Nor98, Nor96].

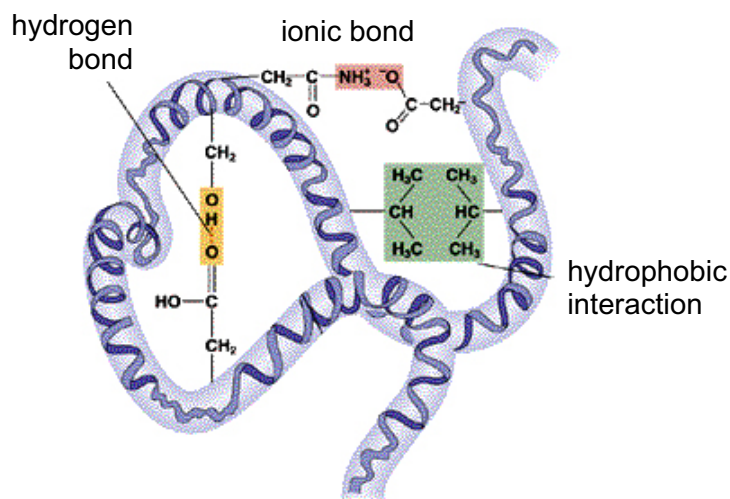


Fig. 4.2. Different possibilities to stabilise a protein molecule in an aqueous medium.

Hydrogen bonds

Peptide unit in a protein backbone contains a hydrogen donor (-NH) and a strong proton acceptor (-C=O) which are the basic components of a hydrogen bond formation (**Figure 4.2**). For a series of globular proteins, *Baker and Hubbard* [Bak84]

found that about 88 % of all peptide carbonyl groups are involved in the hydrogen bond formation. Some amino acid side chains can participate in the hydrogen bond as well, but their contribution to the total number of the internal hydrogen bonds is typically small [Hay94, Bak84, Nor98].

Coulomb interaction

Most of the charged amino acid residues in a protein molecule are located in its aqueous periphery. In the isoelectric region, the positive and negative charges are more or less evenly distributed over the molecule. This results in the intramolecular electrostatic attraction favouring a compact structure. However, excess of either positive or negative charge leads to the intramolecular repulsion and therefore promote an expanded structure. Near the isoelectric point *Coulomb interaction* is expected to favour a compact conformation of a protein molecule. The promotion of the more expanded structure occurs at more extreme pH values. However, the *Coulomb effects* have large dependence on the distribution of the charged residues on a protein molecule [Tan57, Tan57a, Mat86, Nor86, Nor98, Nor96].

Lifshitz - Van der Waals interactions

This interactions originate from interactions between fixed and/or induced dipoles of protein molecules and also of surrounding aqueous medium. They are very sensitive to the separation distance r between the dipoles, varying as r^{-6} . Upon folding the polypeptide chain into a compact structure, dipolar interactions between the protein and water are destroyed. On the other hand, dipolar interactions inside a protein molecule and between the water molecules are newly formed. The overall effect of dipolar interactions on protein stability is not clear, although it is generally assumed that because of the relatively high packing density, dipolar interactions tend to promote a compact structure [Nor98, Hay94, Nir77, Hay91].

Conformational (rotation) mobility along the polypeptide chain

The interactions which are directive limit the rotation along the polypeptide chain and the side chains, prevent the formation of secondary structures as α -helices and pleated β -sheet structures. They also decrease the possibility of folding of the polypeptide chain to form a compact molecule [Nor86].

Bond lengths and bond angles

In order to attain optimum internal interactions, lengths and angles of chemical bonds in a protein molecule may be more or less deformed. Such “stress and strain” implies an increase of the bond enthalpy. Energy minimisation calculations indicate that covalent bond distortions in native (crystallographic) protein provide small but significant contrast to the folded state stability [Lev78, Cre84, Nor86, Hay94].

4.1.3. Protein Adsorption: Fundamental Principles

In protein adsorption studies surface properties such as electrical charge density and hydrophobicity as well as environmental conditions like pH, temperature and ionic strength are often taken as experimental variables. Moreover, the specificity and complexity of the protein structure makes it difficult to investigate all these effects on the protein adsorption process in an unambiguous and systematic way. Several experimental studies [Zso86, Bry86, Han88] showed that the rate of the protein adsorption on a surface of the synthetic linear polymers increases with an increase of the polymer molar mass. Furthermore, it was shown that an increase of the surface hydrophobicity leads to an enhancing protein adsorption [Han88, Hor87, Mal94, Mal95]. The adsorption of a protein at a charged surface involves overlap of the electrical double layers at the solvated surface and the solvated protein surface. This overlap results in the electrostatic attraction between protein and the surface having opposite charge or in repulsion if their electrokinetic charges are of the same charge.

The kinetics of protein adsorption are determined by the adsorption rate at the surface, changes in conformation and/or surface diffusion and mass transport limitations in either adsorption or desorption steps.

Adsorption of protein from aqueous solution on a solid surface is a complex process involving the following steps (**Figure 4.3**) [Kri92, Nor95]: transport toward the interface (1) and attachment at the interface (reorientation) (2), eventual structural rearrangements in the adsorbed state (3), detachment from the interface (4) and transport away from the interface (5).

Each of these steps can, in principle, determine the overall rate of the adsorption process. Protein molecule attached to the surface via several segments may rearrange its structure in order to optimise interaction with a surface. Such structural

changes further contribute to the adsorption free energy. The desorption process is not just the reverse of the adsorption process. Desorption needs a higher free energy than the free energy involved in the initial binding between protein and a surface. After desorption the protein molecules may restructure into its native conformation (6), but also different conformations could equally well remain [Nor86].

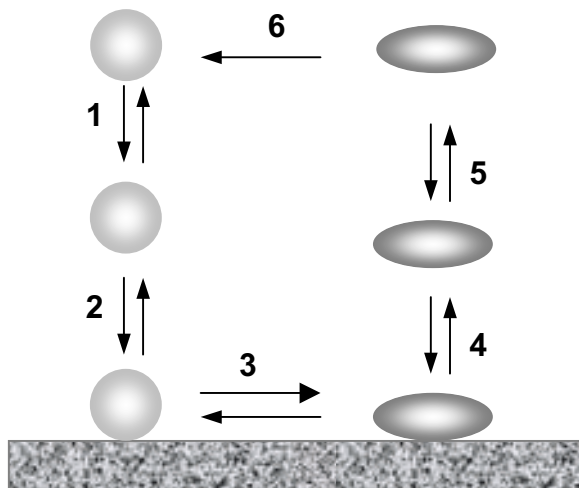


Fig. 4.3. Schematic representation the kinetics of processes occurring during protein adsorption [Kri92, Nor95].

4.1.4. Factors influencing the protein adsorption at solid/liquid interface

Influence of surface hydrophobicity

The extent of adsorption of proteins onto the surfaces of different hydrophobicity is determined by combined effects of interactions between protein molecules and the surface but also within the adsorbed protein layer [Nor98, Nor94, Nor86]. The surface hydrophobicity which is influenced by the chemistry and the morphology of a polymer surface is one of the main factors in the adsorption process and has been a field of fundamental biophysical and biochemical studies [Mal94, Mal95, Mar02, Wer02, Nor95, Arw93, Kra04]. Furthermore, a surface of different hydrophobicity results in different biological response during adsorption of bioactive macromolecules, e.g. enzymes, proteins and antibodies. Generally, it was found that on hydrophobic surfaces, the structural changes in protein molecules and subsequent denaturation of globular proteins during irreversible adsorption are stronger than on hydrophilic ones [Tam93, Mur00]. For these reasons, polymers containing hydrophilic (polar) surface groups, e.g. carboxyl, hydroxyl, amino or phosphate ones, which can create a net electrostatic potential, are often used for investigations of interactions between

protein and substrate [Nor92, But99]. Varying the hydrophobicity/hydrophilicity ratio due to changing the chemical composition of a surface automatically involves variation of protein/substrate (polymer) interactions. The adsorption on hydrophilic surfaces is often driven by charge-related electrostatic attraction and entropic effects arising from changes in conformational structure and hydration/dehydration of a solid substrate and protein molecules [Mal94, Mur00, Nor00, Nor98]. These processes are not independent of each other and the magnitude and prevalence of one over the others is related to the physicochemical properties of protein and polymer surface.

Individual characteristics of protein

Another important factor strongly influencing the adsorption process is the individual characteristics of the used protein, i.e. size, shape and charge distribution [Nor98, Nor00, Wer02, But99]. A high surface activity of protein molecules is governed by an intrinsic property since proteins are complex molecules built up from about twenty different amino acids. For instance, *Norde et. al.* [Nor00, Nor92] divided proteins into two classes according to their electrostatic behaviour: The “soft”, structurally labile proteins (e.g. human serum albumin, bovine serum albumin etc.) are able to display large conformational changes upon adsorption. Their adsorption on a hydrophilic surface is mostly governed by the gain in the conformational entropy and by decreasing the order in the secondary structure. On the other hand, the “hard” proteins (e.g. lysozyme, cytochrome c, RNase, subtilisin etc.) with a high internal cohesion undergo limited or no structural rearrangements during adsorption. They adsorb on a hydrophilic surface only due to electrostatic interactions.

Influence of protein hydrophobicity

Protein molecules contain both polar and non-polar parts. Therefore, their dissolution in water leads to the hydration of hydrophilic groups. The hydrophobic fragments arranged in the interior parts of a molecule. The distribution of the polar and non polar parts on the periphery of a protein molecule is strongly dependent on their size. Large proteins (human serum albumin, fibrinogen etc.) have small amount of non-polar groups on the surface due to similar surface/volume ratio. For small ones (e.g. lysozyme, cytochrome c, ribonuclease etc.), non-polar groups occupy about 50% of the water available surface area [Lee71]. Moreover, the hydrophobicity influences the protein structural stability which affects the adsorption [Ada74, Ohn76, Nor98].

Influence of rearrangements of protein molecules

As just mentioned, the first two steps of a protein adsorption (**Figure 4.3**) are the transport of protein molecules toward the interface and their attachment to a surface. Generally, the intramolecular hydrophobic interactions become less important as a structure-stabilising factor of an adsorbed molecule. This decrease of the hydrophobic interactions between amino acid side groups leads to destabilisation of α -helices and decrease of their content in a protein molecule. In the case of a hydrophilic surface containing oxygen groups (e.g. glass, silica etc.) the peptide units have to form hydrogen bonds to stabilise the protein molecule. Additionally, for a hydrophobic surface, adsorption can induce extra intramolecular hydrogen bonding due to increased or decreased ordering in the protein structure by promoting the formation of secondary structures as α -helices and β -sheets. As a result, the structural rearrangements in a protein molecule could be a major driving force for the adsorption [Ara90, Nor92a, Nor98a, Nor98, Nor86, Nor95].

It should be noted also that adsorption of bioactive macromolecules are strongly influenced by the surrounding environment, i.e. pH, ionic strength and temperature of the solution used. The structure, stability and charge distribution of protein might change dramatically upon changes in the environmental conditions. Therefore, it can be concluded that the cooperative influence of all these factors mentioned above has made it difficult to characterise the behaviour of proteins at interfaces in a systematic and precise way.

4.2. Monitoring the protein adsorption on solid surfaces

Several studies were carried out to characterise the adsorption of proteins on different substrates using different surface sensitive methods [Nor98, Nor92, Nor95, Nor00, Noo99, Elw98, Mar93]. Simple null-ellipsometry was often applied to quantify the level of protein adsorbed onto various solid/aqueous solution interfaces [Mal94, Mal95]. Similar ellipsometric studies were done on the protein adsorption onto crosslinkable hydrogel polymer surface with incorporated phosphorylcholine groups and dodecyl chains [Mur00]. The residual level of protein adsorption on these two polymer surfaces was found to be comparable to that on model surfaces such as silicon oxide and PMMA. X-ray photoelectron spectroscopy and contact angle measurements were applied to characterise the adsorption of BSA on hydrophilic and hydrophobic surfaces [Kra04]. It was shown that BSA adsorbed in an one step process on hydrophobic surface and in a two-step process on hydrophilic one. The combination of two *in situ* techniques, null-ellipsometry and axisymmetric drop shape analysis by profile (ADSA-P) was applied to monitor the protein adsorption at the solid-liquid interface from a sessile solution droplet [Noo99]. It gave a possibility to measure simultaneously the amount of adsorbed protein and the changes in the solid-liquid interfacial tension during adsorption. Additionally, *Van der Veg et al.* [Veg96] showed the pH dependence of the kinetic changes in both the solid-liquid and liquid-vapour interfacial tensions during protein adsorption on FEP-Teflon surface.

Also, there are many different methods applied to study the protein adsorption phenomenon at polymer interfaces using platform technologies of surface engineering situated in *department of Biocompatible Materials of Leibniz-Institute of Polymer Research (Dresden, Germany)*. Some of them are [Htt5]:

- Microslit Electrokinetic Set-up (MES) combined with in-situ reflectometric interference spectroscopy (RIfS) which can provide new insights into protein adsorption phenomena as the in-situ method and allows to analyse simultaneously surface charge characteristics and optical layer thickness.
- Quartz crystal microbalance measurements providing information about mass contribution and viscoelastic properties of the adsorbed biomolecules [Ren04, Ren05].

- High-sensitive differential scanning calorimetry (micro-DSC) allowed to obtain information on a macroscopic level and to assess the overall structure of the protein molecule, e.g. information on protein stability and denaturation temperature [Wei02].

Considering the importance of surface hydrophobicity in protein adsorption applications, the aim of this **Chapter** was to investigate the adsorption of lysozyme and human serum albumin as model proteins with opposite charges at the solid-liquid interface of hyperbranched polymers (HBP) which are extraordinary materials with high application potential [Voi05]. Nevertheless, in spite of prognosticated increasing importance of HBPs for biomedical application, there were no published studies of protein adsorption on hyperbranched aromatic polymers found.

In **Chapter 3.2** of our studies [Mik05] we demonstrated the surface properties and swelling behaviour of hyperbranched aromatic polyester (HBP) thin films in aqueous medium. It was shown that all HBP polymer films used have similar swelling kinetics and reached an equilibrium plateau within half an hour. Therefore, a pre-adsorption period to obtain an equilibrium swollen state of these films was important to consider as the first step in protein adsorption experiments.

In this **Chapter** the protein adsorption on the surfaces of the HBP-OH, HBP-OAc and HBP-OH/OAc-1 was investigated at room temperature ($23 \pm 1^\circ\text{C}$) using a combination of *in situ* spectroscopic ellipsometry, ATR-FTIR spectroscopy and Axisymmetric Drop Shape Analyses by Profile (ADSA-P). The results were compared to those obtained for a polystyrene surface which was used as a more hydrophobic reference material. Unfortunately, thin films of HBP-COOH were not stable enough at pH 7.4 that did not allow us to use them in protein adsorption experiments.

4.2.1. Materials used in the adsorption experiments: polymers (HBP-OH, HBP-OH/OCOCH₃, HBP-OCOCH₃, PS), proteins (LSZ, HSA), buffer

4.2.2.1. Polymers

Hydroxyl (phenolic groups, HBP-OH), hydroxyl/acetate (HBP-OH/OAc-1) and acetate (HBP-OAc) terminated hyperbranched aromatic polyesters (M_w , M_n , T_g , T_{DTG} are given in Chapter 2) and polystyrene (PS, 148H BASF, Germany, M_w 188000 g/mol, M_n 97000 g/mol, $T_g = 100^\circ\text{C}$) were used as polymers to built up model hydrophilic and hydrophobic surfaces. HBPs and PS were spin coated onto polished silicon

wafers (20 seconds, 3000 rpm) as thin films from a 1.0 wt% tetrahydrofuran (THF) or toluene solutions (both from Merck, Germany), respectively.

As reported in Chapter 3.2, the film thickness and annealing procedure have a significant influence on the values of water contact angle and the refractive index that can be correlated to the film density (**Table 4.1**) [Mik05].

Table 4.1. Mean thickness d^{dry} and refractive index n^{dry} , advancing θ_a and receding θ_r contact angles of polymer films used in protein adsorption experiments.

Polymer	Initial state of surface	d^{dry} [nm]	n^{dry}	θ_a [deg]	θ_r [deg]
HBP-OH*	untreated	30 ± 5	1.660 ± 0.007	54.0 ± 0.4	20.1 ± 1.3
	annealed*		1.679 ± 0.005	75.8 ± 0.6	33.7 ± 1.4
HBP-OH/OAc-1	untreated	30 ± 5	1.606 ± 0.004	74.2 ± 1.2	53.0 ± 1.6
HBP-OAc	untreated	35 ± 5	1.589 ± 0.002	76.1 ± 0.1	53.8 ± 0.4
PS	untreated	32 ± 4	1.602 ± 0.004	89.4 ± 0.3	87.9 ± 0.3

* annealed at 240°C for 3 hours

4.2.2.2. Proteins

Chicken egg white lysozyme (LSZ, Sigma, Germany) with molecular weight 16 600 g/mol and IEP of 10.7 (positively charged at pH 7.4) was used as supplied. Lysozyme has a roughly ellipsoidal globular structure with dimension of 4.5 nm x 3.0 nm x 3.0 nm [Mal95]. Lysozyme is a small multidomain protein with high content of secondary structure containing 42% of α -helix.

Human Serum Albumin (HSA) with molecular weight 66 000 g/mol and isoelectric point (IEP) of 4.7 (negatively charged at pH 7.4) was purchased from Sigma (Germany) and used as received without further purification. It is a globular but rather flexible protein with an overall dimension of 15 nm x 3.8 nm x 3.8 nm. The protein molecule consists of three globular units held together by short flexible regions. The secondary structure contains 48% of α -helix and 15% of β -pleated sheet [Wer99].

4.2.2.3. Buffer

Phosphate buffer saline (PBS, pH 7.4, Sigma, Germany) was used to prepare single protein solutions with concentration $c = 2.5$ mg/ml and $c = 20$ mg/ml. The prepared solutions were bottled in plastic vials and immediately frozen at the temperature of -20 °C. Before use, the protein solution was taken out from a refrigerator and kept at room temperature for 1 hour. After that, a solution was used directly for the protein adsorption experiments or for the preparation of the protein solutions of lower concentration.

4.2.2. *In situ* ellipsometry studies of protein layers adsorbed at solid-liquid interfaces: Comparison between experimental data for adsorption kinetics of LSZ and HSA on HBP-OH films

The ellipsometric measurements of adsorption of model proteins were performed using a variable angle multiwavelength ellipsometer M-2000VI, J.A. Woollam Co. Inc. (USA) in the spectral range from 428 to 763 nm. It is a Diode Array Rotating Compensator Ellipsometer (DARCE™) in PCSA configuration. As described in the Chapter 3.2 [Mik05], the ellipsometric WVASE 32 software package was used to evaluate the thickness d and refractive index n of the dry film from obtained ellipsometric experimental data Ψ and Δ at three angles of incidence (65° , 70° , 75°). The optical two layer model (Si substrate/SiO₂/polymer) was used for the data analysis. Optical constants of silicon and silicon dioxide at $\lambda = 630$ nm were taken from [Wer99, Woo]. First of all, the SiO₂ layer thickness was determined. In order to determine d and n of the polymer film the fit was performed using the *Cauchy* equation [Woo] over the measured spectral region, where the HBPs and PS films are non-absorbing ($k = 0$).

The dynamic measurements of protein adsorption were performed in the special quartz cell at an angle of incidence of 68° (**Figure 3.2.2**). The sample was placed in the middle of the cell, and the measurement at the air-solid interface was done before the buffer was added for the solid-liquid experiment to consider a windows effect. The subsequent time dependent measurements were started from the injection of buffer solution with volume of 3 ml by an Eppendorf syringe as it was described earlier (Chapter 3.2) [Mik05]. In this way the equilibrium swollen state of the polymer film was precisely determined. After that, the dynamic scan was stopped

and the single spectroscopic scan was recorded. Then, a new dynamic scan was started. One minute later, a protein solution of high concentration of desired volume was injected. The record of the ellipsometric angles Ψ and Δ allows to determine the thickness of the protein layer as a function of time. The different steps of a protein adsorption experiment are schematically shown in **Figure 4.4**. For every experiment, single spectroscopic ellipsometry scans were recorded prior to the introduction of the protein solution and at the end of the adsorption period.

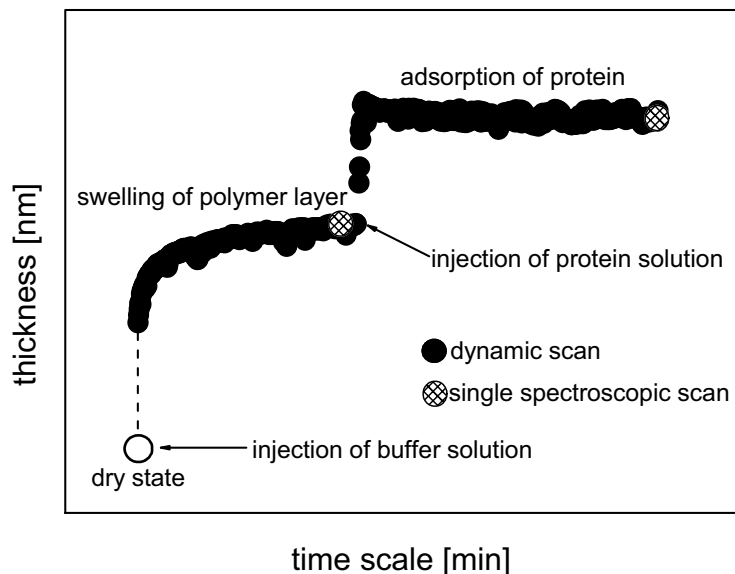


Fig. 4.4. Schematic representation of experimental steps in protein adsorption experiments measured by ellipsometry.

At the same time, the large data sets of Ψ , Δ -pairs are available to carry out a successful fit to the assumed optical model as well as for crosschecking results. Typical data of an adsorption experiment are shown in **Figure 4.5**. All experimental data were of good reproducibility allowing the best fit. Differences between two sets of data indicate the adsorbed amounts of HSA and LSZ. It can be seen that adsorption causes changes in both Ψ and Δ (**Figure 4.5a**). The largest difference in Δ occurs between 428 and 550 nm. Interestingly, with increase of λ the difference of Δ decreases. In the near vicinity of 633 nm, which is a typical wavelength of a null-ellipsometer, the difference in Δ is relatively small. Changes in Ψ are more pronounced in the full wavelength range.

Figure 4.5b shows the Ψ and Δ profiles at $\lambda = 450$ nm recorded for the adsorption from HSA and LSZ solutions ($c = 1.0$ mg/ml) onto the surface of the untreated HBP-OH during the first 10 minutes. The first set of Ψ and Δ was measured when the surface was in contact with the pure buffer solution (dashed line). The second set of

Ψ and Δ was recorded during adsorption of a protein (solid line). The difference between the end point of the first set and the starting point of the second set is due to a re-alignment of the sample before recording the protein adsorption (**Figure 4.4**). Clear difference can be seen between the Ψ and Δ of the swollen polymer film and after protein is adsorbed. The strong increase of both angles corresponded to the adsorbed protein layer, suggesting that the adsorbed amount varies little after just 2 minutes.

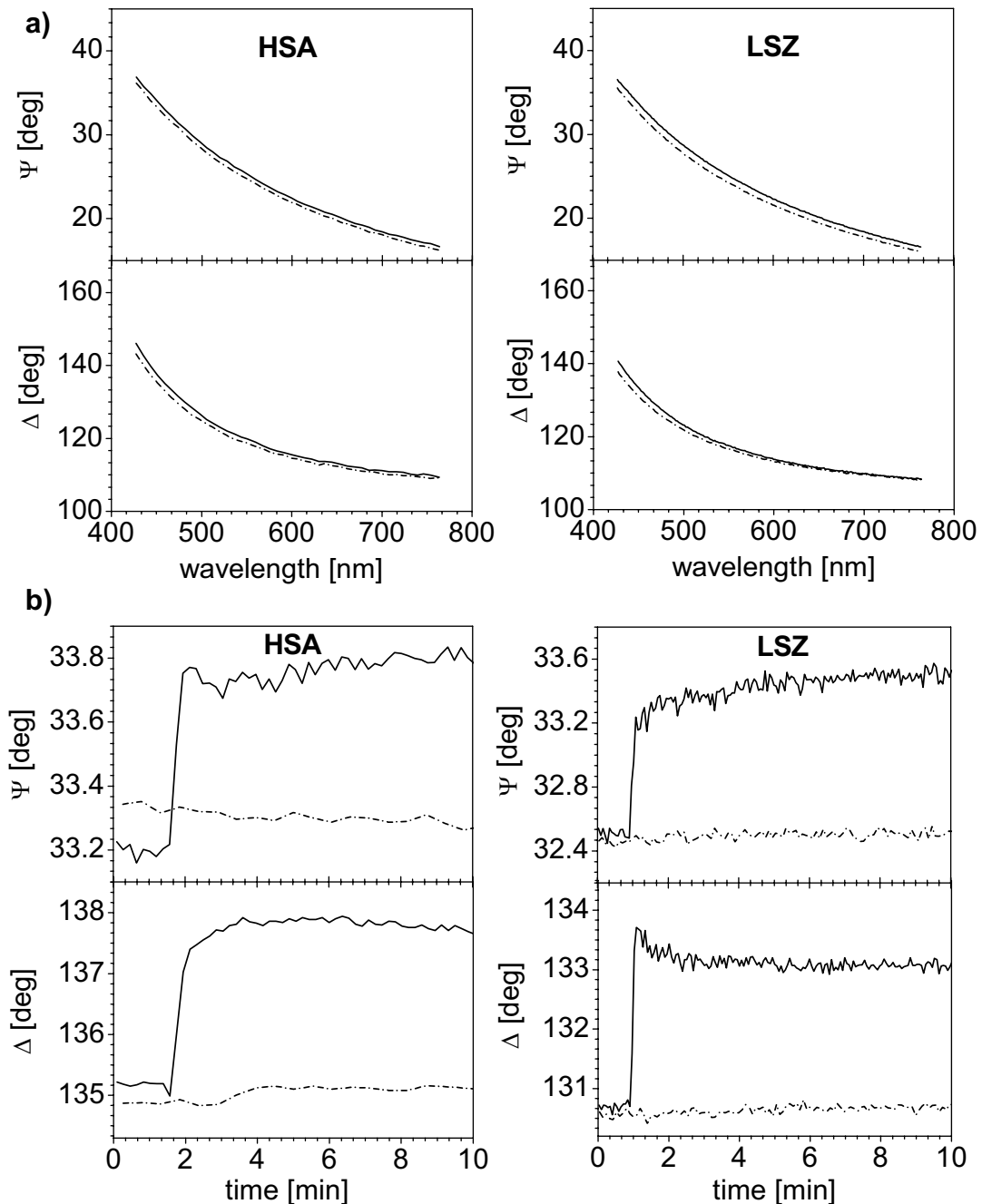


Fig. 4.5. Spectroscopic ellipsometry data measured at the polymer/solution interface (untreated HBP-OH / PBS) before (---) and after (—) adsorption of HSA (left) and LSZ (right) from solutions with concentration of 1.0 mg/ml: **2a)** – wavelength dependence, **2b)** – time dependence at $\lambda = 450$ nm.

Changes in the thickness of a protein layer adsorbed on the polymer substrate were evaluated using the optical model illustrated in **Figure 4.6**. Note, it was assumed that the protein adsorption does not change the structure of the underlying polymer layer, and proteins do not penetrate into the swollen HBP layer. Unfortunately, often it is not possible to determine simultaneously n and d of very thin layers ($d < 10\text{-}20$ nm) such as the adsorbed protein layers because of a possible correlation of these parameters. Moreover, the situation is more complicated for dynamic and non-dense aqueous protein layer. This was the main reason why it was decided to use a constant mean value of the refractive index $n_{pl} = 1.375$ to describe the adsorbed aqueous protein layer [Mal94, Mal95, Wer99] and to fit the corresponding layer thickness d_{pl} .

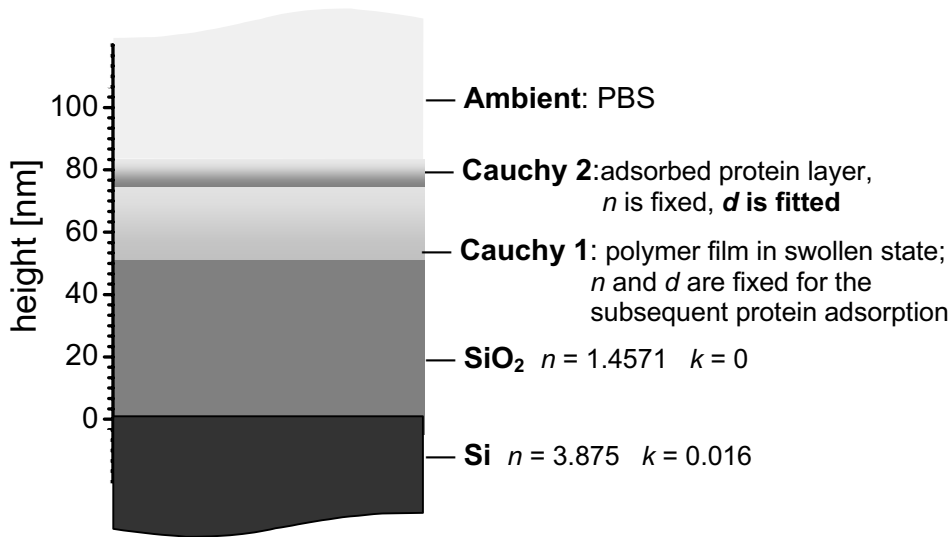


Fig. 4.6. Optical model used for fitting of the experimental ellipsometric data Ψ and Δ to evaluate the thickness d of adsorbed protein layer. The refractive index n of the protein layer was fixed at 1.375 [Wer99].

The average thickness d_{pl} calculated in such manner from the data obtained by the single spectroscopic scan after reaching the adsorption equilibrium, was finally used to evaluate the adsorbed amount (Γ) of protein according the *de Feijter et al.* equation [Fei78]:

$$\Gamma = d_{pl} \frac{(n_{pl} - n_{am})}{\left(\frac{dn}{dc}\right)_p} \quad (4.1)$$

where Γ is the adsorbed amount of protein [mg/m^2], d_{pl} is the protein adsorbed layer thickness [nm], n_{pl} is the effective refractive index of the protein layer fixed at 1.375

[Wer99]; $(dn/dc)_p$ is the refractive index increment of HSA ($0.187 \text{ cm}^3/\text{g}$) [Mal95, Wer99] and LSZ ($0.188 \text{ cm}^3/\text{g}$) [Mal95, Fei78]. n_{am} is the refractive index of buffer solution used as an ambient medium ($n = 1.327$ at $\lambda = 630 \text{ nm}$) [Mik05]. From the point of view of the ellipsometry data evaluation Γ should show an independence on a possible n_{pl} , d_{pl} parameter correlation because here the unequivocally determined “optical thickness” of the protein layer (product of d_{pl} and n_{pl}) is used for the calculation (see Eq.1).

4.2.3. *In situ* Attenuated Total Reflection Fourier Transform Infrared (ATR-FTIR) Spectroscopy: a complementary analytical tool for protein adsorption studies

ATR-FTIR spectroscopy was applied to obtain further molecular evidence of protein adsorption on HBP films. ATR-FTIR measurements were performed using an FTIR spectrometer (IFS 28, Bruker-Optics GmbH, Germany) consisting of a special mirror set-up and a removable *in situ* ATR sorption cell (**Figure 4.7**) surrounding a trapezoidal ATR-Si-crystal of 50 mm x 20 mm x 2 mm and providing an incidence angle of 45° [Mül02]. The Single Beam Sample Reference (SBSR) concept applied by M. Müller [Mül02] in *Leibniz Institute of Polymer Research (Dresden, Germany)* based on alternate recording of the intensities of the upper sample half (I_S) and lower reference half (I_R) of the ATR plate allows for convenient compensation of background absorptions from the silicon ATR plate, polymer film, water vapour and liquid water (from the buffer). Both half's are sealed by O-rings and the front plate of the *in situ*-cell forming two separate compartments, which can be filled by aqueous solutions.

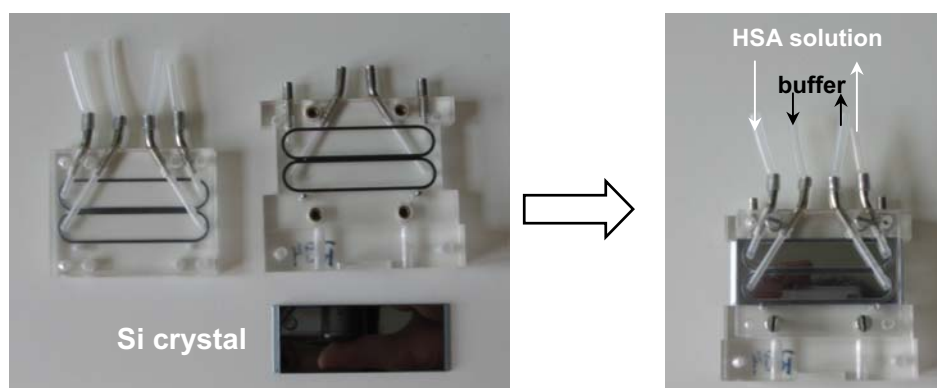


Fig. 4.7. *In situ* ATR sorption cell (M. Müller, IPF, Dresden, Germany).

Intensity spectra were recorded in the spectral range of 4000 - 400 cm^{-1} with a resolution of 2 cm^{-1} and 100 scans for both sample and reference half and were processed to give absorbance spectra according to Equation 2:

$$A_{SBSR} = -\log\left(\frac{I_S}{I_R}\right) \quad (4.2)$$

HBP-OH was coated onto the total front area of the ATR-Si-crystal from a 0.5 wt% THF solution by a special spin coating set-up. The film thickness was ellipsometrically determined to be 32 nm after annealing for three hours at 240 °C in a vacuum oven. At first, HBP-OH was equilibrated in the sample and reference half for one hour with the buffer solution to obtain the swollen state of the HBP-OH film. After that, in the sample compartment the buffer solution was replaced by 5 ml of the HSA solution in order to avoid dilution of the protein solution by the buffer, whereas in the reference compartment the buffer solution remained. Subsequently, 12 spectra were measured with an interval of 5 minutes. After that the flow cell was rinsed with PBS to remove non attached protein molecules and 3 spectra were recorded for the following 30 minutes. Four protein concentrations of 0.05, 0.1, 0.5 and 1.0 mg/ml starting from the lowest one were used. Thereby, the respective higher concentrated solution was injected onto the bound layer adsorbed from the lower concentrated protein solution. Protein adsorption was monitored by determining the integrated absorbance value of the Amide-II band, which is located near 1550 cm^{-1} and shows almost not interference with the $\delta(\text{OH})$ band of liquid water from the buffer solution.

4.2.4. Axisymmetric Drop Shape Analysis by Profile applied *in situ* to study kinetics of protein adsorption at HBPs and PS surfaces

In previous investigations [Noo99, Gru99], it was shown that contact angle measurements based on Axisymmetric Drop Shape Analysis by Profile (ADSA-P, **Figure 1.5**) can be used to access the changes in the surface energetics due to protein adsorption. In the present study, the experiments with sessile solution droplets were performed to measure changes in the contact angle and interfacial tensions due to the adsorption of the proteins.

In the first type of experiments, a droplet of a protein solution with a volume of 50 μl was gently deposited onto an untreated polymer surface and the changes in contact

angle and liquid surface tension were measured during the protein adsorption up to 30 minutes. The set-up was covered by a small glass cell to prevent evaporation effects.

In the second type of experiments, a buffer solution droplet with a volume of 200 μl was placed onto the polymer surface and 30 minutes later, a protein solution (4 - 10 μl) with desired concentration was directly injected into the middle of the drop using an Eppendorf syringe. From changes in droplet volume the final concentration of protein was recalculated. This type of experiments was applied to simulate the experimental steps used in the ellipsometric experiments. HBP-OH polymer substrates were used as pre-swollen films. For this, the prepared HBP-OH films were kept in a desiccator for three days to remove the residual solvent. After that, the HBP-OH films were annealed in a vacuum oven at 240 $^{\circ}\text{C}$ for 3 hours. Pre-swollen state was obtained by immersion of annealed HBP-OH films into PBS solution for a half hour [Mik05]. After that, films were rinsed with reagent-grade water produced by Milli-Q filtration system. The rest of water was removed from the surface with argon stream and the sample was immediately used for the measurements. PS films were used as prepared without any treatment.

It is well known that the adsorption of protein molecules at interfaces is accompanied by changes in the interfacial tension. The change in the interfacial tension is influenced by molecular characteristics of protein, protein solution concentration and properties of a polymer surface. Usually, at higher protein concentrations more rapid changes of the interfacial tension are observed [Noo99, Gru99]. The contact angle $\theta(t)$ and the liquid-vapour interfacial tension $\gamma_{lv}(t)$ data were obtained as function of time from a sessile solution droplet on a polymer substrate by ADSA-P. These data were combined with Young's equation (Eq. 1.7) to yield the overall changes of the solid-liquid interfacial tension $\gamma_{sl}(t)$ at any time t during the adsorption process. The solid-vapour interfacial tension γ_{sv} was estimated separately from water contact angle measurements using the equation of state approach for solid-liquid interfacial tension (Eq. 1.8). The changes in the solid-liquid interfacial tension $\Delta\gamma_{sl}(t)$ due to protein adsorption were quantified by the following equation:

$$\Delta\gamma_{sl}(t) = \gamma_{sl}(0) - \gamma_{sl}(eq) \quad (4.3)$$

where $\gamma_{sl}(0)$ and $\gamma_{sl}(eq)$ are the initial and final average values of the solid-liquid interfacial tension. In the experiments using pre-adsorption time, it was assumed that

$\gamma_{sl}(0)$ and $\gamma_{sl}(eq)$ are the solid-liquid interfacial tensions of buffer solution and polymer before injection and of a protein solution and polymer after injection of a protein solution, respectively.

4.2.5. Adsorption kinetics of LSZ and HSA at solid/liquid interface of HBP-OH, HBP-OH/OCOCH₃, HBP-OCOCH₃ and PS films

Figure 4.8 shows the ellipsometric results of the adsorption process using a protein solution with concentration of 1.0 mg/ml. There were no significant differences between the adsorption kinetics of LSZ and HSA on different types of surfaces, showing a very fast adsorption process. However, the adsorbed amount of these proteins on the untreated HBPs and PS surfaces was different.

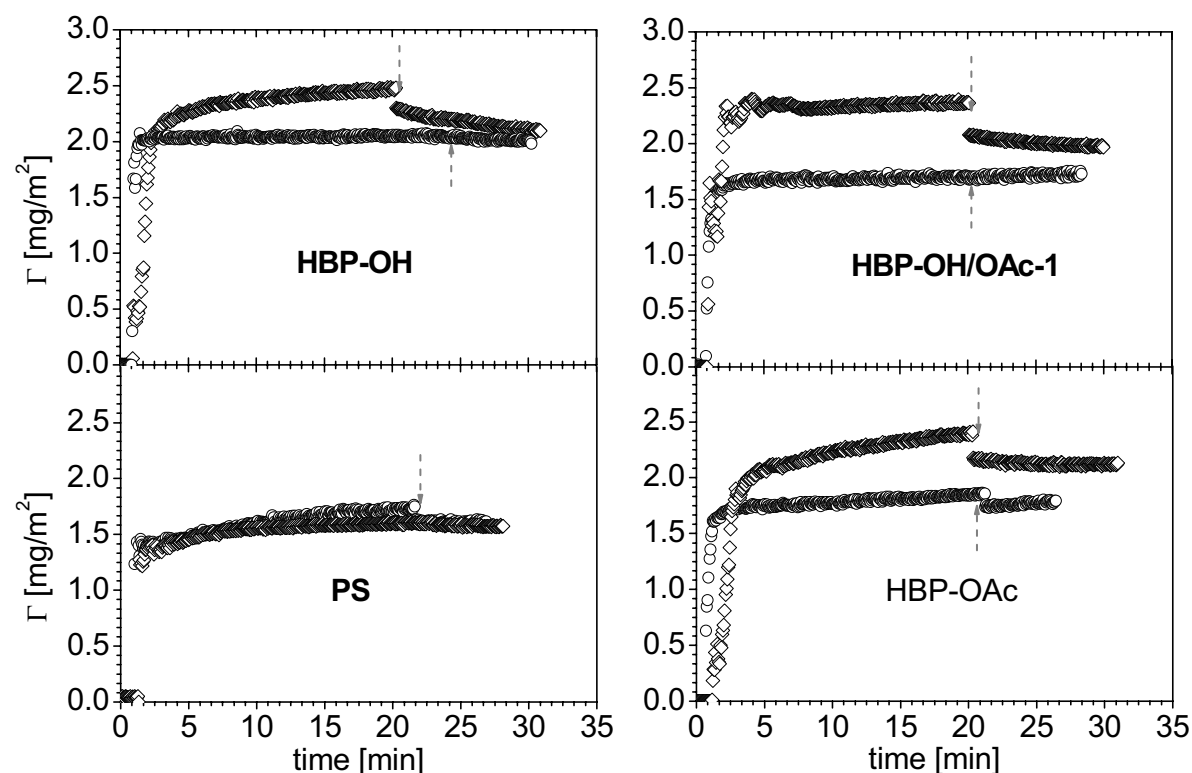


Fig. 4.5. Adsorption kinetics of HSA (○) and LSZ (◇), $c = 1.0$ mg/ml, with following rinsing with PBS (-----) on HBP and PS films.

These results might be explained by different mechanisms of adsorption on more hydrophilic HBPs and more hydrophobic PS surfaces (see values of the advancing contact angle, **Table 4.1**). Thus, the adsorption of the first layer of LSZ on the weak negatively charged HBP surfaces should be affected by the attractive electrostatic interaction between surface and protein. Further adsorption is controlled by other

factors, e.g. hydrophobic interactions between proteins in two layers and dynamic movements of the first adsorbed layer [Wah95]. On the PS surface, the situation is quite different. The adsorption of LSZ should be governed in that case mainly by the hydrophobic interaction between the PS surface and the hydrophobic domains of LSZ. The result of a low desorption due to rinsing with buffer from the hydrophobic PS surface showed that LSZ has also a relatively high affinity to the hydrophobic surface and the adsorption is essentially irreversible. The adsorption of LSZ on several hydrophobic surfaces was previously documented by different groups [Nor95, Mal94, Wer02]: They supposed that the adsorption of LSZ is determined by the “hardness” of protein molecules adsorbed at the surface, i.e. physical interactions are responsible for the protein-surface interactions and affecting the structure and stability of the adsorbed molecules. For example, *Wertz and Santore* [Wer02] found that LSZ undergoes interfacial orientation but resists to significant conformational changes at the interface.

Surprisingly, the adsorbed amount of HSA (at $c = 1.0$ mg/ml) on the polar surface of HBPs having a weak negative surface charge is higher than on the more hydrophobic PS. In contrast to HBP-OH and HBP-OH/OAc-1, the rinsing of PS and HBP-OAc films with buffer reveals a decrease in the amount of adsorbed HSA.

However, *Ballauff et. al.* [Wit03, Jac04] have observed a strong interaction between the negatively charged BSA and spherical polyelectrolyte brushes, e.g. poly(acrylic acid) and poly(styrene sulfonic acid). They supposed that due to the heterogeneity of the surface charge distribution of globular proteins, the protein adsorption also takes place on the “wrong side” of the isoelectric point of a protein ($\text{pH} > \text{IEP}_p$), i.e. due to electrostatic interactions between negatively charged polymer and positively charged protein patches. Therefore, depending on the number of these positively charged patches the adsorption might be more or less strong.

On the other hand, the relative higher adsorption of HSA at the hydrophilic (polar) surface can be also attributed to the rearrangements of the densely folded structure of globular protein over time in order to optimise their interaction with a surface [Nor95, Bar92]. In this case, the driving force of the adsorption must overcompensate the opposite effects of hydrophilic dehydration and electrostatic repulsion [Nor92]. The hydrophobic parts of the protein which are located in the interior of the dissolved molecule might be exposed to the shell due to adsorption. Such structure rearrangement in the “soft” HSA molecule involving a reduction of intramolecular

hydrophobic bonding and a decrease of the secondary structure [Nor00] should play a major role in the adsorption process on the more hydrophilic HBP surfaces.

The adsorption kinetics in terms of contact angle was studied by ADSA-P to reveal changes in the solid-liquid interfacial tension γ_{sl} which can be used as a measure of protein adsorption as well. Three different experimental runs of protein adsorption for HSA solution ($c = 1.0$ mg/ml) at the untreated HBP-OH, HBP-OAc and PS surfaces are shown in **Figure 4.9**. As expected [Voi91], in general the changes obtained in γ_{lv} and θ due to adsorbed proteins are more or less dependent on the type of protein and the concentration used.

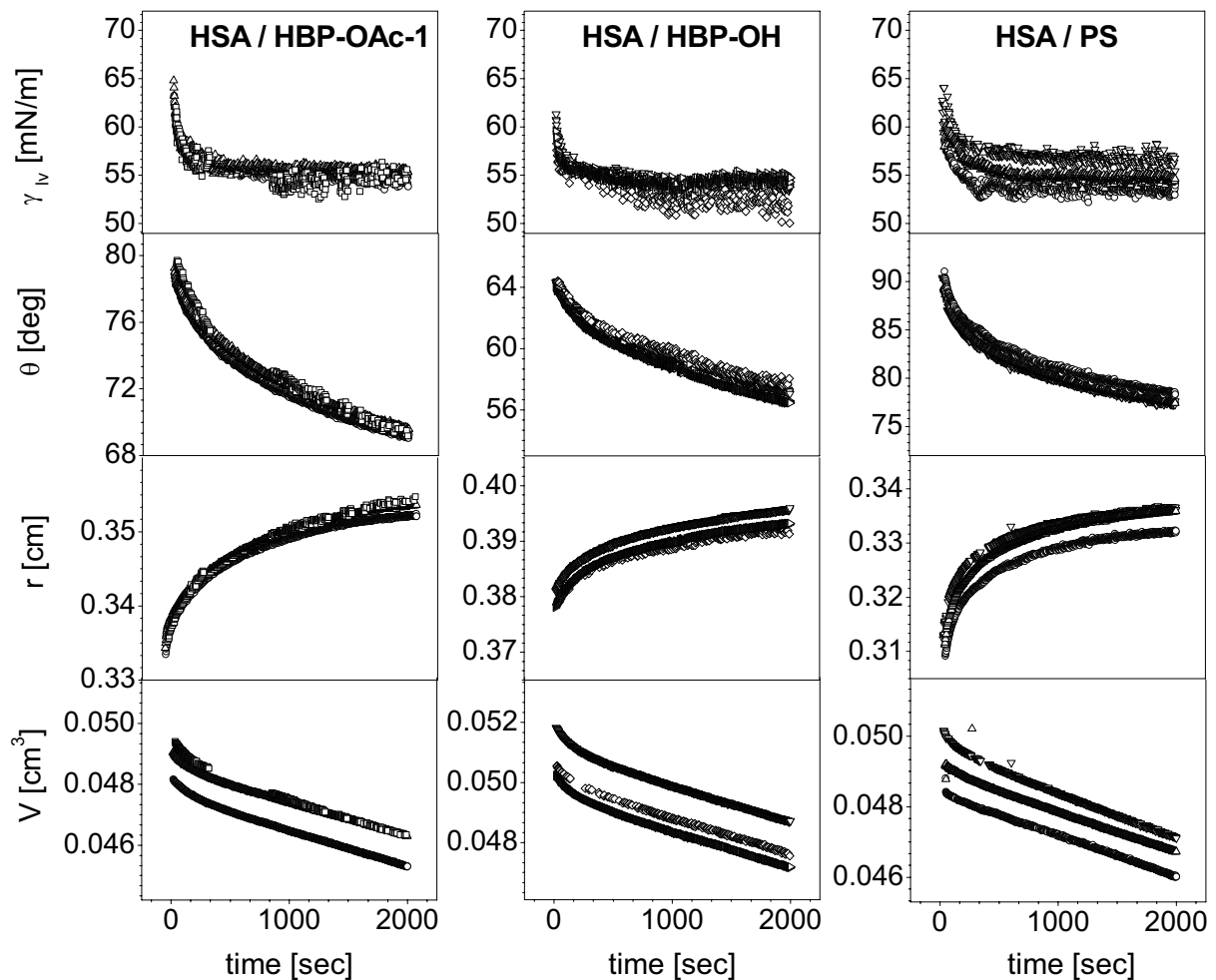


Fig. 4.9. Different runs of liquid-vapour interfacial tension γ_{lv} , contact angle θ , contact radius r and volume V during protein adsorption from HSA solutions ($c = 1.0$ mg/ml) at untreated HBPs and PS surfaces.

The evaluated results of changes in the solid-liquid interfacial tension $\Delta\gamma_{sl}$ according to Eq. (3) due to adsorbed proteins on HBP-OH, HBP-OAc and PS surfaces are shown in **Figure 4.10**. The adsorption of HSA on PS and HBP-OAc films is accompanied by a significant change in γ_{sl} compared with HBP-OH ones. Only small differences in $\Delta\gamma_{sl}$ were observed when HSA or LSZ adsorb on hydrophilic HBP-OH surfaces.

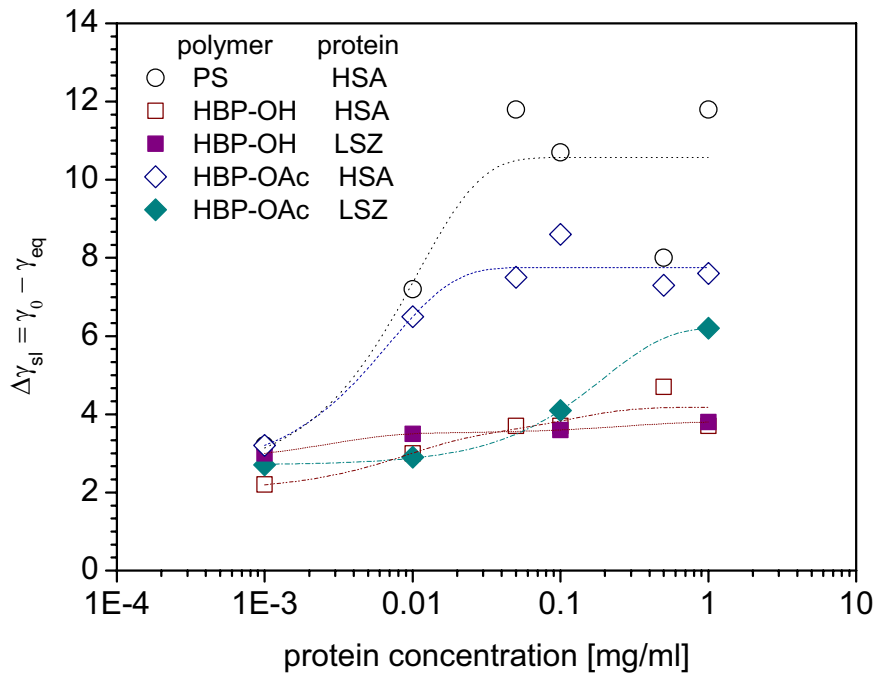


Fig. 4.10. Changes in solid-liquid interfacial tension $\Delta\gamma_{sl}$ due to protein adsorption on different polymer surfaces.

In **Figure 4.11**, the results obtained from the wetting and ellipsometric experiments for the adsorption kinetics of HSA on HBP-OH and PS are compared. HSA adsorbs very fast on both types of surfaces. After a certain time there is (nearly) no further change in the adsorbed amount of HSA but the solid-liquid interfacial tension γ_{sl} is further decreased with time. This behaviour was also found by *Noordmans et al.* [Noo99] and was explained by conformational changes of the adsorbed HSA molecules. These changes are more pronounced for the more hydrophobic polymer surface. The kinetics of the γ_{sl} and thickness changes of the LSZ showed similar time dependence as HSA with a distinct influence of concentration.

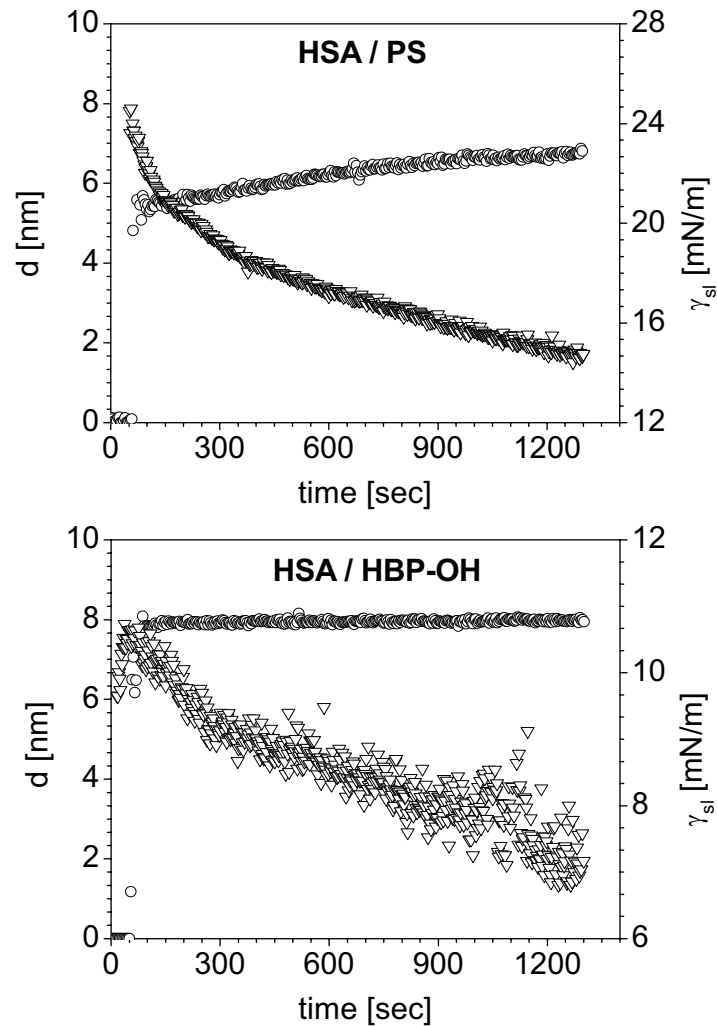


Fig. 4.11. Time-dependent changes in γ_{sl} (∇) and thickness d (\circ) due to adsorbed HSA ($c = 0.1$ mg/ml) at the untreated HBP-OH and PS surfaces.

Measurements using a pre-adsorption period in the buffer solution were carried out exemplarily for HBP-OH to simulate the experimental conditions used in the ellipsometric measurements. **Figure 4.12** illustrates the time dependence of γ_{lv} , γ_{sl} and θ during adsorption of HSA on PS compared to pre-swollen HBP-OH films. The pronounced decrease in θ during contact with a pure PBS solution droplet can be attributed mainly to the buffer penetration within the polymer film and an increase in the hydrophilic character due to reorientation of polar surface groups of the HBP-OH. Injection of HSA solution resulted in a rapid and pronounced increase in the contact angle. The observed effect is very complex and it can not be excluded that this behaviour is caused by a pinning of the contact line as there was no further change in the contact angle with time. The decrease in γ_{lv} over time, which can be simultaneously measured, is due to the adsorption of HSA molecules at the liquid-

vapour interface. Generally, on the polar hydrophilic surface of HBP-OH, a gradual increase of θ was observed for *both proteins* at different concentrations (**Table 4.2**). On the more hydrophobic PS surface, the contact angle decreases in the presence of adsorbed protein molecules showing a decrease in γ_{sl} during adsorption. The calculated increase in γ_{sl} during the adsorption of proteins at the HBP-OH surfaces for this special type of experiments is still not clear.

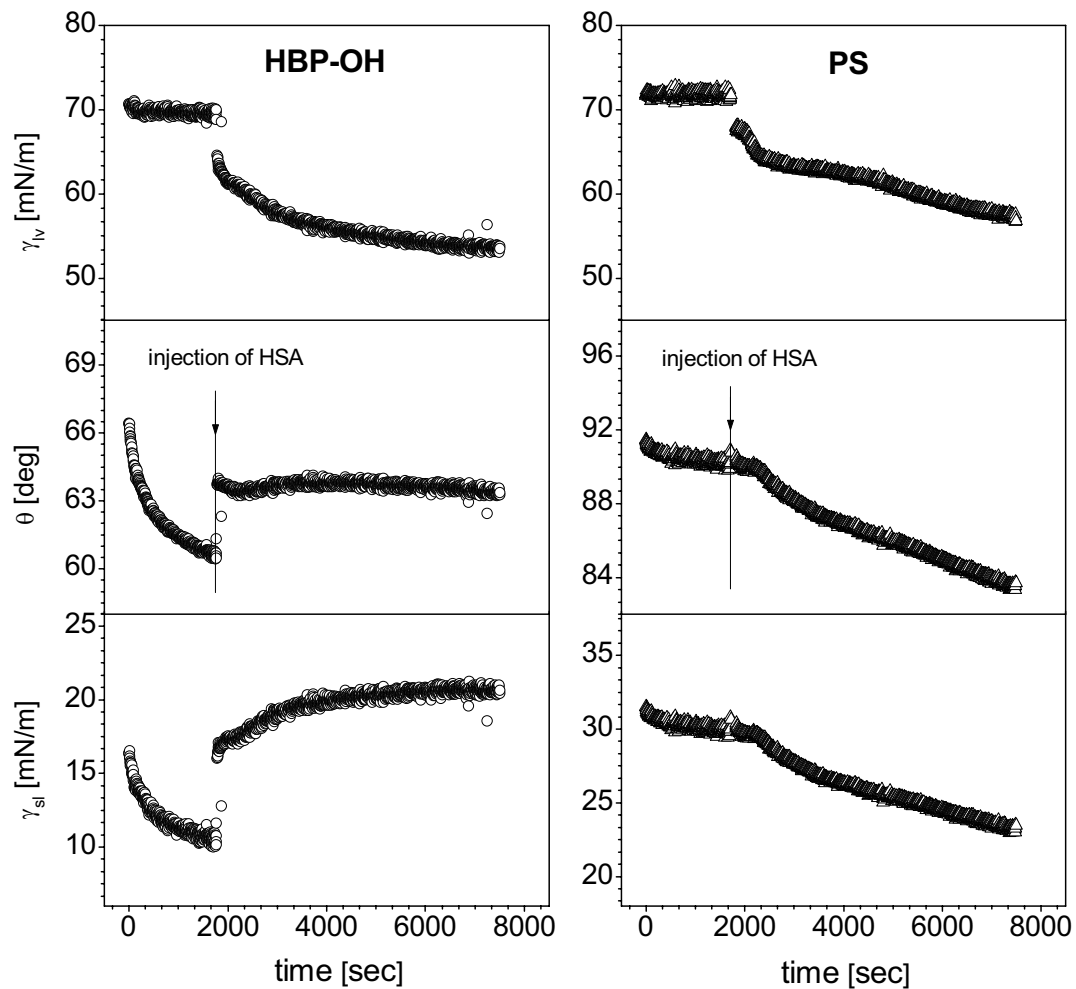


Fig. 4.12. The changes in γ_{lv} , γ_{sl} and θ during HSA adsorption of final concentration of 0.1 mg/ml on PS and pre-swollen HBP-OH films.

Table 4.2. Changes in γ_{lv} , γ_{sl} and θ due to LSZ and HSA adsorption on PS and pre-swollen HBP-OH films (experiments with pre-adsorption period).

Polymer	Protein	c protein [mg/ml]	$\Delta\gamma_{lv}$ [mN/m]	$\Delta\gamma_{sl}$ [mN/m]	$\Delta\theta$ [deg]
HBP-OH	HSA	0.1	15.9	-8.6	-2.9
		0.5	17.4	-11.1	-2.8
	LSZ	0.1	11.0	-5.9	-2.2
		0.5	15.3	-9.5	-2.3
PS	HSA	0.1	13.9	+7.4	+7.2
		0.5	17.0	+10.7	+10.8
	LSZ	0.1	5.2	+2.9	+2.6
		0.5	8.9	+4.8	+4.5

Figure 4.13 shows the results obtained by a consecutive increase of protein concentration during one ellipsometric experiment which gave the values of adsorbed amount on HBPs and PS films corresponding to the results obtained from individual measurements at a selected protein concentration.

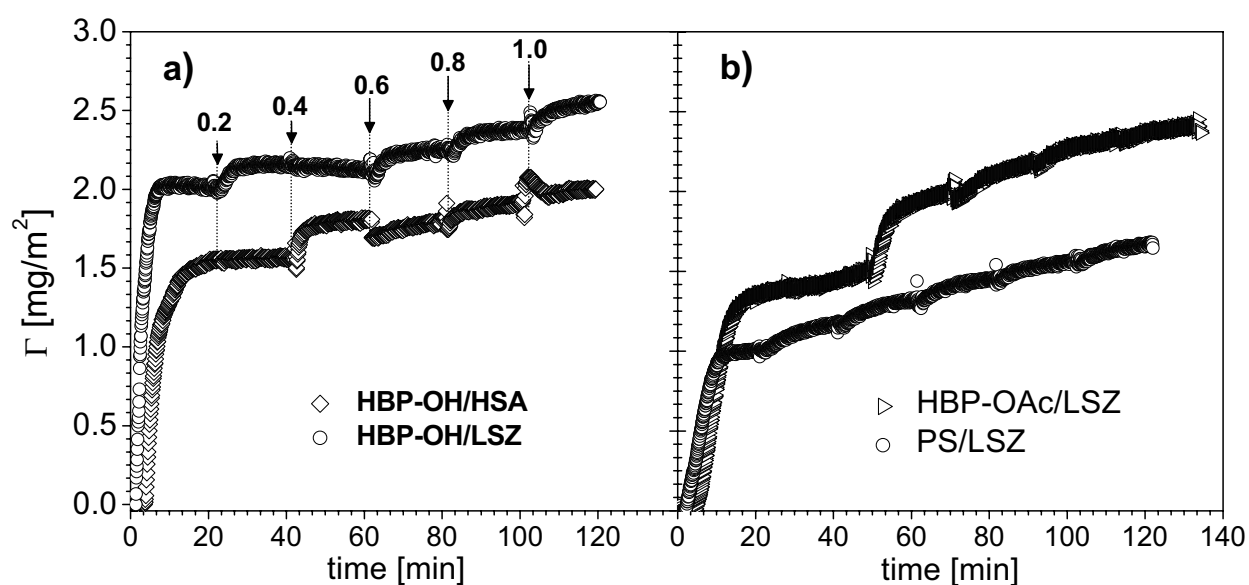


Fig. 4.13. Consecutive adsorption of LSZ and HSA on untreated HBPs and PS films (c protein [mg/ml]: 0.1 → 0.2 → 0.4 → 0.6 → 0.8 → 1.0).

At the lowest concentration tested ($c = 0.1$ mg/ml) the adsorption kinetics is diffusion-limited and the initial slope of the adsorption curves is clearly seen. Further injection of a protein solution leading to the structural rearrangements involves an expanding contact area between the protein molecules and the surface or with already adsorbed molecules or displacement of neighbouring molecules [Nor95]. Such behaviour is the reason for the increase in the adsorbed amount for LSZ as well as for HSA with increasing the protein concentration. It is interesting to note that the adsorbed amount increases more gradually in the case of LSZ than for HSA adsorbed on HBP-OH films (**Figure 4.13a**). The mean values of the adsorbed amount at the adsorption plateau at $c = 1.0$ mg/ml were found to be 2.0 and 2.5 mg/m² for HSA and LSZ, respectively.

To confirm the results and conclusions obtained by the ellipsometry and ADSA-P, the adsorption kinetics of HSA at the HBP-OH surface was characterised by ATR-FTIR spectroscopy as a complementary *in situ* technique. **Figure 4.14** shows typical absorbance spectra (A_{SBSR}) recorded during the adsorption of HSA from buffered solutions of four different concentrations onto the HBP-OH film, which was pre-swollen by PBS. The spectra are related to the respective end state of adsorption for each of the four concentrations used. These absorbance spectra reflect the direct differences between the swollen HBP-OH film in contact to PBS and the swollen HBP-OH film in contact to the buffered protein solution. In the spectral range of 1800 – 1400 cm⁻¹ the characteristic Amide-I and Amide-II bands at around 1653 and 1547 cm⁻¹ are visible, from which protein adsorption can be confirmed on the molecular level [Mül97]. The obvious presence of noise in these spectra prevents a further detailed analysis of the conformational fractions, which is principally provided by IR spectroscopy [Miy60, Byl86, Jac95]. However, both wavenumber positions point to a considerable amount of α -helical structure, as it is claimed by the above mentioned authors based on theoretical and empirical results [Mül02, Mül01]. Furthermore, in **Figure 4.14** a significant increase of the Amide-I and Amide-II integrated band areas (IBA) in dependence of the protein concentration is obtained, which is consistent with an increased amount of adsorbed protein. For quantitative analysis of the adsorbed amounts only the Amide-II band can be used, since the Amide-I band is interfered by the $\delta(\text{OH})$ due to water.

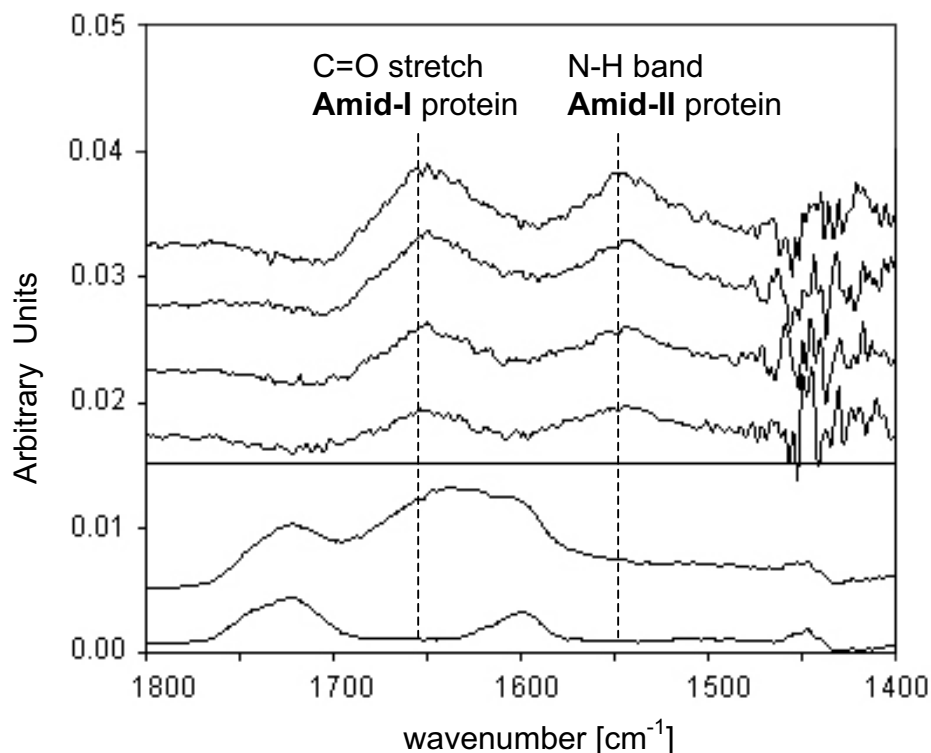


Fig. 4.14. ATR-FTIR spectra, from bottom to top: HBP-OH in dry and swollen state, HBP-OH in contact with 0.05, 0.1, 0.5 and 1.0 mg/ml HSA solutions (difference spectra of the adsorbed proteins, see text).

The kinetics of the consecutive HSA adsorption on HBP-OH surface is shown in **Figure 4.15** for the four applied concentrations. The average IBA values attributed to the end state before and after rinsing with PBS indicate the increase of the amount of adsorbed HSA with increasing protein concentration. Further rinsing with buffer gave only a slight decrease of IBA of Amide-II due to desorption of non attached HSA molecules from the top of the HBP-OH surface. This indicates again the irreversible character of adsorption of HSA onto the surface of HBP-OH. Further injection of HSA solution provides the formation of new interactions between polymer surface and protein molecules.

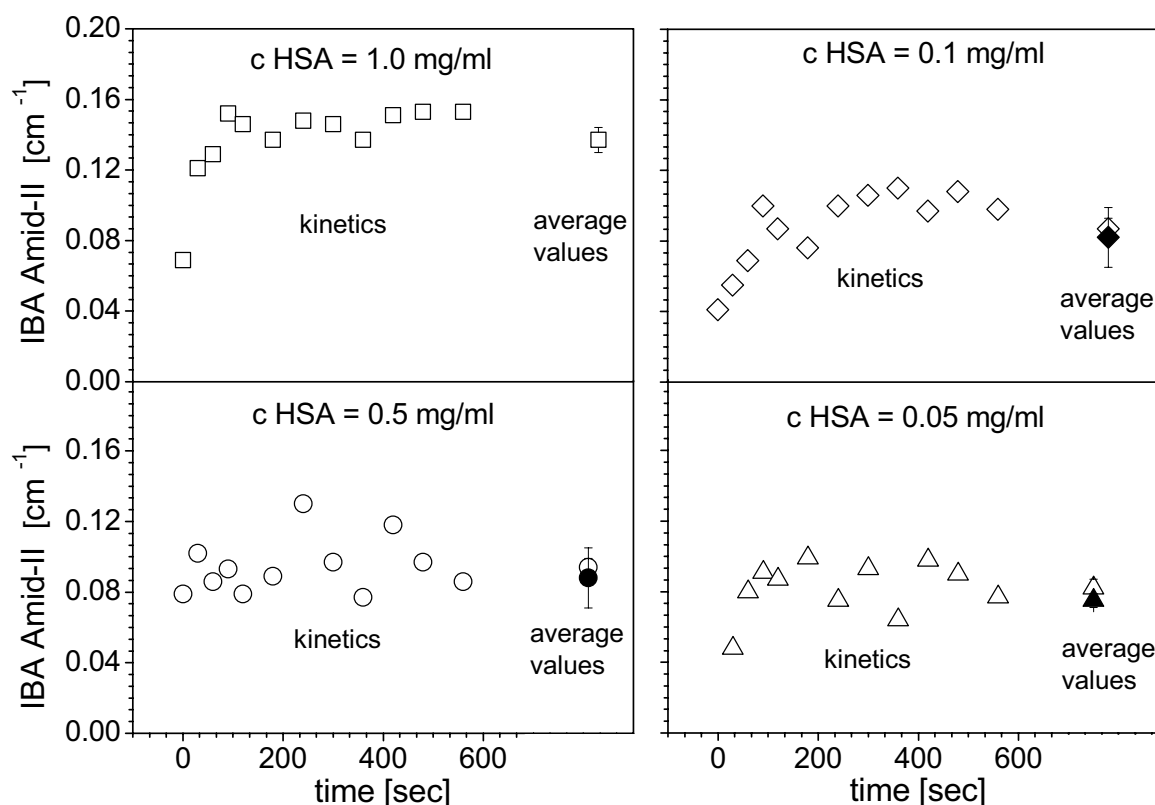


Fig. 4.15. Integrated band area (IBA) of Amid II determined during protein uptake (blank symbols) and rinsing with PBS (full symbols) for HSA solutions and HBP-OH.

4.2.6. Adsorption isotherms and adsorbed layer structure

The concentration dependence of the adsorption process for both proteins is shown in **Figure 4.16**. The adsorbed amount slightly increases with protein concentration, however, this increase is not linearly dependent on the concentration. At $c(\text{LSZ}) = 1.0 \text{ mg/ml}$ it was found 2.5 mg/m^2 on HBP-OH, 2.5 mg/m^2 on HBP-OH/OAc-1, 2.4 mg/m^2 on HBP-OAc and 1.6 mg/m^2 on PS, respectively. For comparison, on hydrophilic silica and hydrophobic methylated silica surfaces the amount of adsorbed LSZ determined by *Malmsten* [Mal94, Mal95] was found to be 3.5 mg/m^2 ($d \sim 11 \text{ nm}$) and 2.8 mg/m^2 ($d \sim 4 \text{ nm}$). *Malmsten* compared the values of the ellipsometrically determined thickness d of the adsorbed protein layer with the molecular dimension of the protein (see 2.2). The evaluation of our ellipsometric data (using a constant $n_{pl} = 1.375$) gave adsorbed LSZ layer thicknesses of $9.9 \pm 0.2 \text{ nm}$ on HBP-OH, $9.4 \pm 0.4 \text{ nm}$ on HBP-OAc, $10.0 \pm 0.3 \text{ nm}$ on HBP-OH/OAc-1 and $6.4 \pm 0.2 \text{ nm}$ on PS films,

respectively. Following the proposal of *Malmsten* [Mal94, Mal95] this should indicate the formation of more than one layer of adsorbed LSZ on both surfaces.

In our HSA experiments, the maximum ellipsometrically determined layer thickness (again with a constant $n_{pl}=1.375$) obtained by adsorption from HSA solution ($c = 1.0$ mg/ml) was 8.0 ± 0.1 nm (2.0 mg/m²) on HBP-OH, 6.8 ± 0.3 (1.7 mg/m²) on HBP-OH/OAc-1, 8.2 ± 0.4 (2.1 mg/m²) on HBP-OAc films and 6.6 ± 0.1 nm (1.7 mg/m²) on PS films. Comparing again the HSA dimension ($15 \times 3.8 \times 3.8$ nm) and layer thicknesses the formation of non compact adsorbed HSA layers on both surfaces can be concluded [Mal94, Mal95, Fle93, Nor92b]. For the similar BSA, *Norde* [Nor00] found also irreversibly adsorbed non-closely packed monolayers on hydrophilic silica and hydrophobic polystyrene particles.

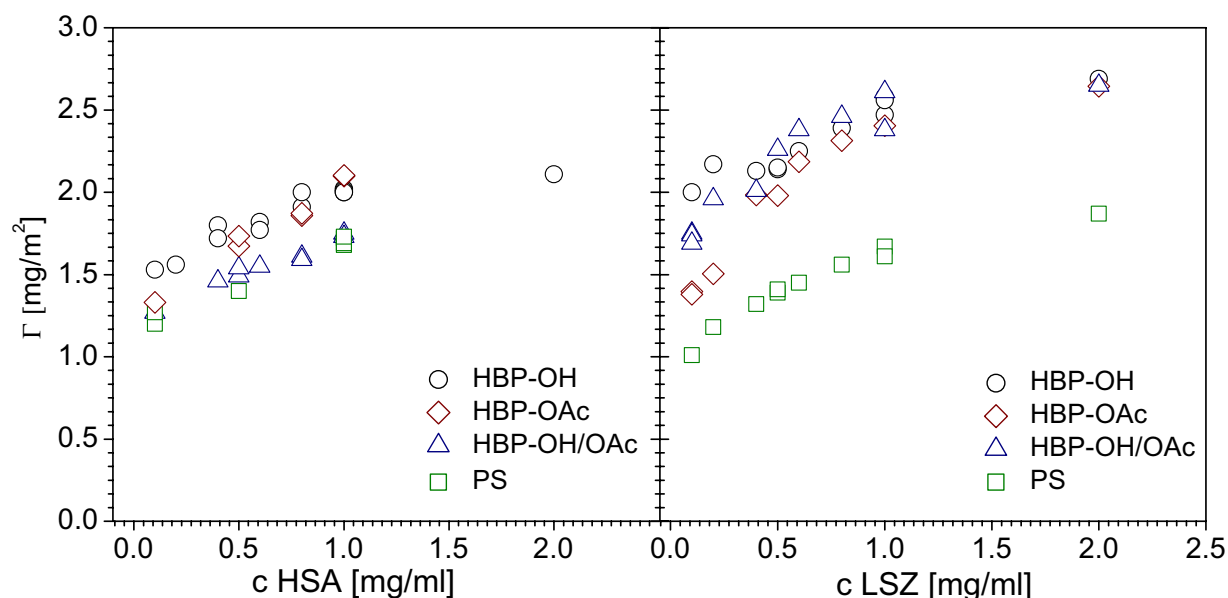


Fig. 4.16. Adsorption isotherms of LSZ and HSA adsorbed on HBPs and PS films.

4.2.7. Summary, remarks to protein adsorption

In the present Chapter, a brief overview of the protein adsorption phenomenon and experimental results confirming good binding ability of hyperbranched aromatic polyesters (HBP) to several proteins are given. It is also proposed that only a *combination* of different surface-sensitive techniques is able to give a better understanding and a comprehensive description of the complex adsorption processes of protein molecules on different polymer surfaces. In this connection

several *in situ* techniques were applied to monitor the adsorption process of several model proteins (LSZ and HSA) at the solid-liquid interface of the HBP thin films as well as for PS (reference) films.

Using *in situ* spectroscopic ellipsometry, it has been found that a higher amount of positively charged LSZ adsorbs on the hydrophilic HBP surfaces compared to the hydrophobic PS surface.

In contrast to this, only the adsorption of non compact HSA layers on the surface of HBPs was obtained. Moreover, compared to PS films, a higher amount of HSA absorbed on HBP which have a weak negative surface charge.

The formation and build up of a HSA layer at the surface of HBP-OH was also monitored *in situ* by ATR-FTIR spectroscopy. The irreversible adsorption of HSA was examined and confirmed by the formation of Amid-I and Amid-II bands.

The kinetics of the protein adsorption was studied using *in situ* spectroscopic ellipsometry and ADSA-P showing very fast adsorption process on HBPs and PS surfaces.

There have been many studies done in the field of protein adsorption showing the high adsorption rate of globular negatively charged proteins (e.g., HSA, IEP=4.7; α -lactalbumin, IEP=4.3; β -lactoglobulin, IEP=5.3) on hydrophobic surfaces compared to hydrophilic ones [Mal95, Nor95, Mar02]. However, as just mentioned, no studies were done using *hyperbranched aromatic polyesters* as a substrate. Therefore, the difference between the adsorbed amount of HSA on hydrophilic HBPs surfaces and more hydrophobic PS surface is marked.

5. Summary and outlook of dissertation

The framework of this thesis aims to investigate the adsorption-relevant properties of thin films of hyperbranched aromatic polyesters (HBP) with the same backbone structure but different functional groups. These results may be employed to a variety of different applications such as bio-active materials, bio-sensors, etc. Before carrying out the protein adsorption experiments, the HBPs were studied by different techniques in order to obtain the total information of properties and behaviour of the polymers in dissolved and solid state.

One category of experiments was concerned with the characterisation of chemical composition and typical structural elements, purity and physical properties of HBPs which strongly influence the properties of polymer coatings. The HBPs show relatively high glass transition temperatures and good thermal stability up to 300 °C. The formation of large HBP aggregates in solution was revealed due to absolute molar masses determination along the separation process and taking into account the actual compactness of the dissolved HBP molecules.

A second group of experiments was carried out on HBP films revealing a strong dependence of the annealing procedure on various properties of these coatings. The formation of a better ordered and thermally more stable hydrogen bonding network through the inter- and intramolecular interactions between the hydroxyl groups or hydroxyl and ester groups of hydroxyl (phenolic groups) terminated hyperbranched aromatic polyester (HBP-OH) with temperature was clarified. Film thickness and annealing procedure were found to have a significant influence on the value of the refractive index which can be correlated to the film density. We showed that the surface properties (hydrophilicity/hydrophobicity) of HBP thin films are strongly influenced by the annealing procedure. The stability and swelling dynamics of HBP thin films in an electrolyte solution were significantly influenced by the type of the functional groups and time of annealing. The temperature and ageing time dependent character of the grafting reaction of the carboxyl terminated hyperbranched aromatic polyester (HBP-COOH) was used for the fabrication of surfaces with multiple carboxyl groups providing the grafting capability and including the surface functionality. The high ageing temperature applied for the grafting

reaction also promoted the formation of an inter- and intramolecular hydrogen bonded network (self-cross linking) increasing the hydrophobicity of the surface.

The protein adsorption onto the surfaces of HBPs and polystyrene has been monitored by lysozyme (LSZ) and human serum albumin (HSA) adsorption experiments in order to find out the availability of these surfaces for the bio-applications. The positively charged LSZ shows higher adsorption and formation of interfacial multilayers on hydrophilic HBP surfaces compared to the more hydrophobic PS surface. The adsorption of non compact HSA layers on the surfaces of HBPs was obtained. Additionally, HSA shows a higher adsorbed amount on HBPs having a weak negative surface charge than on PS films. The irreversible adsorption of HSA on the surface of the HBP-OH was detected by the formation of Amid-I and Amid-II bands. The kinetics of the protein adsorption was studied using *in situ* spectroscopic ellipsometry and ADSA-P showing a very fast adsorption process on HBPs and PS surfaces.

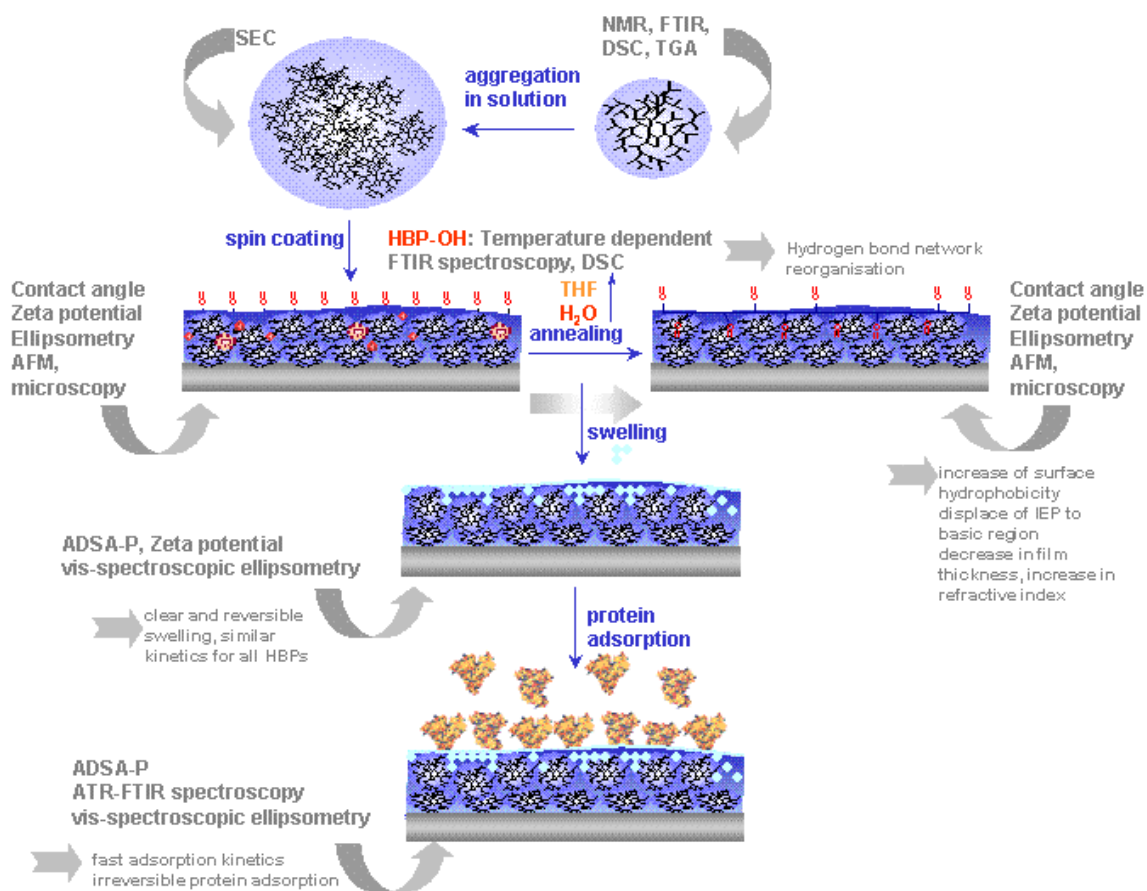


Fig. 5.1. Experimental steps to study hyperbranched aromatic polyesters.

The main conclusion is that HBPs thin films showed good stability with predictable variable properties in aqueous media and a higher bioactivity was found for all HBPs tested compared to linear PS. Thus, HBPs might be used as a suitable potential support for protein immobilization, and may open new perspectives for the development of bio-objects with tuned binding affinity and structural stability.

However, there were only hyperbranched **aromatic** polyesters used in this work. The aromatic backbone structure gives hardness and no flexibility to the hyperbranched macromolecules. Therefore as a further research, it will be interesting to compare the behaviour of HBPs with different backbone structure and the same terminal groups for the better similarity (**Figure 5.2**), i.e. differences (or not) of the surface properties, hydrogen bonded network formation and reorganisation due to high temperatures, swelling behaviour in aqueous media and protein binding ability.

As the "motivation" implies, one present and future aim might be to find new potential bio-chemical and bio-physical applications for the HBPs, e.g. in biosensors or bio-carriers. For this reason, the stability of these polymers in aqueous media is a very important factor. Therefore, the fabrication of surface attached HBP layers using different kind of techniques (**Figure 5.3**) can be used as next step for further research. Part of these ideas has been already realised in the project *B 6 IPF SFB 287*.

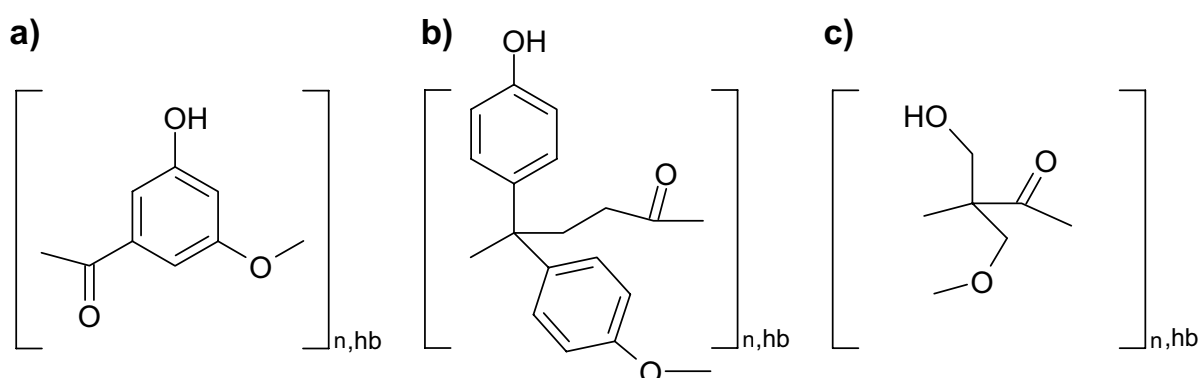
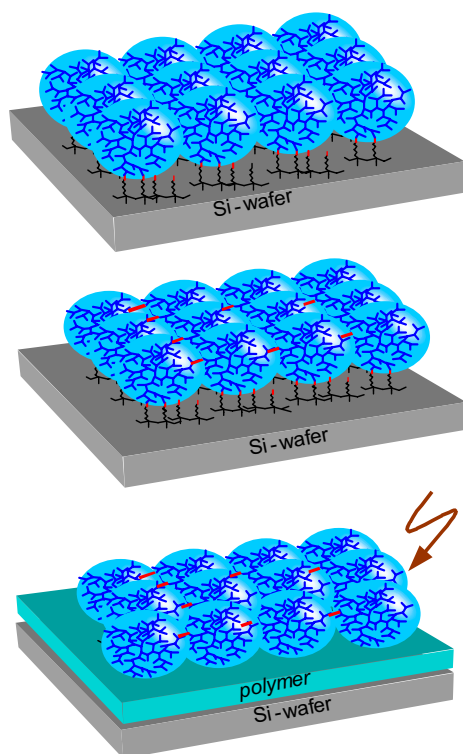


Fig. 5.2. Schematic representation of hyperbranched aromatic (a), aromatic-aliphatic (b) and aliphatic (c) polyesters with terminal hydroxyl groups.



Immobilisation on modified wafers using couplers: *PGMA* (*polyglycidylmethacrylate*)
GPS (*3-glycidoxy-propyltrimethoxy silane*)
Aminosilane /MSA-Copolymer

Cross-linking reaction within the layers using bifunctional coupling agents
Bis-Oxazoline
DiisocyanateHexamethylenediisocyanat

Simultaneous immobilisation and cross-linking on thick polymer layers (*Teflon AF, PTFE, PET*) using low pressure plasma
Optimisation of process parameters: gas, time, excitation

Fig. 5.3. Different possibilities of immobilisation of hyperbranched macromolecules to a substrate.

As the second idea, the modification of already synthesised hydroxyl or carboxyl terminated hyperbranched aromatic polyesters by linear aliphatic polymers of different chain length (**Figure 5.4**) is proposed. Thus, it will be possible to obtain macromolecules with hard core and long flexible chains (charged or not charged). Such molecules having a quite open structure might be used as potential biomolecules (protein, enzyme, antibody) carriers.

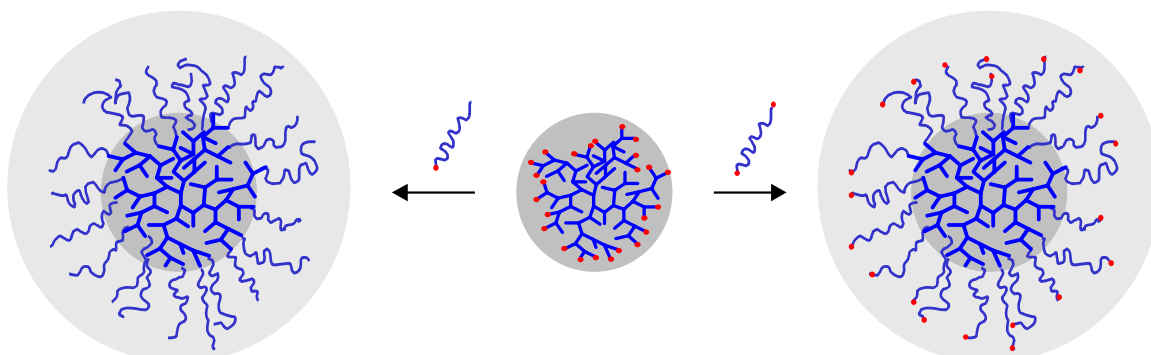


Fig.5.4. Schematic representation of modification of hyperbranched molecule by linear polymer (red dots are charged groups).

List of symbols and abbreviations

ADSA-P	Axisymmetric Drop Shape Analysis by Profile
AFM	Atomic Force Microscope
ATR	Attenuated Total Reflection
DSC	Differential Scanning Calorimetry
FTIR	Fourier Transform Infrared spectroscopy
HAC	Heating-annealing-cooling cycle
HBP	Hyperbranched polymer
-OH	hydroxyl group
-OAc	acetate group
-OH/OAc	hydroxyl/acetate group (mixed composition)
-COOH	carboxyl group
IEP	Isoelectric Point
IR	Infrared
KBr	Potassium bromide
LS	Light Scattering
MALLS	Multi Angle Laser Light Scattering detector
min	minute
ml	Millilitre
nm	nanometre
NMR	Nuclear Magnetic Resonance
PDI	Polydispersity index
ppm	parts per million (concentration)
PS	Polystyrene
PVP	poly(2-vinyl pyridine)
RI	Refractive Index detector
sec	second
SEC	Size Exclusion Chromatography
THF	tetrahydrofuran
TGA	Thermo Gravimetric Analysis
UV	Ultraviolet detector
wt%	weight per cent

α	absorption coefficient
A_n, B_n, C_n	Cauchy parameters
d	film thickness
Δ	relative phase shift
H	contact angle hysteresis
γ	surface tension
i	complex number
I	intensity
κ	extinction coefficient
λ	wavelength
n	refractive index
N	complex refractive index
T_g	glass transition temperature
T_{DTG}	temperature of maximum decomposition
θ	contact angle
ψ	relative amplitude ratio
M_n	number-average molecular weight
M_w	weight-average molecular weight
M_w / M_n	polydispersity

References

- [Ada74] K. Adachi, T. Asakura, *Biochemistry* **1974**, *13*, 4976.
- [Ara90] T. Arai, W. Norde, *Colloids and Surfaces* **1990**, *51*, 1.
- [Arw93] H. Arwin, S. Welin-Klintström, R. Jansson, *J. Coll. Int. Sci.* **1993**, *156*, 377.
- [Azz87] R.M.A. Azzam, N.M. Bashara: *Ellipsometry and polarized light*. Elsevier, Amsterdam, **1987**.
- [Bak84] E.N. Baker, R.E. Hubbard, *Prog. Biophys. Mol. Biol.* **1984**, *44*, 97.
- [Bar92] R. Barbucci, A. Casolaro, A. Magnani, *Clin. Mater.* **1992**, *11*, 37.
- [Bel02] G. Belge, D. Beyerlein, C. Betsch, K.-J. Eichhorn, G. Gauglitz, K. Grundke, B. Voit, *J. Anal. Bioanal. Chem.* **2002**, *374*, 403.
- [Bel02a] C. Bellmann, C. Klinger, A. Opfermann, F. Böhme, H.-J.P. Adler, *Prog. Org. Coat.* **2002**, *44*, 93.
- [Bel04] C. Bellmann, *Chem. Eng. Technol.* **2004**, *27*, 937.
- [Bey01] D. Beyerlein, K.-J. Eichhorn, K. Grundke, M. Eigner, D. Schmaljohann, B. Voit, *Polymer Materials: Science and Engineering* **2001**, 84.
- [Bey01a] D. Beyerlein, G. Belge, K.-J. Eichhorn, G. Gauglitz, K. Grundke, B. Voit, *Macromol. Symp.* **2001**, *164*, 117.
- [Bey02] D. Beyerlein, *Hochverzweigte Polyester in Dünnen Schichten: Charakterisierung der Material- and Grenzflächeneigenschaften*, Dissertation, Technische Universität Dresden, **2002**, Tenea, Berlin.
- [Bru97] M.L. Bruening, Y. Zhou, G. Aguilar, R. Agee, D.E. Bergbreiter, R.M. Crooks, *Langmuir* **1997**, *13*, 770.
- [Bry86] E. Brynda, M. Houska, F. Lednicky, *J. Colloid Interface Sci.* **1986**, *113*, 164.
- [Bur03] S.E. Burke, C.J. Barrett, *Langmuir* **2003**, *19*, 3297.
- [But99] A.M. Butler, M.A. Tracy, R.D. Tilton, *Journal of Controlled release* **1999**, *58*, 335.
- [Byl86] M. Byler, H. Susi, *Biopolymers* **1986**, *25*, 469.
- [Ces93] L.C. Cesteros, E. Meaurio, I. Katime, *Macromolecules* **1993**, *26*, 2323.
- [Ces93a] L.C. Cesteros, J.R. Isasi, I. Katime, *Macromolecules* **1993**, *26*, 7256.
- [Col99] M.M. Coleman, J.F. Graf, P.C. Painter, *Specific Interactions and the Miscibility of Polymer Blends*, Technomic Publishing Co., Lancaster, **1991**.
- [Cos00] M.E. Cosulich, S. Russo, S. Pasquale, A. Mariani, *Polymer* **2000**, *41*, 4951.

- [Cre84] T.E. Creghton *Proteins: Structures and Molecular Principles*, W.H. Freeman, New York, **1984**.
- [Eic03] K.-J. Eichhorn, A. Fahmi, G. Adam, M. Stamm, *Journal of Molecular Structure* **2003**, 661-662, 161.
- [Elw98] H. Elwing, *Biomaterials* **1998**, 19, 397.
- [Far01] T.R Farhat, J.B. Schlenoff, *Langmuir* **2001**, 17, 1192.
- [Fei78] J.A. de Feijter, J. Benjamins, F.A. Veer, *Biopolymers* **1978**, 17, 1759.
- [Fle93] G.J. Fler, M.A. Cohen Stuart, J.M.H.M. Scheutjens, T. Cosgrove, B. Vincent, *Polymer at Interfaces*, Chapman & Hall, London, **1993**.
- [Flo52] P.J. Flory, *J. Am. Chem. Soc.* **1952**, 74, 2718.
- [Fow64] F.M. Fowkes, *Ind. Eng. Chem.* **1964**, 12, 40.
- [Fre02] H. Frey, R. Haag, *Rev. Mol. Biotechnol.* **2002**, 90, 257.
- [Gao04] C. Gao, D. Yan, *Prog. Polym. Sci.* **2004**, 29, 183.
- [Ger04] M. Gernert, *Thermal structuring of esterprotected sulfonatpolymers*, Presented in the Institute of Polymer Research, Dresden, Germany, 28.01.**2004**, Lecture.
- [Goo92] R.J. Good, C.J. van Oss, *The modern theory of contact angles and the hydrogen bond components of surface energies*, in: M. Schrader, G. Loeb Eds. , *Modern Approaches to Wettability: Theory and Applications*, Plenum Press, New York, **1992**, 1.
- [Gru96] K. Grundke, T. Bogumil, C. Werner, A. Janke, K. Pöschel, H.-J. Jacobasch, *Colloids and Surfaces Part A: Physicochemical and Engineering Aspects*, **1996**, 116, 79.
- [Gru96a] K. Grundke, T. Bogumil, T. Gietzelt, H.-J. Jacobasch, D.Y. Kwok, A.W. Neumann, *Prog. Colloid Polym. Sci.*, **1996**, 101, 58.
- [Gru99] K. Grundke, C. Werner, K. Pöschel, H.-J. Jacobasch, *Colloids and Surfaces Part A: Physicochemical and Engineering Aspects* **1999**, 156, 19.
- [Gru01] K. Grundke in "*Handbook of Applied Surface and Colloid Chemistry: Wetting, Spreading and penetration*", Ed. by K. Holmberg, **2001**, Chapter 7, V. 2, 119.
- [Han88] J. Hansen, K. Ely, D. Horsley, J. Herron, V. Hlady, J.D. Andrade, *Macromol. Chem. Macromol. Symp.* **1988**, 17, 135.
- [Haw91] C.J. Hawker, R. Lee, J.M.J. Fréchet, *J. Am. Chem. Soc.*, **1991**, 113, 4583.
- [Haw99] C.J. Hawker, *Advances in Polymer Science* **1999**, 147, 143.

- [Hay91] C.A. Haynes, K. Tamura, H.R. Körfer, H.W. Blanch, J.M. Prausnitz, *J Phys. Chem.* **1991**, *96*, 905.
- [Hay94] C.A. Haynes, W. Norde *Colloids and Surfaces B: Biointerface* **1994**, *2*, 517.
- [Haz93] Hazlett, R.D., in *Contact Angle, Wettability and Adhesion*, (Mittal, K.L., Ed.) VSP, **1993**, 173.
- [Hen04] A. Henning, K.-J. Eichhorn, U. Staudinger, K. Sahre, M. Rogalli, M. Stamm, A.W. Neumann, K. Grundke, *Langmuir* **2004**, *20*, 6685.
- [Hes97] M. Hesse, H. Meier, B. Zeeh, *Spectroscopic methods in organic chemistry*, Georg Thieme Verlag Stuttgart – New York, **1997**.
- [Hie98] A. Hierlemann, J.K. Campbell, L.A. Baker, R.M. Crooks, A.J. Ricco, *J. Am. Chem. Soc.*, **1998**, *120*, 5323.
- [Hor87] D. Horsley, J. Herron, V. Hlady, J.D. Andradý, *ACS Symp. Ser.* **1987**, *343*, 290.
- [Höl97] D. Hölder, A. Burgath, H. Frey, *Acta Polym* **1997**, *48*, 30.
- [Htt1] <http://www.uta.edu/optics/research/ellipsometry/ellipsometry.htm>
- [Htt2] <http://www.ntmdt.ru/SPM-Techniques/Principles/>
- [Htt3] http://www.nanotech-now.com/images/Art_Gallery/AS-AFM.jpg
- [Htt4] <http://www.chemie.uni-hamburg.de/tmc/kulicke/analytic/analytic.htm>
- [Htt5] <http://www.ipfdd.de/inst/departments/bm/bm.html>
- [Hun81] Hunter, R.J., *Zeta Potential in Colloid Science: Principles and Applications*, Academic Press, London, **1981**.
- [Hun86] R.J. Hunter, *Foundations of Colloid Science*, Clarendon Press, Oxford, V. 1, **1986**.
- [Jac95] M. Jackson, H.H. Mantsch, *Critical Reviews in Biochem. and Mol. Biology* **1995**, *30*, 95.
- [Jac04] G. Jackler, A. Wittemann, M. Ballauff, C. Czeslik, *Spectroscopy* **2004**, *18*, 289.
- [Jac96] H.-J. Jacobasch, F. Simon, C. Werner, C. Bellmann, *tm-Technisches Messen* **1996**, *63*, 439.
- [Jik01] M. Jikei, M. Kakimoto, *Prog. Polym. Sci.* **2001**, *26*, 1233.
- [Joh93] M. Johansson, E. Malmström, A. Hult, *J. Polym. Sci. Part A: Polym. Chem.* **1993**, *31*, 619.
- [Jön85] B.A. Ivarsson, P.-O. Hegg, K.I. Lundström, U. Jönsson, *Colloids Surfaces*, **1985**, *13*, 169.

- [Illu92] M.E. Norman, P. Williams, L. Illum, *Biomaterials* **1992**, 13, 841.
- [Kad98] J. Kadokawa, M. Sato, M. Karasu, H. Tagaya, K. Chiba, *Angew. Chem. Int. Ed.* **1998**, 37, 2373.
- [Ker93] W. Kern, *Handbook of Semiconductor Wafer Cleaning Technology - Science, Technology, and Applications*, William Andrew Publishing/Noyes, **1993**.
- [Kim88] Y.H. Kim, O.W. Webster, *Polym. Prepr. (Am. Chem. Soc., Div. Polym. Chem.)*, **1988**, 29, 310.
- [Kim90] Y. H. Kim, O.W. Webster, *J. Am. Chem. Soc.* **1990**, 112, 4592.
- [Kis99] E. Kiss, E.I. Vargha-Butler, *Colloids and Surfaces B. Biointerfaces* **1999**, 15, 181.
- [Kra04] B. Sweryda-Krawiec, H. Devaraj, G. Jacob, J.J. Hickman, *Langmuir* **2004**, 20, 2054.
- [Kri82] H.R. Kricheldorf, Q-Z. Zang, G. Schwarz, *Polymer* **1982**, 23, 1821.
- [Kri92] V. Krisdhasima, J. McGuire, R. Sproull, *J. Colloid Interface Sci.* **1992**, 154, 337.
- [Kuo03] S.-W. Kuo, C.-L. Lin, H.-D. Wu, F.-C. Chang, *J. of Polymer Research* **2003**, 10, 87.
- [Kwo99] D.Y. Kwok, A.W. Neumann, *Adv. Colloid Interface Sci.* **1999**, 81, 167.
- [Led02] A. Lederer, D. Voigt, C. Clausnitzer, B. Voit, *J. Chromatogr. A* **2002**, 976, 171.
- [Lee71] B. Lee, F.M. Richards, *J. Mol. Biol.* **1971**, 55, 379.
- [Lee98] J.Y. Lee, P.C. Painter, M.M. Coleman, *Macromolecules* **1998**, 21, 954.
- [Lev78] M. Levitt, *Biochemistry* **1978**, 17, 4277.
- [Lim01] Y. Lim, S.M. Kim, Y. Lee, W. Lee, T. Yang, M. Lee, H. Suh, J. Park, *J. Am. Chem. Soc.* **2001**, 123, 2460.
- [Luz00] I. Luzinov, D. Julthongpiput, H. Maiz, J. Pionteck, V.V. Tsukruk, *Macromolecules* **2000**, 33, 1043.
- [Mac01] M.E. Mackay, G. Carmezini, *Langmuir* **2001**, 17, 1708.
- [Mal95] M. Malmsten, *Colloids and Surfaces B: Biointerfaces* **1995**, 3, 297.
- [Mal94] M. Malmsten, *J. Colloid Interface Sci.*, **1994**, 166, 333.
- [Mar93] J. Martensson, H. Arwin, I. Lundström, Th. Ericson, *J. Colloid Interface Sci.*, **1993**, 155, 30.
- [Mar94] Marmur, A., *Adv. Coll. Int. Sci.* **1994**, 50, 121.

- [Mar98a] Marmur, A., *Colloid and Surfaces A: Physicochem. Eng. Aspects* **1998**, 136, 209.
- [Mar02] R.J. Marsh, R.A.L. Jones, M. Sferrazza, *Colloids Surf. B: Biointerfaces* **2002**, 23, 31
- [Mat67] H. Matsuura, T. Miyazawa, *Spectrochimica Acta* **1967**, 23, 2433.
- [Mat86] J.B. Matthew, F.R.N. Gurd, *Methods Enzymol.* **1986**, 130, 413.
- [McC03] M. McCormick, R.N. Smith, R. Graf, C.J. Barrett, L. Reven, H.W. Spiess, *Macromolecules* **2003**, 36, 3616.
- [Mik05] Y. Mikhaylova, V. Dutschk, C. Bellmann, K. Grundke, K.-J. Eichhorn, B. Voit, *Colloids and Surfaces A: Physicochemical and Engineering Aspects*, **in print**.
- [Mik04] Y. Mikhaylova, E. Pigorsch, K. Grundke, K.-J. Eichhorn, B. Voit, *Macromol. Symp.* **2004**, 210, 271.
- [Min02] S. Minko, S. Patil, V. Datsyuk, F. Simon, K.-J. Eichhorn, M. Motornov, D. Usov, I. Tokarev, M. Stamm, *Langmuir* **2002**, 18, 289.
- [Mir04] V.L. Mironov, *Fundamentals of the scanning probe microscopy*, Nizhniy Novgorod, **2004**.
- [Miy60] T. Miyazawa, *J. Chem. Phys.* **1960**, 32, 1647.
- [Mor03] H. Mori, A.H.E. Müller, *Prog. Polym. Sci.* **2003**, 28, 1403.
- [Mur00] E.F. Murphy, J.R. Lu, A.L. Lewis, J. Brewer, J. Russell, P. Stratford, *Macromolecules* **2000**, 33, 4545.
- [Mül02] M. Müller, *ATR-FTIR Spectroscopy at Polyelectrolyte Multilayer Systems* 'Handbook of Polyelectrolytes and Their Applications', Eds. S.K. Tripathy, J. Kumar, H. S. Nalwa, Vol. 1, American Scientific Publishers (ASP), **2002**, 293.
- [Mül97] M. Müller, C. Werner, K. Grundke, K.-J. Eichhorn, H. J. Jacobasch, *Microchim. Acta* **1997**, 14, 671.
- [Mül01] M. Müller, T. Rieser, P.L. Dubin, K. Lunkwitz, *Macromol. Rapid Commun.* **2001**, 22, 390.
- [Nor86] W. Norde, *Advances in Colloid and Interface Science* **1986**, 25, 267.
- [Nor91] W. Norde, J. Lyklema, *J. Biomater. Sci. Polymer Edn.* **1991**, 2, 183.
- [Nor92] W. Norde, J.P. Favier, *Colloids and Surfaces* **1992**, 64, 87.
- [Nor92a] W. Norde, A.C.I. Anusiem, *Colloids Surfaces* **1992**, 66, 73.
- [Nor92b] M.E. Norman, P. Williams, L. Illum, *Biomaterials* **1992**, 13, 841.

- [Nor95] W. Norde, *Cells and Materials* **1995**, 5, 97.
- [Nor96] W. Norde, *Macromol. Symp.* **1996**, 103, 5.
- [Nor98] W. Norde in M. Malmsten (Eds), *Biopolymers at interfaces, Surfactant science series, v. 75, New York*, **1998**, 27.
- [Nor98a] W. Norde, T. Zoungrana, *Biotechnol. Appl. Biochem.* **1998**, 28, 133.
- [Noo99] J. Noordmans, H. Wormeester, H.J. Busscher, *Colloids and Surfaces B. Biointerfaces* **1999**, 15, 227.
- [Nor00] W. Norde, C.E. Giacomelli, *J. Biotechnology* **2000**, 79, 259.
- [NorX] W. Norde in K.L. Mittal and P. Bothorel (Eds), *Surfactants in Solution, v. 5, Plenum Press, New York*, 1027.
- [Ohn76] T. Ohnishi, T. Asakura, *Biochem. Biophys. Acta* **1976**, 453, 93.
- [Orl02] J.A. Orlicki, N.O.L. Viernes, J.S. Moore, *Langmuir* **2002**, 18, 9990.
- [Oss88] C.J. van Oss, M.K. Chaudhury, R.J. Good, *Chem. Revs.* **1988**, 88, 927.
- [Owe69] D.K. Owens, R.C. Wendt, *J. Appl. Polym. Sci.* **1969**, 13, 1741.
- [Pai99] P.C. Painter, R. Prunthikul, M.M. Coleman, *Macromol. Symp.* **1999**, 141, 57.
- [Pee98] R. F. Peez, D. L. Dermody, J. G. Franchina, S. J. Jones, M. L. Bruening, D. E. Bergbreiter, R. M. Crooks, *Langmuir* **1998**, 14, 4232.
- [Pru01] R. Prunthikul, M.M. Coleman, P.C. Painter, N. Beck Tan, *Macromolecules* **2001**, 34, 4145.
- [Ren04] L. Renner, T. Pompe, K. Salchert, C. Werner, *Langmuir* **2004**, 20, 2928.
- [Ren05] L. Renner, T. Pompe, K. Salchert, C. Werner, *Langmuir* **2005**, 21, 4571.
- [Sed96] R.V. Sedev, J.G. Petrov, A.W. Neumann, *J. Colloid Interface Sci.* **1996**, 180, 36.
- [Ser05] A. Serghei, Y. Mikhailova, K.-J. Eichhorn, B. Voit, F. Kremer, *European J. of Physics E*, **2005**, 17, 199.
- [Sch98] D. Schmaljohann, *Funktionalisierung von hochverzweigten Polyestern für den Einsatz als Beschichtungs- und Blendmateria,* Herbert Utz Verlag, Dissertation, TU München **1998**.
- [Sch02] B. Schwarz, M. Schönhoff, *Langmuir* **2002**, 18, 2964.
- [Sch03] D. Schmaljohann, H. Komber, J.G. Barratt, D. Appelhans, B. Voit, *Macromolecules* **2003**, 36, 97.
- [Sha69] Shaw, D.J., *Electrophoresis*, Academic Press, London, **1969**.
- [Sid01] A. Sidorenko, X.W. Zhai, S. Peleshanko, A. Greco, V.V. Shevchenko, V.V. Tsukruk, *Langmuir* **2001**, 17, 5924.

- [Sid02] A. Sidorenko, X.W. Zhai, A. Greco, V.V. Tsukruk, *Langmuir* **2002**, *18*, 3408.
- [Sid02a] A. Sidorenko, X.W. Zhai, F. Simon, D. Pleul, V.V. Tsukruk, *Macromolecules* **2002**, *35*, 5131.
- [Ste24] O. Stern Z. *Elektrochem.* **1924**, *30*, 508.
- [Sty99] D. Styrkas, S. J. Doran, V. Gilchrist, J. L. Keddie, J. R. Lu, E. Murphy, R. Sackin, T.-J. Su, A. Tzitzinou, *Polymer Surfaces and Interfaces III* edited by R.W. Richards and S.K. Peace, **1999**.
- [Sun02] L. Sun, R.M. Crooks, *Langmuir* **2002**, *18*, 8231.
- [Tam93] Y. Tamada, Y. Ikada, *J. Colloid Interface Sci.* **1993**, *155*, 334
- [Tan57] C Tanford, J.G. Kirkwood, *J. Am. Chem.Soc.* **1957**, *79*, 5333.
- [Tan57a] C Tanford, J.G. Kirkwood, *J. Am. Chem.Soc.* **1957**, *79*, 5340.
- [Tan01] Y. Tang, J.R. Lu, A.L. Lewis, T.A. Vick, P.W. Stratford, *Macromolecules*, **2001**, *34*, 8768.
- [Tan02] Y. Tang, J.R. Lu, A.L. Lewis, T.A. Vick, P.W. Stratford, *Macromolecules*, **2002**, *35*, 3955.
- [Tan04] O.M. Tanchak, C.J. Barrett, *Chem. Mater.* **2004**, *16*, 2734.
- [Veg96] W. Van der Vegt, W. Norde, H.C. Van der Mei, H.J. Busscher, *Colloid Polym. Sci.* **1996**, *274*, 27.
- [Vog04] B. D. Vogt, C. L. Soles, H.-J. Lee, E. K. Lin, W.-I. Wu, *Langmuir* **2004**, *20*, 1453.
- [Voi93] B. Voit, S. R. Turner, T. Mourey, *Macromolecules* **1993**, *26*, 4617.
- [Voi00] B. Voit, *J. Polym. Sci. Part A: Polym. Chem.* **2000**, *38*, 2506.
- [Voi02] B. Voit, D. Beyerlein, K.-J. Eichhorn, K. Grundke, D. Schmaljohann, T. Loontjens, *Chem. Eng. Technol* **2002**, *25*, 704.
- [Voi05] B. Voit, *J. Polym. Sci. Part A: Polym. Chem.* **2005**, *43*, 2679.
- [Vol05] M. Vollprecht, F. Dieterle, G. Wernet, G. Gauglitz, K.-J. Eichhorn, B. Voit, *Anal. Chem.* **2005**, *77*, 5542.
- [Vre75] J.S. Vrentas, C.M. Jarzebski, C.M. Duda, *J.L. AIChE J.* **1975**, *21*, 894.
- [Voi91] A. Voigt, O. Thiel, D. Williams, Z. Policova, W. Zingg, A.W. Neumann, *Colloids and Surfaces* **1991**, *58*, 315.
- [Wah95] M. Wahlgren, T. Arnebrant, I. Lundström, *J. Colloid Interface Sci.* **1995**, *175*, 506.
- [Wel96] M. Wells, R.M. Crooks, *J. Am. Chem. Soc.* **1996**, *118*, 3988.
- [Wel02] P.B. Welzel, *Thermochimica Acta* **2002**, *382*, 175.

- [Wer99] C. Werner, K.-J. Eichhorn, G. Grundke, F. Simon, W. Grählert, H.-J. Jacobasch, *Colloids and Surfaces A: Physicochemical and Engineering Aspects* **1999**, 156, 3.
- [Wer02] C.F. Wertz, M.M. Santore, *Langmuir* **2002**, 18, 1190.
- [Wit03] A. Wittemann, B. Haupt, M. Ballauff, *Phys. Chem. Chem. Phys.* **2003**, 5, 1671.
- [Woo] J.A. Woollam, User Manual VASE and M-44 Ellipsometers, WVASE 32™, J.A. Woollam Co., Lincoln, Nebraska, USA.
- [Wooa] J.A. Woollam Co., Inc. (Lincoln/USA) Website, <http://www.jawoollam.com/>
- [Woo99] J. A. Woollam et al „Overview of Variable Angle Spectroscopic Ellipsometry (VASE). Part 1: Basic Theory and Typical Applications,” Proceedings of the 44th” SPIE meeting, **1999**.
- [Yas94] T. Yasuda, T. Okuno, *Langmuir* **1994**, 10, 2435.
- [Yhe01] Y. He, N. Asakawa, Y. Inoue, *Macromol. Chem. Phys.* **2001**, 202, 1035.
- [Zag02] E. Zagar, M. Zigon, *Macromolecules* **2002**, 35, 9913.
- [Zag03] E. Zagar, J. Grdadolnik, *Journal of Molecular Structure* **2003**, 658, 143.
- [Zag04] E. Zagar, M. Zigon, *J. of Chromatography A* **2004**, 1034, 77.
- [Zho96] Y. Zhou, M. L. Bruening, D. E. Bergbreiter, R. M. Crooks, M Wells, *J. Am. Chem. Soc.* **1996**, 118, 3773.
- [Zie03] A. Ziemer, K.-J. Eichhorn, G. Adam, C. Froeck, B. Voit, M. Kreitschmann, P. Kierkus, *Macromol. Chem. Phys.* **2003**, 204, 1275.
- [Zim01] R. Zimmermann, S. Dukhin, C. Werner, *J. Phys. Chem. B.* **2001**, 105, 8544.
- [Zso86] R.J.L. Zsom *J. Colloid Interface Sci.* **1986**, 111, 434.

Curriculum vitae

born September 20, 1976 in Tver, Russia
married

Education

- 09/1983–06/1993** Secondary School, Tver, Russia
Certificate of profession: dressmaker of light clothes
- 09/1993–05/1996** Tver State Chemical-Technological College, Russia
Field of study: Production of factory-goods and surface covers from polymeric materials
Final predicate: Technician-Technologist, excellent
- 07/1995–12/1995** Diploma practice in textile laboratory of physical-mechanical tests, company "Tver ChimVolokno", department of viscose textile fibres
Certificate of laboratory worker
- 09/1996–06/2000** Tver State University, Russia, Bachelor Studies in Chemistry
Speciality: Organic Chemistry
Thesis: Study of the cationic surfactants adsorption on aluminised glass fibres
Final predicate: Bachelor's degree in Chemistry, excellent
- 09/2000–07/2002** Tver State University, Russia, Master Studies in Chemistry
Speciality: Macromolecular Chemistry
Thesis: Structural features of physically and chemically modified polymers
Final predicate: Master's degree in Chemistry, excellent
- 07/2002–to date** PhD student at Dresden Technical University, Germany
Field of study: Macromolecular Chemistry
Thesis: Investigation of adsorption of model proteins on hyperbranched aromatic polyester thin films in aqueous media

Employment

- 07/2002–to date** Scientific co-worker at the Leibniz Institute of Polymer Research, Dresden, Germany
Analytical Department

Grants

Grant of the Russian Federation Government N 95

Articles

7. Y. Mikhaylova, V. Dutschk, M. Müller, K. Grundke, K.-J. Eichhorn and B. Voit, Study of the solid-liquid interface of hydroxyl-terminated hyperbranched aromatic polyesters (HBP-OH) in aqueous media. II. Adsorption of model proteins
Colloids and Surfaces A: Physicochemical and Engineering Aspects, submitted **2006**.
6. Y. Mikhaylova, V. Dutschk, C. Bellmann, K. Grundke, K.-J. Eichhorn, B. Voit, Study of the solid-liquid interface of hydroxyl-terminated hyperbranched aromatic polyesters (HBP-OH) in aqueous media. I. Characterisation of the properties and swelling behaviour of HBP-OH thin films
Colloids and Surfaces A: Physicochemical and Engineering Aspects, **in print**.
5. Y. Mikhaylova, G. Adam, L. Häussler, K.-J. Eichhorn, B. Voit, Temperature-dependent FTIR spectroscopic and thermoanalytic studies of hydrogen bonding of hydroxyl (phenolic group) terminated hyperbranched aromatic polyesters
Journal of Molecular Structure, **in print**.
4. A. Serghei, F. Kremer, L. Hartmann, Y. Mikhailova, K.-J. Eichhorn, B. Voit Dynamics of Polymers in Confining Geometries of Different Topology
Polymer Preprints, ACS Meeting, San Diego, **2005**, submitted 11/04
3. Serghei, Y. Mikhailova, K.-J. Eichhorn, B. Voit and F. Kremer Discrepancies in the characterization of the glass transition in thin films of hyperbranched polyesters
Journal of Polymer Science Part B, submitted, **2005**.
2. A. Serghei, Y. Mikhailova, K.-J. Eichhorn, B. Voit, F. Kremer, Molecular dynamics of hyperbranched polyesters in the confinement of thin films
European J. of Physics E **2005**, 17, 199.
1. Y. Mikhaylova, E. Pigorsch, K. Grundke, K.-J. Eichhorn, B. Voit, Surface properties and swelling behaviour of hyperbranched polyester films in aqueous media
Macromol. Symp. **2003**, 210, 271.

Y. Mikhaylova, M. Müller, K. Grundke, K.-J. Eichhorn, B. Voit
In-situ study of protein adsorption on hyperbranched aromatic polyester thin films
Presented at the 94th Bunsen colloquium, Bayreuth, Germany, March 6-7, **2006**,
Lecture.

Y. Mikhaylova, M. Müller, K.-J. Eichhorn, B. Voit
In-situ spectroscopic vis-ellipsometry at the solid/liquid interface of hyperbranched
aromatic polyesters: swelling and protein adsorption
Presented at the 4th Workshop Ellipsometry, Berlin, Germany, February 20-22, **2006**;
Lecture.

Y. Mikhaylova, M. Müller, K. Grundke, K.-J. Eichhorn, B. Voit,
Adsorption of model proteins on thin films of hyperbranched aromatic polyesters.
Presented at the Tver State University, Russia, June 16-19, **2005**; Lecture.

Y. Mikhaylova, K. Grundke, K.-J. Eichhorn, B. Voit,
Surface properties and swelling behaviour of hyperbranched polyester films in
aqueous media.
Presented at the 5th International Symposium Molecular Mobility and Order in
Polymer System, Saint Petersburg, Russia, June 20-24, **2005**; Lecture.

Y. Mikhaylova, V. Dutschk, K. Grundke, K.-J. Eichhorn, B. Voit,
Adsorption of model proteins on thin films of hyperbranched aromatic polyesters.
Presented at the 10th Dresden Polymer Discussion "Characterization of polymer
surfaces and thin films", Evangelische Akademie Meißen, Germany, April 10-13,
2005; Poster.

Y. Mikhaylova, V. Dutschk, K. Grundke, K.-J. Eichhorn, B. Voit,
Adsorption of model proteins on thin films of hyperbranched aromatic polyesters
Presented at the 2nd Max-Bergmann-Symposium, IPF, Dresden, Germany, Feb. 17-
18, **2005**; Poster.

Y. Mikhaylova, C. Bellmann, V. Dutschk, K. Grundke, K.-J. Eichhorn, B. Voit,
Surface properties and characterization of thin films of hyperbranched aromatic
polyesters.
Presented at the workshop NANOFUN-POLY on polymer chemistry and polymer
processing, IPF, Dresden, Germany, Jan. 28-29, **2005**; Poster.

K.-J. Eichhorn, K. Grundke, Y. Mikhaylova, E. Pigorsch,
Immobilisierung und Stabilisierung von funktionellen Schichtsystemen aus
unterschiedlich verzweigten Polymeren auf Festkörperoberflächen
Tagung: "SFB 287", TU Dresden, Germany, July 20-21, **2004**; Poster.

Y. Mikhaylova, V. Dutschk, K. Grundke, K.-J. Eichhorn, B. Voit,
Characterization of protein adsorption onto different polymer surfaces by
Axisymmetric Drop Shape Analysis by Profile and Ellipsometry
Presented at the "Fortschritte bei der Synthese und Charakterisierung von
Polymeren" Vortragstagung der GDCh-Fachgruppe Makromolekulare Chemie,
Düsseldorf, Germany, March 15-16, **2004**; Poster.

Y. Mikhailova, E. Pigorsch, K. Grundke, K.-J. Eichhorn, B. Voit,
Surface properties and swelling behaviour of hyperbranched polyester films in
aqueous media
Presented at the International Symposium on „Reactive Polymers in Inhomogeneous
Systems, in Melts and at Interfaces” Dresden, Germany, Sep. 28 to Oct. 01, **2003**;
Poster.
Issue of a special volume of the contributions of the REACT2003 in “Macromolecular Symposia”
edited by WILEY-VCH Verlag GmbH, Weinheim

Y. Mikhaylova, E. Pigorsch, K. Grundke, K.-J. Eichhorn, B. Voit,
Investigating behaviour of Hyperbranched polyesters in aqueous media
Presented at the 7th Nachwuchstage der Kolloid- und Grenzflächenforschung,
Ruprecht-Karls-Universität Heidelberg, Germany, April 03-04, **2003**; Poster.

Versicherung (insurance).

Hiermit versichere ich, dass ich die vorliegende Arbeit ohne unzulässige Hilfe Dritter und ohne Benutzung anderer als der angegebenen Hilfsmittel angefertigt habe; die aus fremden Quellen direkt oder indirekt übernommenen Gedanken sind als solche kenntlich gemacht. Die Arbeit wurde bisher weder im Inland noch im Ausland in gleicher oder ähnlicher Form einer anderen Prüfungsbehörde vorgelegt.

Frühere Promotionsverfahren haben nicht stattgefunden.

Die vorliegende Arbeit wurde unter der wissenschaftlichen Betreuung von Prof. Dr. Brigitte Voit, Dr. Klaus-Jochen Eichhorn und Dr. Karina Grundke im Rahmen des Sonderforschungsbereiches 287 (Projekt B6 der Deutschen Forschungsgemeinschaft) am Institut für Polymerforschung Dresden e. V. in der Zeit von Juli 2002 bis März 2006 angefertigt.

Die Promotionsordnung der Technischen Universität Dresden vom 16. April 2003 der Fakultät Mathematik und Naturwissenschaften erkenne ich an.

Dresden, 06.03.2006

Yulia Mikhaylova